AN ANALYTICAL AND EXPERIMENTAL STUDY OF FABRIC-REINFORCED, CEMENT-BASED LAMINATED COMPOSITES

by

Sachiko Sueki

A Thesis Presented in Partial Fulfillment
of the Requirements for the Degree
Master of Science

ARIZONA STATE UNIVERSITY

December 2003

AN ANALYTICAL AND EXPERIMENTAL STUDY OF FABRIC-REINFORCED, CEMENT-BASED LAMINATED COMPOSITES

by

Sachiko Sueki

has been approved

December 2003

APPROVED:

_____, Chair

_____

_____

Supervisory Committee

ACCEPTED:

_____

Department Chair

_____

Dean, Graduate College

ABSTRACT

Fabric reinforced cement based composites are a new class of reinforced composites which have the potential for becoming load bearing structural members. Recent studies conducted at ASU point out to superior tensile strength and ductility of these materials. The behavior of fabric-reinforced composites is primarily governed by interfacial bond characteristics between fiber and matrix. One of the methods to evaluate such characteristics is a pullout test. A series of pullout tests was conducted using several different fabric cement manufacturing techniques, matrix, and fabric types. There were four fabric types: alkali-resistant glass (AR-glass), polypropylene (PP), polyethylene (PE), and Polyvinyl Alcohol (PVA); two different mix designs (control and with fly ash); and three different procedures for making samples (control, pultrusion, and vacuum). In addition, there were two different fabric embedded lengths (0.3 and 0.5 inches) and three different free fabric lengths (1, 2 and 3 inches). In order to verify experimental results, two mathematical models addressing straight yarn and woven yarns were developed. These models use a shear lag approach to address the debonding growth and pullout of a single yarn under frictional and adhesion bond. The yarn model was modified into addressing the curvature on the surface in the case of a woven fabric by implementing the restraint caused by fill yarn in the yarn model. The experimental results showed that fabric, mix design and procedural variations highly affected the interfacial bonding. Model predictions verified the experimental results well. The interfacial surface between fiber and cement was observed using the scanning electron microscope and there were significant visible differences on the surface.

To develop analytical design formulations for these composites, the effects of fabric composites under shear load were studied by mathematically calculating the load and deformation response using a laminate theory. Since propagation of cracks between fiber and concrete might be the governing factor in failure of composite under shear load, a model was developed taking the damage due to matrix cracking into account. The model simulated similar trends to those of experimental results, especially when fibers were placed in directions appropriate to carry the tension caused by shear load.

….To My Parents

ACKNOWLEDGEMENTS

I express my sincere gratitude to my advisor and committee chair, Dr. Barzin Mobasher, for his constant guidance, support and help throughout the course of the study. I would also like to extend sincere gratitude to Dr. Subramaniam D. Rajan who inspired me to learn FEM and other programming tools which are going to be invaluable. Thanks also to Dr. Apostolos Fafitis for his encouragement and serving on my committee. I also extend my thanks to Dr. Alva Peled for her guidance and help for the extensive summer experiments. I greatly appreciate the help provided by Dr. Dallas Kingsbury and Peter Goguen in day to day laboratory work. Thanks are also extended to my laboratory mates, Jitendra Pahilajani and Nora Singla for providing me with friendly help. I am grateful to Chaitanya Deenadayalu for his help with Abaqus and C++. Finally, I would like to acknowledge all my friends, especially Srihari, Paul and Suresh for their support and help without which it would have been difficult to complete in time. I would also like to express my gratitude to all the CEE administrative staffs and folks at International Student Office for their Kind help and support. At the end, nothing would have been possible without the encouragement, sacrifice, and blessings of my beloved parents, Masahiko and Mieko Sueki, and sister, Hiroko Iizuka.

TABLE OF CONTENTS

LIST OF TABLES

LIST OF FIGURES

CHAPTER 1

INTRODUCTION

1.1 Introduction

Materials scientists, engineers and scientists are always striving to produce either improved traditional materials or completely new materials to find better performance of materials. Composite materials are an example of the latter category. There is no really adequate definition of a composite material. However, there are three main points to be included in a definition of an acceptable composite material for use in structural applications.

a. It consists of two or more physically distinct and mechanically separable materials.
b. It can be made by mixing the separate materials in such a way that the dispersion of one material in the other can be done in a controlled way to achieve optimum properties.
c. The properties are superior, and possibly unique in some specific respects, to the properties of the individual components.

The examples of composite materials are wood, bone, metallic alloys (e.g. steels), reinforced concrete beams etc. The broad classification of composite materials with some examples is in Table 1.1. In addition to the construction materials, other general applications of these composite materials are aircrafts, automobiles, boats, furniture, sport's equipment etc.

Table 1.1

Broad Classification of Composite Materials (From: D. Hull, 1981 An introduction to composite materials, Cambridge university press)

	Examples
Natural composite materials	Wood Bone Bamboo Muscle and other itssue
Microcomposite materials	Metallic alloys: e.g. steels Toughened thermoplastics: e.g. impact polystyrene, ABS Sheet moulding compounds Reinforced thermoplastics
Macrocomposites (Engineering products)	Galvanised steel Reinforced concrete beams Helicopter blades Skis

Within the last fifty years there has been a rapid increase in the production of synthetic composites, those incorporating fine fibres in various plastics. A fibrous reinforcement is characterized by its length being much greater than its cross-sectional dimension. However, the ratio of length to the cross-sectional dimension, known as the aspect ratio, can vary considerably. In single-layer composites long fibres with high aspect ratios give what are called continuous fibre reinforced composites, whereas discontinuous fibre composites are fabricated using short fibres of low aspect ratio. The orientation of the discontinuous fibres may be random or preferred. The frequently encountered preferred orientation in the case of a continuous fibre composite is termed unidirectional and the corresponding random situation can be approximated to by bi-directional woven reinforcement. Multilayered composites are another category of fibre

reinforced composites. These are classified as either laminates or hybrids. Laminates are sheet constructions which are made by stacking layers in a specified sequence. Hybrids are usually multilayered composites with mixed fibres and are becoming commonplace. The fibres may be mixed in a ply or layer by layer and these composites are designed to benefit from the different properties of the fibres employed. The most commonly used fibers in the cement-based matrix are steel, glass polymeric and natural fibers.

The reason for using fibers in composite is to enhance the properties of an inherently weak, brittle and crack-prone cementitious matrix. Fiber in hardened cement paste, mortar or concrete may have at least three important effects. First, they may tend to increase the stress at which the matrix starts to crack. Second, they may improve the strain capacity or ductility of the inherently brittle cementitious matrix, thus increasing its energy absorption capability or toughness characterized in general by the area under a stress-strain or load-deformation curve or some defined portion of it. A third important effect of fibers is their tendency to inhibit or modify crack development in terms of reducing crack width and average crack spacing. The degree of improvements depends on the mode of loading and the type and amount of fibers. Any type of fiber effective for reinforcing relatively weak and brittle cementitious matrices must have higher tensile strength, ductility (or elongation), elastic modulus, elasticity and Poisson's ratio than those of matrix. However, realization of full reinforcing potential depends strongly on the interfacial shear bond between fiber and matrix.

In the simplest case of very long fibers aligned in the direction of uniaxial tensile stress, just like conventional straight reinforcing bars, it should be obvious that if

adhesive interfacial shear bond does not exist no tensile stress can develop in the fibers. In this case the strength of the composite is the same as the strength of the matrix because the fibers pull out of the matrix without resistance. In contrast, when there is very strong interfacial shear, whether by adhesion, friction or mechanical interlock, the fibers become subject to the entire load carried by the composite once the matrix cracks, and the ultimate strength depends only on the amount and intrinsic strength of the fibers. However, if the toughness of the composite was concerned, the interface must not be so strong that it does not fail and allow toughening mechanisms such as debonding and fibre pullout to take place.

In addition, shear failure in composite structures is of equally important phenomena. Use of fibers in cement concrete helps to make concrete less brittle. Fibers generally help to withstand tougher tensile load conditions than cement alone. However, when fiber reinforced composite was considered as a laminated composite, such use of fibers with cement concrete has a tendency to reduce interfacial bonding between the fibers and the matrix. Practically, when the mechanical properties of fiber reinforced composites are calculated mathematically, it is often considered that the composite consist of laminates. In each laminate, all the fibers are aligned in one direction. This is also termed as ‘laminate theory’. In recent years, cement-based laminates are considered to be an ideal material for structural, seismic, and other severe loading applications. Due to such specialized nature of the structures, their shear characteristics are vital to understand. However, there are very few studies reported on how fibers perform in shear

failure conditions. Therefore understanding the role of fibers in withstanding or enhancing shear resistance is very critical.

1.2 Review of Related Literature

The behavior of fiber-reinforced composites is primarily governed by the interfacial bond characteristics between the fiber and the matrix. Several methods have been developed to evaluate the bonding strength between fiber and matrix. In one of the earlier researches by Kelly and Tyson in 1965, they measured the force required to pullout a fiber embedded in a matrix as the bonding strength. This method, in addition to its relative simplicity of sample preparation and measurement, is expected to give realistic information when one considers the pullout of fibres from the fracture surfaces of composites. Based on this experiment, they found that the force required for extracting a stiff metal wire from a softer metal matrix is a linear function of the embedded length of wire. This is a case in which a uniform shear strength of the interface can be assumed along a fibre.

In another study by Greszczuk (1969), he considered a general relationship between the fibre strength and the interface strength theoretically as a function of the embedded length of fibre using the assumptions of the shear lag theory, assuming that the extensional stresses in the matrix are negligible relative to those in the fibre and that the shear stresses in the fibre are small compared to those in the matrix. He also assumed that complete fibre-matrix debonding takes place when the maximum inter facial shear stress, $\tau_{i,max}$, is equal to the maximum interfacial bond shear strength, $\tau_{ib,max}$. Later in

1972, Lawrence developed a theory on the effect of partial debonding on the maximum debonding stress including the effect of friction, instead of using Greszczuk's assumption that immediate, catastrophic fibre-matrix debonding takes place when the shear forces reaches maximum.

These theoretical approaches are based on maximum shear strength criterion using shear lag based models. Based on maximum shear strength criterion, debonding takes place when the maximum shear stress at interface reaches a critical value. An alternative approach is a formulation based on fracture mechanics principles using the energy release rate criterion suggested by Gurney and Hunt (1967). Such formation is based on the assumption that the propagation of the debonding zone requires a certain energy and that debonding zone requires a certain energy and that debonding will occur only when the energy flowing into the interface exceeds the value of the specific resistance energy.

Much later in 1990, Stang et al. described the whole debonding process, including a criterion for the initiation of debonding and the load-versus-displacement relationship during debonding.

As mentioned earlier, the behavior of fiber-reinforced composites is primarily governed by the interfacial bond characteristics between the fiber and the matrix. In 1973, Aveston and Kelly proposed the fundamental concepts and relationships among matrix crack spacing, interfacial debonding (or sliding) length, and interfacial shear stress of a continuous fiber-reinforced composite. Advancing the concept, in 1996 Mobasher and Li conducted a theoretical analysis interfacial properties and crack opening.

Above mentioned theoretical models are for a yarn condition. However, in recent years, considerable attention has been devoted to woven fabric composite materials by many scientists. e.g. Peled et al. in 1994 showed the increase of bond strength in woven fabric reinforcement materials using the pullout experiment.

1.3 Objectives of the Thesis

There are two major parts, interfacial shear bonding and shear failure, in this thesis. The primary objective of the first part is to study the effect of fiber debonding and pullout to predict the stress-strain relation under tensile load in fabric reinforced concrete. After the cracks have formed in the material under the tensile load, fiber debonding and pullout process have a significant influence to the crack opening since fiber works as a crack bridging. However, the geometrical condition of fibers and matrix in pullout specimens are different from that in a composite subjected to a tensile load. Note that the pullout test is conducted under the existence of free fiber which does not apply to the tensile test. Therefore, the interface response of pullout test might not be the same as that for tensile test. Pullout test was conducted under various free fiber lengths to modify different conditions between pullout and tensile tests as explained in the following chapters.

The specific objectives of the first part are as follows.

a. To conduct the pullout test under various free fiber lengths, fabric types and mix designs.

b. To model the load-deformation relationship using results of objective ‘a’ and existing theory of a yarn condition.
c. To model the load-deformation relationship using the results of objective ‘a’ and existing theory for woven condition.
d. To compare two models and study the sensitivity of various parameters that have been used in the model.

The objective of the second part is to understand material properties of fiber reinforced concrete under shear load better. Haup (1997) conducted a series of experiments for shear failure in various composite samples. However, it is also important to generalize the behavior of composite material for such failure conditions. Therefore, a model for shear failure was developed and simulation results were compared with their experimental data.

The specific objectives of the second part are as follows.

a. To model the load-deformation relationship using existing theory of laminate theory.
b. To compare the experimental and simulated results.

Details of pullout test (experiments) are explained in Chapter 2. Chapter 3 discusses the models to fit the results of experiments from the pullout test. Details of shear model are explained in Chapter 4 and conclusions are outlined in Chapter 5.

CHAPTER 2

EXPERIMENTAL ANALYSIS AND RESULTS

2.1 Pullout Test

A series of pullout test were designed to obtain the bond strength and other properties of the fabric/matrix interface. Using the combination of 4 different fabrics and 2 different mix designs, specimens were made by 3 different procedures. Specimens were made of cement paste with thickness of .32 inches (8 mm) and contained a layer of fabric in the middle.

2.1.1 Specimen Preparation

Fabric

Four different types of fabrics were used in the experiment, which are alkali-resistant AR-glass (AR-glass), polypropylene (PP), polyethylene (PE), and Polyvinyl Alcohol (PVA) fabrics. Fabrics are shown in figure 2.1. The properties for these fabrics are given below (Table 2.1).

Table 2.1

Properties of Yarns

Yarn Type	Yarn Nature	Strength (MPa)	Modulus of Elasticity (MPa)	Strain at Peak (mm/mm)	Filament size (mm)	Number of filaments in a bundle	Approximate Bundle diameter (mm)
AR-glass	Bundle	1276-2448	78600	-	0.0135	400	0.27
PP	Bundle	500	6900	0.27	0.04	100	0.40
PE	Monofilament	260	1760	0.21	0.25	1	0.25
PVA	Bundle	227	3938	0.11	-	-	0.97

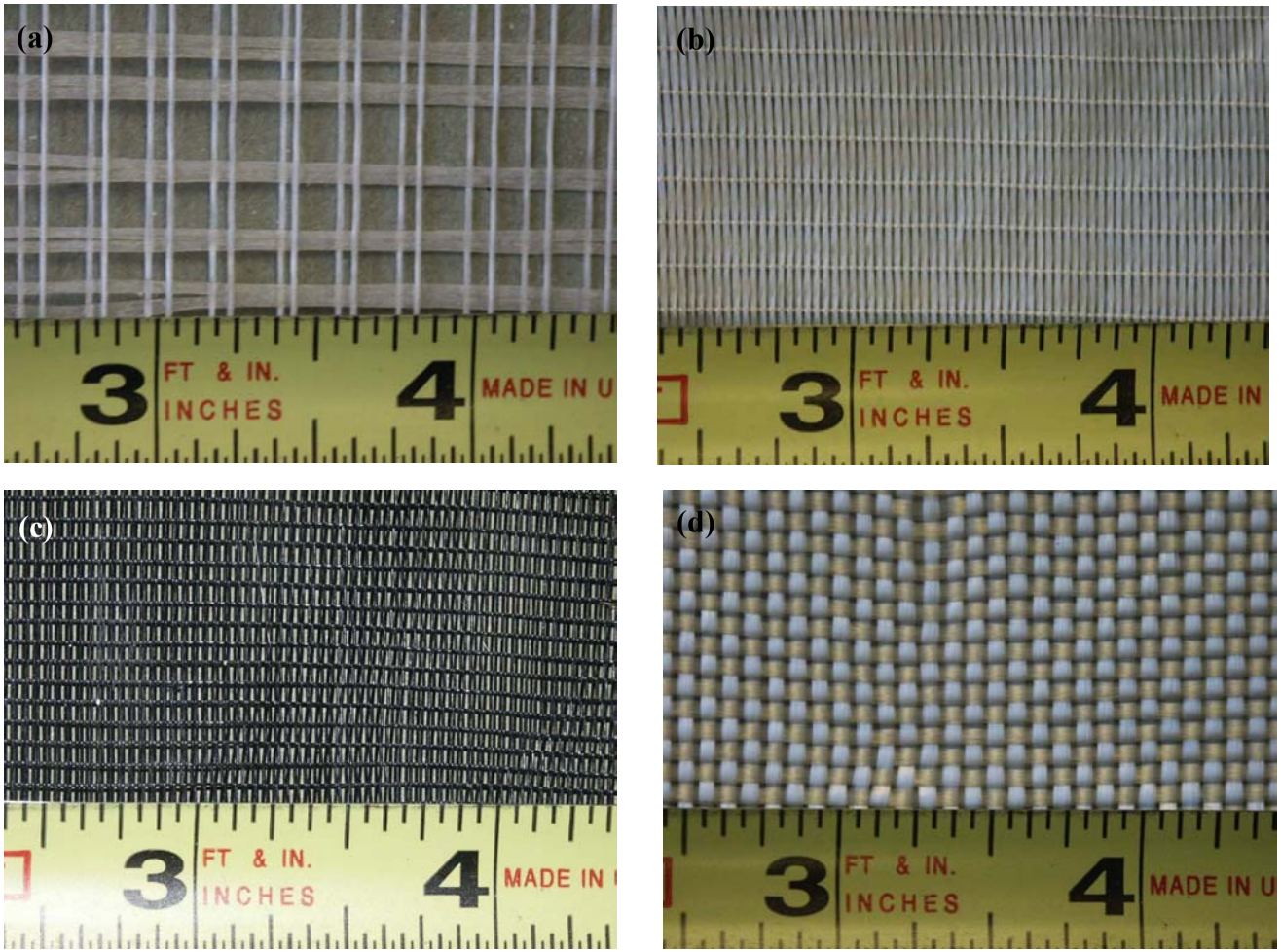

Fig. 2.1. Fabric types (a) AR-glass (b) PP (c) PE (d) PVA

Mix Design

Two types of mix design were used with their details provided in table 2.2. Mix design 1 was a plain Portland cement paste. To enhance the workability of this mix superplasticizer was added. Mix design 2 contained 40% fly ash as cement replacement and had enough workability that no superplasticizer was needed. Both mixtures had 5% silica fume and a water to cementitious solids of 2.7.

Table 2.2

Mix Design Detail

	Mix Design 1	Mix Design 2
Water Cementitious Ratio	2.7	2.7
Water	829 g	829 g
Cement	2040 g	1224 g
Silica Fume	169 g	169 g
Fly Ash	-	816 g
Superplasticizer	5.25 ml	-

Procedure

Samples were prepared by three different methods to evaluate the interaction between the processing and the interfacial bond development. These procedures include the cast, the pultrusion, and vacuum mixing procedures. The all the specimens were made in a single mold with dimensions of 10 x 6 inches (254 x 152.4 mm) as shown in figure 2.2. The thickness of the mold was adjustable since its sides were made of thin strips and several strips could be used to make up a specific thickness. In the cast

procedure which was the control process, the paste mixture was poured into the mold in several layers, layer by layer. The mix was first poured into the mold and then a fabric layer was laid on it. This was followed by another layer of paste (Fig. 2.3). In the pultrusion process, the fabrics were passed through a cement bath, and then pulled through a set of rollers to squeeze the paste in the openings of the fabric and remove excessive paste (Fig. 2.4). Then, the fabrics were laid on the cement in the mold. The third procedure was done by using the vacuum (Fig. 2.5) mixing process. After the ingredients were blended in a stationary mixer, the fresh mixture was transferred to a container and additional mixing was conducted under vacuum. The mix was vacuumed for two minutes to take out the air babbles inside. The mix was then pored into the mold. The specimens were removed from the mold after 24 hours, and kept in an oven at 80 ^{o}C with a RH about 100%. 2 days after steam curing, the samples were cut to the specified embedded fiber lengths using a water cooled saw with a diamond edge blade as shown in figure 2.6. The specimens were stored in room temperature until the time of testing.

Fig. 2.2. Specimen mold (a) Base plate (b) Flame (c) Mold (d) Mold with base

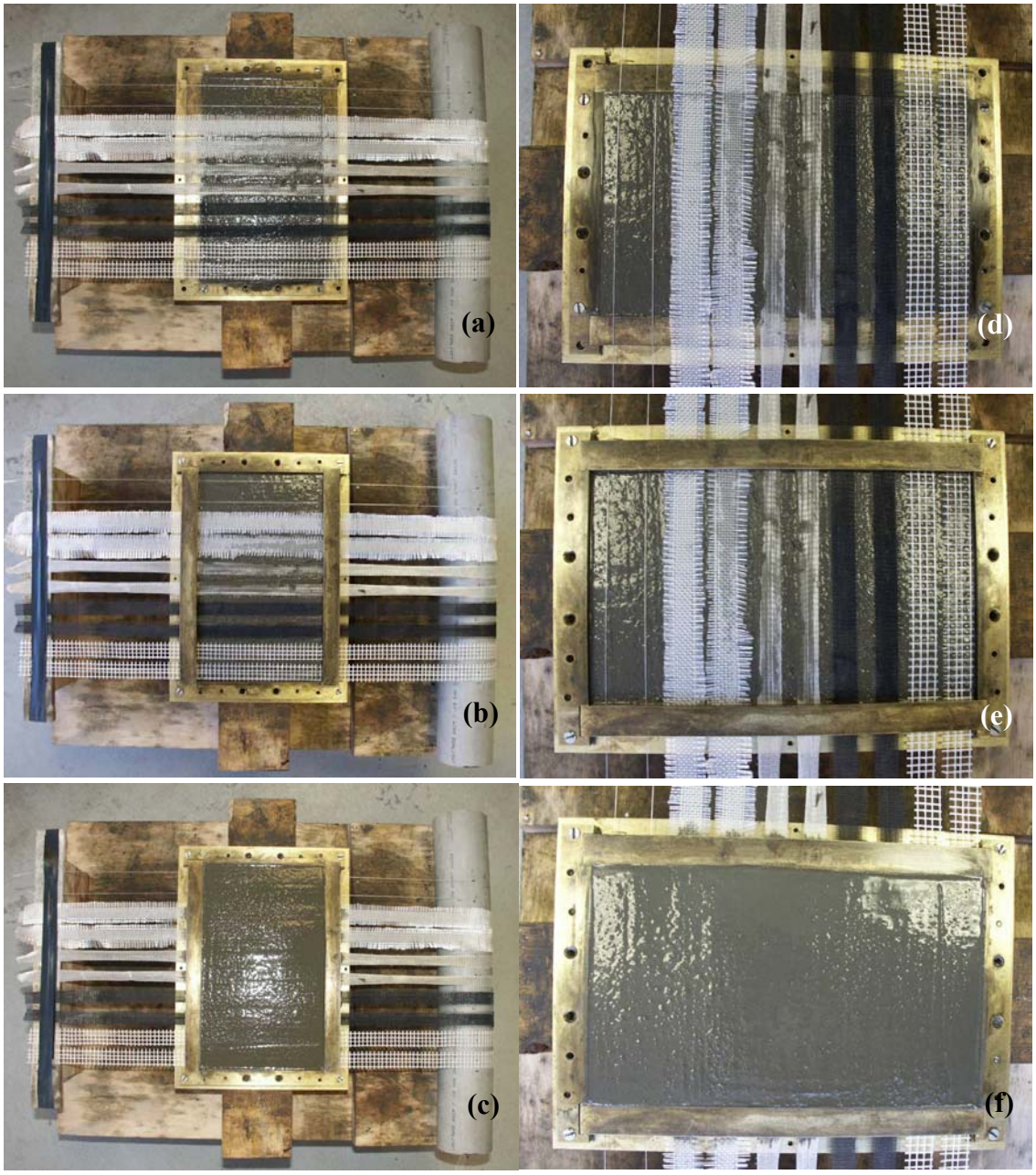

Fig. 2.3. Sample Preparation (a) Step 1 (b) Step 2 (c) Step 3 (d), (e) and (f) Close up of (a), (b) and (c)

Fig. 2.4. Pultrusion process

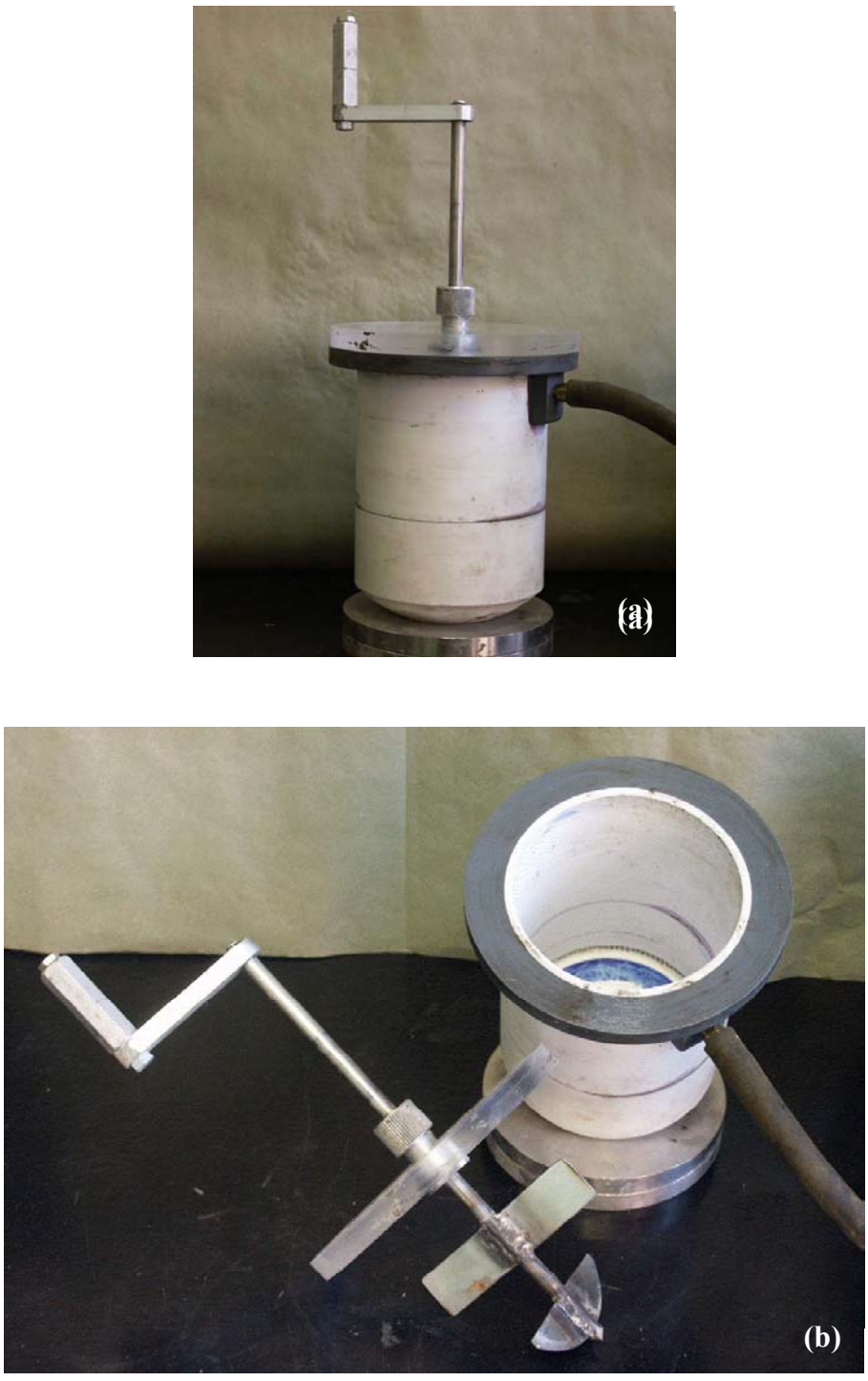

Fig. 2.5. Vacuum (a) Side view (b) Top view with lid off

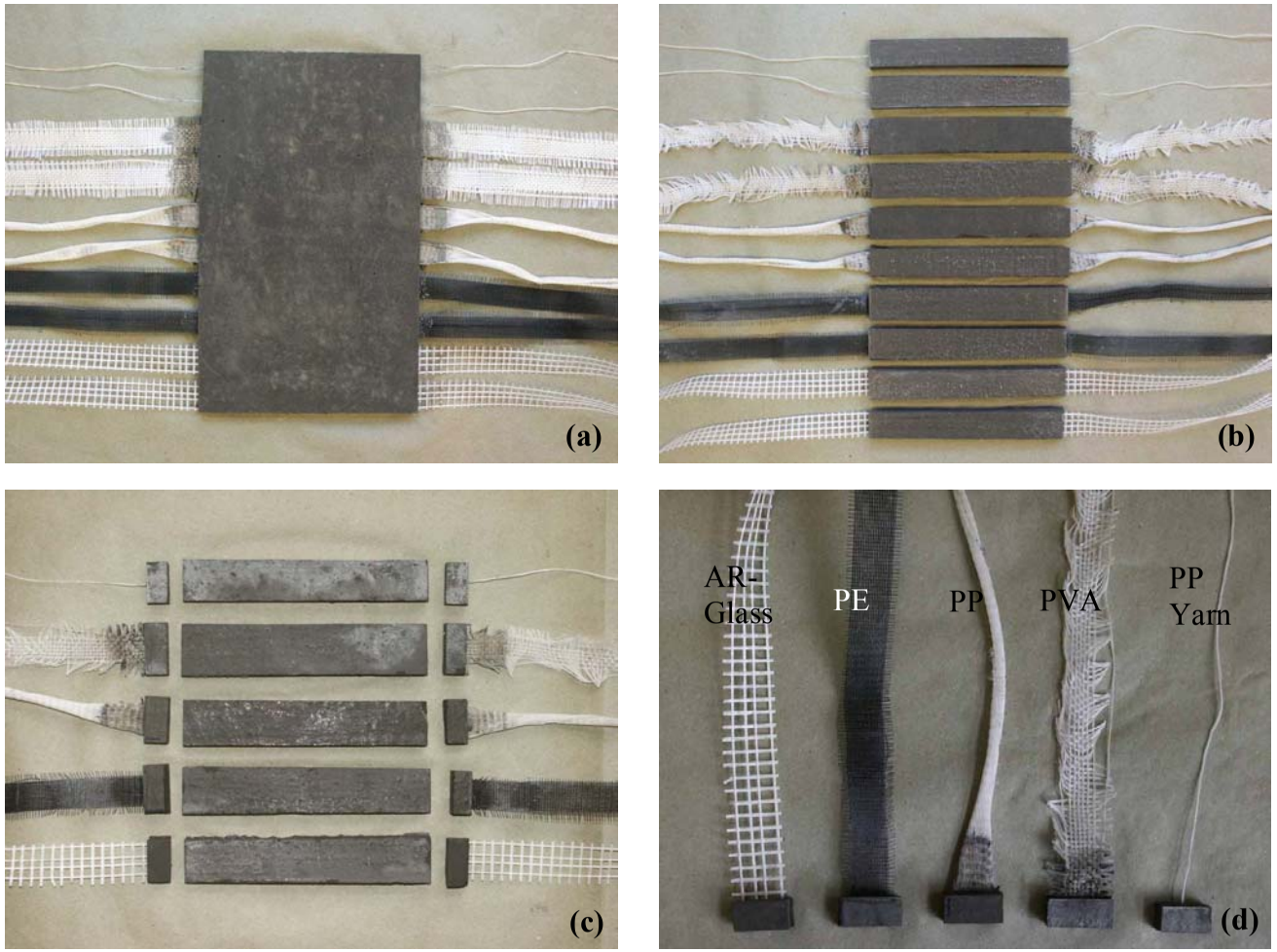

Fig. 2.6. Specimens (a) Sample taken out from the mold (b) & (c) Cut into specific size (d) Each sample

Specimen

The dimensions of specimens were 1.0 inch wide by 0.32 inches thick (25.4 mm wide by 8.1 mm thick) as shown in figure 2.7. The experimental design matrix is shown in table 2.3 listing all the variables studied. There were four types of fabrics, two formulations for matrix, and three procedures to make the samples. In addition, there were two different embedded and three different free fiber lengths used. The test was conducted by pulling out 8 yarns or 1 yarn from the matrix. For the case of 1 yarn condition, a yarn is pulled out from the matrix embedded as fabric or a yarn condition. The details of each sample are in table 2.3. Two embedded lengths of 0.3 or 0.5 inches (7.62 or 12.7mm) were used.

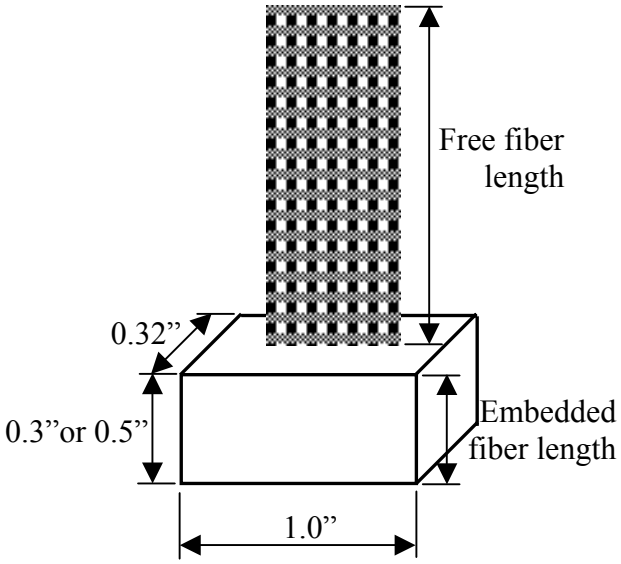

Fig. 2.7. Schematic drawing of a specimen

Table 2.3

Summary of Specimens

8 yarns

Fabric	Mix	Procedure	Free length (inch)	Embedded length (inch)	Sample ID
AR-glass	Control	Cast	1	0.5	G105
AR-glass	Control	Cast	2	0.5	G205
AR-glass	Control	Cast	3	0.5	G305
AR-glass	Control	Pultrusion	1	0.5	GP105
AR-glass	Control	Vacuum	1	0.5	GV105
AR-glass	w/ FA	Cast	1	0.5	FG105
AR-glass	w/ FA	Pultrusion	1	0.5	FGP105
PP	Control	Cast	1	0.3	PP103
PP	Control	Cast	1	0.5	PP105
PP	Control	Cast	2	0.5	PP205
PP	Control	Cast	3	0.5	PP305
PP	Control	Pultrusion	1	0.3	PPP103
PP	Control	Pultrusion	1	0.5	PPP105
PP	Control	Vacuum	1	0.3	PPV103
PE	Control	Cast	1	0.5	PE105
PE	Control	Cast	2	0.5	PE205
PE	Control	Cast	3	0.5	PE305
PVA	Control	Cast	1	0.3	PVA103
PVA	Control	Pultrusion	1	0.3	PVAP103
PVA	w/ FA	Pultrusion	1	0.3	FPVAP103
PVA	w/ FA	Pultrusion	1	0.5	FPVAP105

1 yarn

Fabric	Mix	Condition	Procedure	Free length (inch)	Embedded length (inch)	Sample ID
PP	Control	Yarn	Cast	1	0.3	PPY103
PP	Control	Yarn	Pultrusion	1	0.3	PPPY103
PP	Control	Yarn	Vacuum	1	0.3	PPVY103
PP	Control	Fabric	Cast	1	0.3	PPFY103
PP	Control	Fabric	Pultrusion	1	0.3	PPPFY103

2.1.2 Test Procedure and Data analysis

Pullout tests were carried out using the setup as shown in figure 2.8. The lower portion of the test grip was a rectangular piece with a slot to allow for the insertion of the fabric. Individual samples were inserted inside this grip such that the free length portion of the fabric was protruding out and clamped by the frictional grips at the top (see figure 2.9). The test was conducted by pulling the fabric out and resisting the load by reacting against the lower grip. The test was conducted using a constant displacement rate of 0.25 mm/sec. The test was continued until embedded fabric was completely pulled out.

Fig. 2.8. Setup for pullout test

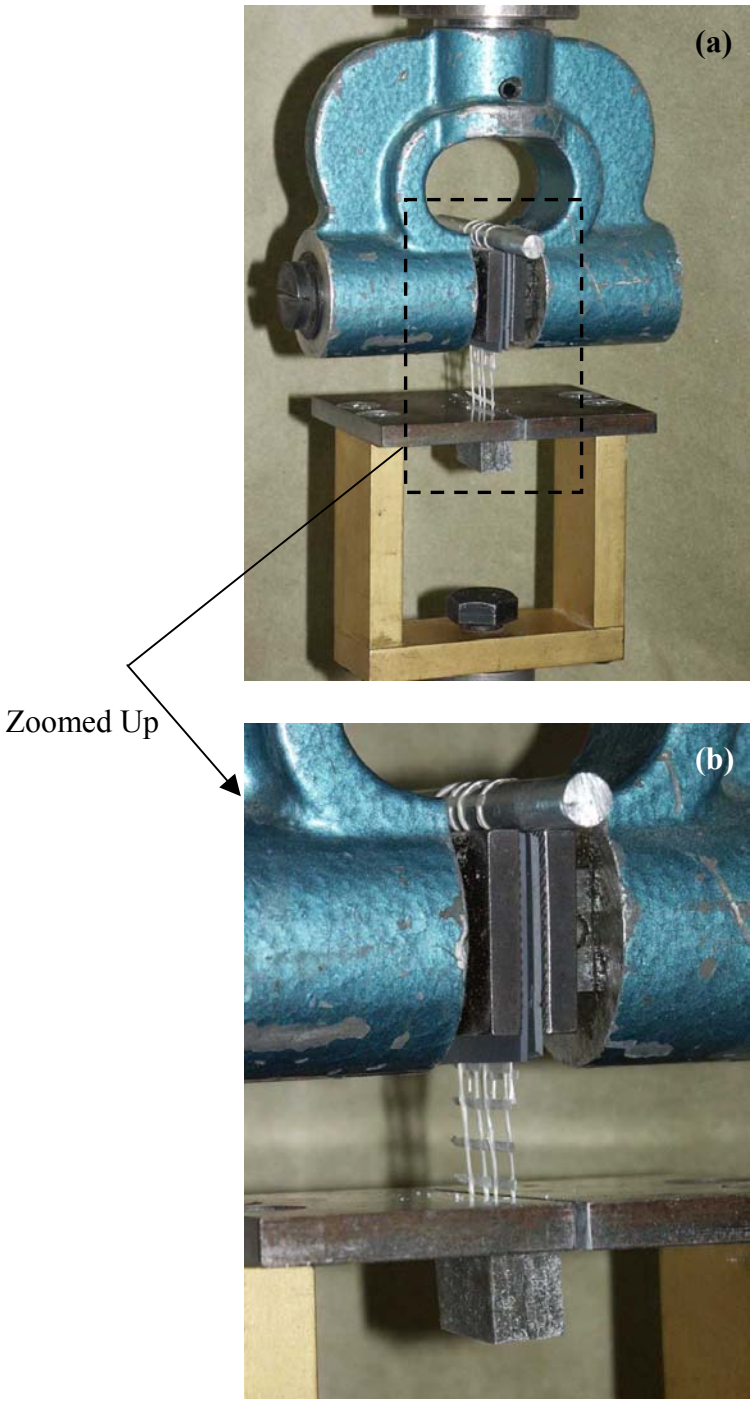

Fig. 2.9. Specimen set up (a) Specimen under grips (b) Close up of (a)

The load and deformation data thus obtained were smoothed using a five point smoothing operation as follows:

$$X_i = \frac{1}{5}\left(x_{i-2} + x_{i-1} + x_i + x_{i+1} + x_{i+2}\right) \tag{2.1}$$

where X_i is the smoothed data at i[th] point and x_{i-2}, x_{i-1} *and* x_{i+1}, x_{i+2} are the data points before and after i[th] point. Five data points, two points before and two after the target point, are necessary to smoothen the data. Therefore first two and last two data points were kept as it is. Then, the data were reduced to 50% of the total data using cubic spline interpolation to reduce excess data for easier handling. Total number of acquired data was about 700 points. Finally, the load-deformation results were used to calculate the initial slope of the graph (K), toughness and maximum shear strength, τ_{max}. τ_{max} was calculated using the following equation

$$\tau_{max} = \frac{P_{max}}{n\pi dl} \tag{2.2}$$

where, P_{max} is maximum load, n is number of yarns pulled out, d is diameter of a yarn and l is the embedded length of a yarn.

2.1.3 Results

Table 2.4 shows the summary of experiment results. The experimental results (deformation versus load) are shown from figure 2.10 to 2.16. Figures 2.10 to 2.14 show the results of eight yarns pullout. Figure 2.15 and 2.16 are for the single yarn pullout.

Table 2.4

Summary of Calculation Results

Sample ID	Average K (lbf/inch)	Standard Deviation K	Average Max load (lbf)	Standard Deviation Max Load	Average Toughness (lbf-inch)	Standard Deviation Toughness	Average τ_{max} (psi)	Standard Deviation τ_{max}	Comments
G105	1407.62	333.09	41.27	4.05	5.22	2.01	330.76	23.87	
G205	1092.51	168.24	33.67	6.52	4.54	1.55	275.34	54.84	
G305	1038.58	78.45	39.23	6.63	4.34	1.64	316.37	45.15	
GP105	1247.36	239.37	32.71	10.02	3.26	1.14	255.43	81.21	Most of the sample's yarn broken
GV105	1881.57	269.76	58.28	7.04	8.04	1.48	426.66	47.84	Most of the sample's yarn broken
FG105	1363.12	197.96	54.56	18.28	5.90	2.28	456.72	148.23	Some of the sample's filament broken
FGP105	1484.43	282.02	45.64	14.80	4.45	2.72	380.42	122.43	Some of the sample's yarn broken and matrix split
PP103	461.71	221.18	26.47	11.21	3.65	2.09	224.13	89.56	
PP105	627.86	77.36	39.21	5.69	7.49	1.53	209.31	27.30	
PP205	361.10	50.21	34.34	4.80	8.60	1.51	181.26	21.41	
PP305	293.72	13.34	36.39	11.35	8.47	2.76	190.48	54.07	
PPP103	534.11	117.80	53.80	15.76	9.23	3.63	422.13	96.90	
PPP105	520.85	79.58	60.83	16.49	11.90	6.18	310.61	71.91	Some of the sample's yarn broken
PPV103	638.17	79.98	28.13	5.60	3.76	1.58	242.92	55.62	Some of the sample's matrix broken

Table 2.4

Continued

Sample ID	Average K (lbf/inch)	Standard Deviation K	Average Max load (lbf)	Standard Deviation Max Load	Average Toughness (lbf-inch)	Standard Deviation Toughness	Average τ_{max} (psi)	Standard Deviation τ_{max}	Comments
PE105	40.87	5.91	17.04	1.27	8.31	2.32	146.86	4.82	
PE205	28.53	2.53	16.03	4.02	8.13	3.28	138.31	33.44	
PE305	20.65	3.12	17.52	2.68	11.52	5.03	157.35	23.39	
PVA103	273.75	49.59	32.80	8.52	4.23	0.69	223.88	50.22	
PVAP103	263.74	50.41	61.31	3.49	13.63	3.09	464.15	38.01	Most of the sample's yarn broke
FPVAP103	352.29	32.67	50.86	7.27	7.10	0.78	442.46	102.37	Most of the sample's yarn broke
FPVAP105	434.68	41.22	73.48	3.76	12.96	2.28	374.73	25.99	Most of the sample's yarn broke
PPY103	88.61	19.89	5.54	3.44	1.10	0.82	365.58	221.69	
PPPY103	107.34	14.38	6.17	2.20	1.21	0.38	413.88	186.98	
PPVY103	95.83	18.88	8.94	2.46	1.76	0.37	589.65	158.72	All the sample’s few filaments did not pull out.
PPFY103	103.54	25.92	6.27	2.31	1.30	0.54	396.49	144.19	
PPPFY103	71.01	7.96	9.11	1.92	1.65	0.42	623.17	164.72	Half of the sample's yarn broke

Our results suggested that the increase in free fiber length reduces the stiffness proportionally as seen in figure 2.10. The ratio of reduction depended on type of fabrics (AR-glass, PE and PP) used as seen in each figure 2.10a, b and c.

It was observed that the AR-glass fabrics required the highest load (≈ 38 lbf) to pullout the yarns (Fig. 2.11). PP was slightly less than AR-glass fabric (> 36 lbf), while PE required less than 50% of the load (<17 lbf) compared to AR-glass. However, PE fabrics had the highest toughness at more than 9 lbf-inch. This compared to AR-glass at less than 5 lbf-inch and PP at about 8 lbf-inch as seen in table 2.4.

Figures 2.12a, b, and c show the effect of use of fly ash (mix design 2) as compared to control mixture (mix design 1) for AR-glass or PVA fabric. The specimens with AR-glass and PVA fabrics were manufactured using the normal casting procedure, and/or pultrusion bath. For the case of AR-glass fabrics with cast procedure, use of fly ash resulted in higher load capacity (≈ 17 lbf higher than mixtures without fly ash). AR-glass fabrics with pultrusion bath also showed a similar trend. Maximum load for mix design 2 was almost 40% (13 lbf) higher than mix design 1. In contrast, in the case of PVA with pultrusion procedure, mixtures without fly ash showed a higher maximum load (> 60 lbf) than with fly ash (≈ 50 lbf). However, it was observed that in most of the samples with mix design 2 the bond was so well developed that the fabrics fractured as opposed to pullout.

Figure 2.13 showed that the load-slip responses depend to a great extent on the manufacturing process employed. This was verified further in PP fabric case. When pultrusion bath was used to make the samples, the maximum load was two times higher

(≈ 25 lbf more) for both 0.3” and 0.5” embedded lengths than cast procedure. The toughness was also improved to levels as high as 3 lbf-inch. When vacuum mixing was used, the improvements were not as visible as compared to the pultrusion bath. On average, vacuum samples are less than 2 lbf higher than control procedure (of all the samples). Use of vacuum for AR-glass fabric resulted in increase of maximum load by more than 20 lbf. However, AR-glass fabric did not show the clear difference like PP when pultrusion bath was used. As a matter of fact, average of maximum load for the AR-glass fabric with pultrusion bath was slightly less (≈ 5 lbf) than that of control procedure for mix design 1. This might be attributed to the damage imparted to the AR-glass fabric during pultrusion. When the mix design 2 was used for AR-glass fabric, while samples made by pultrusion bath were reduced by nearly 9 lbf in maximum load, results were still higher than the cast procedure with mix design 1 (> 7 lbf).

In all the samples, the increase in embedded length resulted in the increase of maximum load as seen in figure 2.14. The relative magnitudes of increase were different for each case. PP with cast procedure and mix design 1 increased by 48% (> 10 lbf) when embedded length was increased from 0.3” to 0.5”. Similarly, PP with pultrusion bath and mix design 1 increased by 13% (≈ 7 lbf), and PVA with pultrusion bath and mix design 2 increased by 44% (> 22 lbf).

Figures 2.15 and 2.16 show the results of a PP yarn pullout test conducted while the yarn was within the woven fabric compared to a stand-alone condition. In each case, a single yarn was pulled out from the matrix, and figure 2.15 shows the difference of these two conditions. Pulling a single PP yarn out from the matrix embedded as woven

needed higher load (nearly 1 lbf) than from the one embedded as a yarn. Figure 2.16 shows the effect of different procedures (cast, with pultrusion bath and with vacuum). When a single yarn was pulled out from the matrix, the maximum load for cast procedure was lowest (< 6 lbf) among the three procedures. The highest maximum load was nearly 9 lbf, and occurred for vacuum samples, possibly due to the lower porosity at the interface transition zone. Samples made with pultrusion bath needed more than 6 lbf to pullout a yarn. When fiber was embedded as woven, pulling a yarn from the samples in pultrusion bath procedure required nearly 3 lbf higher than with the cast procedure.

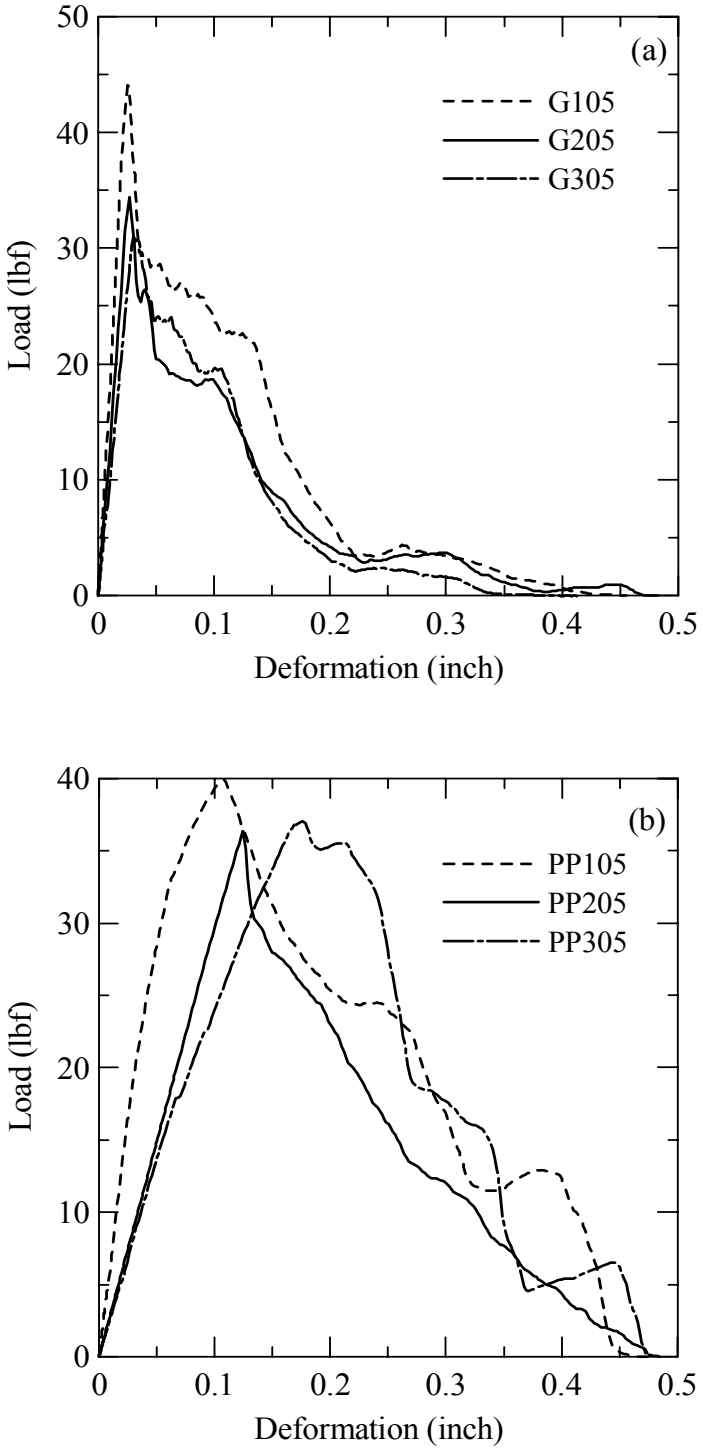

Fig. 2.10. Deformation vs. load for different free fiber lengths (a) AR-glass (b) PP (c) PE

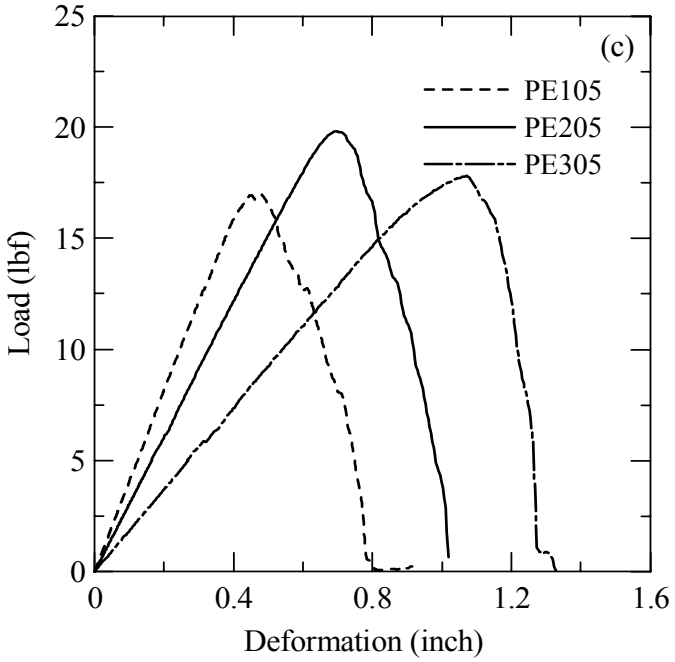

Fig. 2.10. Continued

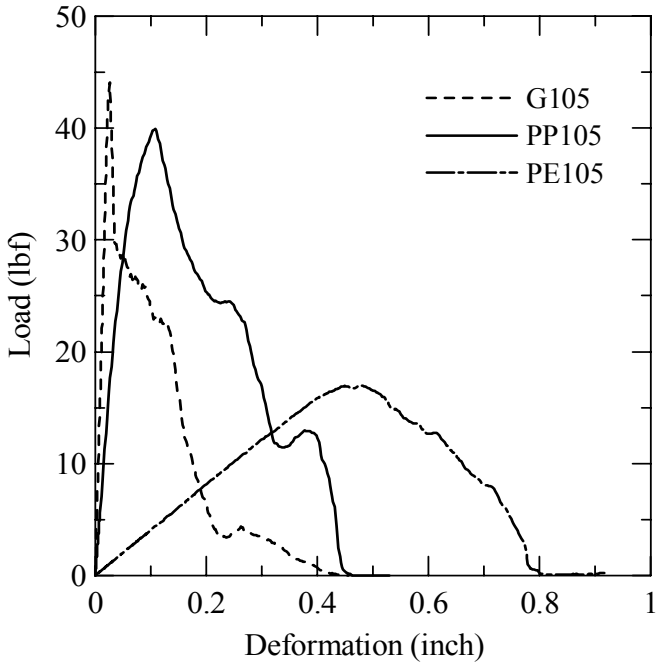

Fig. 2.11. Deformation vs. load for different fabric types

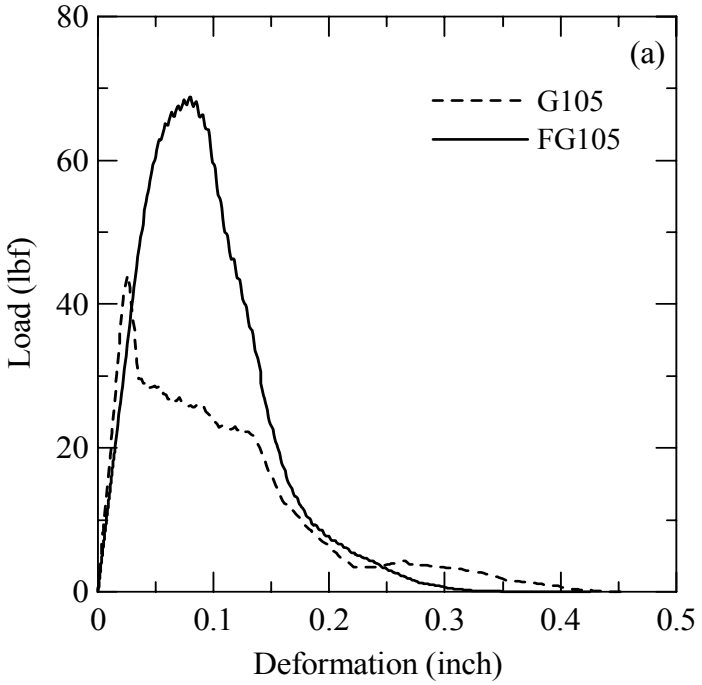

Fig. 2.12. Deformation vs. load for different mix designs (a) AR-glass with cast procedure (b) AR-glass with pultrusion procedure (c) PVA with pultrusion procedure

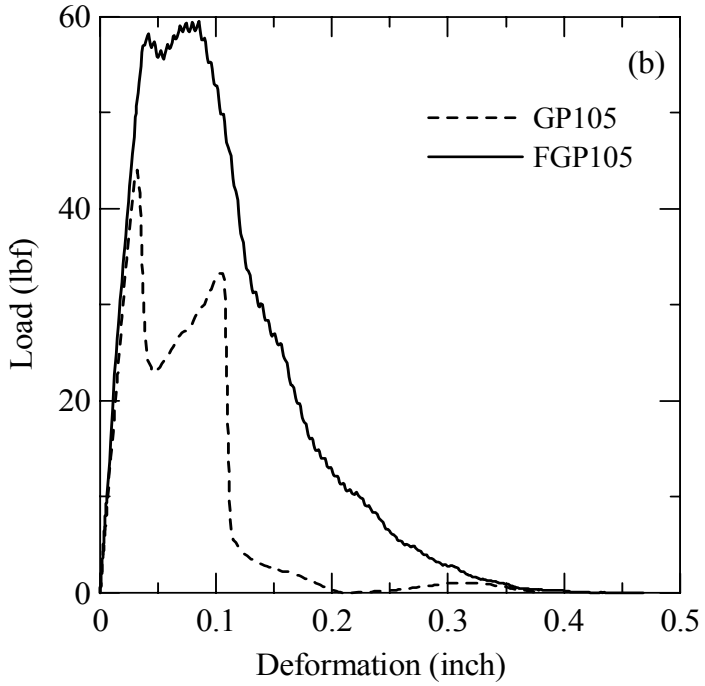

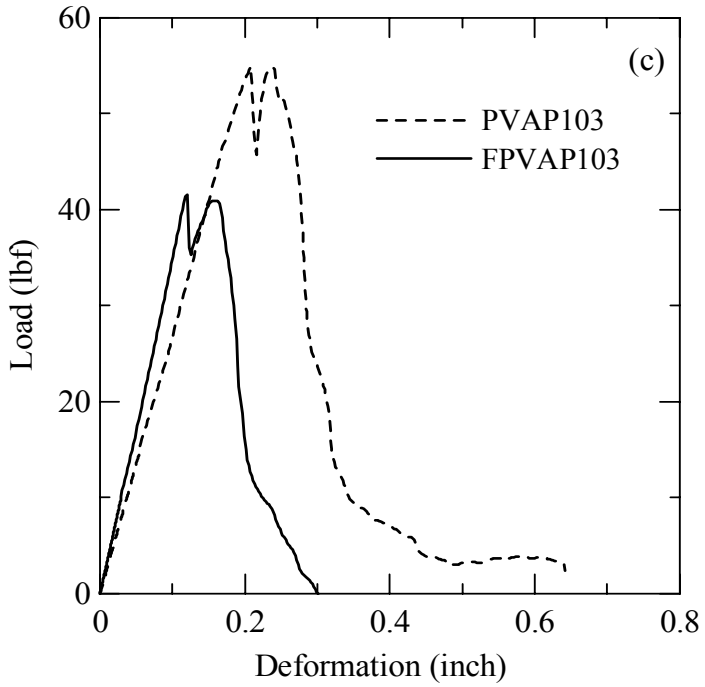

Fig. 2.12. Continued

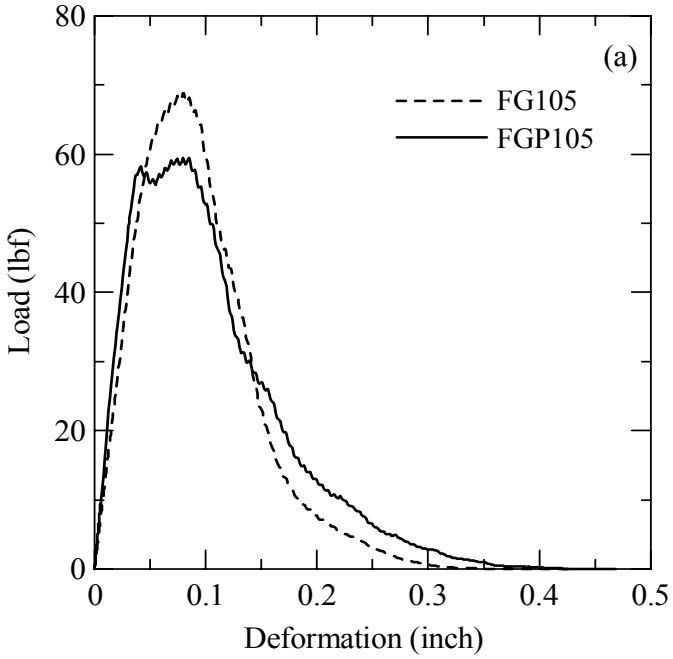

Fig. 2.13. Deformation vs. load for different processes (a) AR-glass with mix design 2 and embedded length 0.5” (b) AR-glass with mix design 1 and embedded length 0.5” (c) PP with mix design 1 and embedded length 0.3” (d) PP with mix design 1 and embedded length 0.5” (e) PVA with mix design 1 and embedded length 0.3”

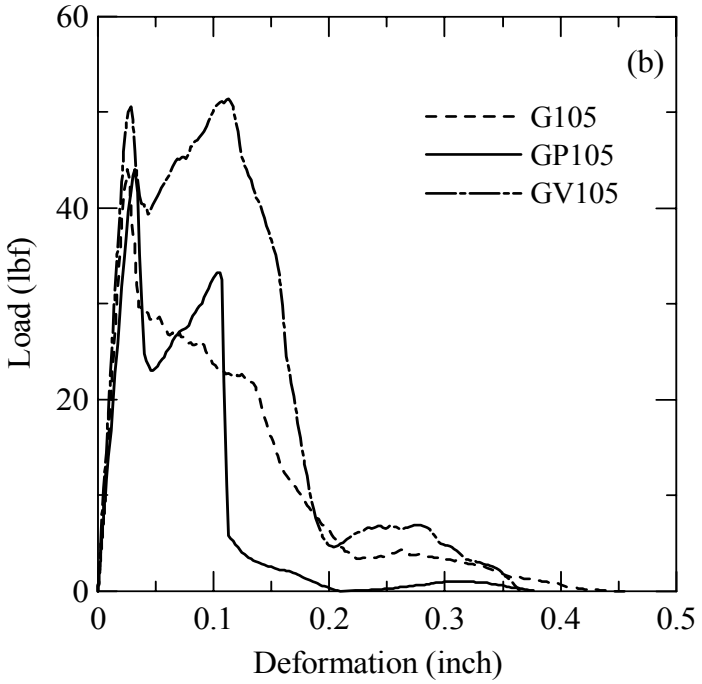

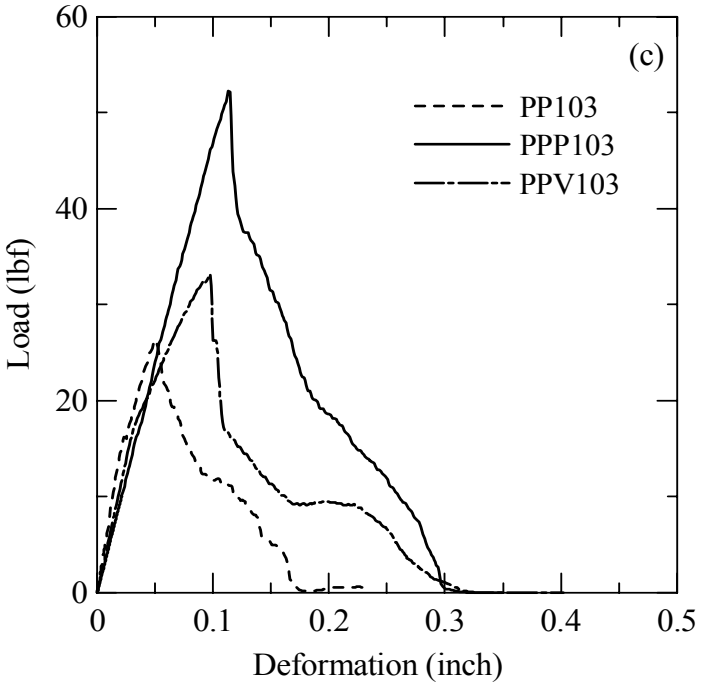

Fig. 2.13. Continued

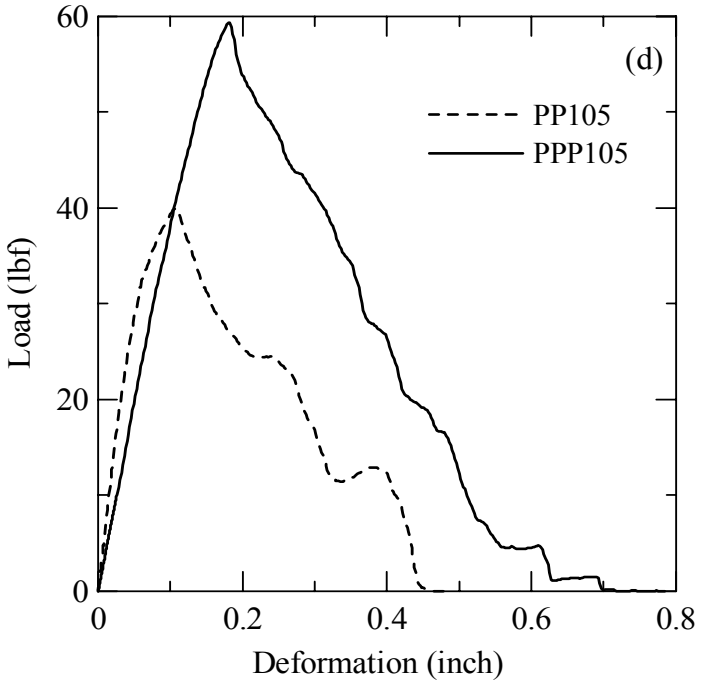

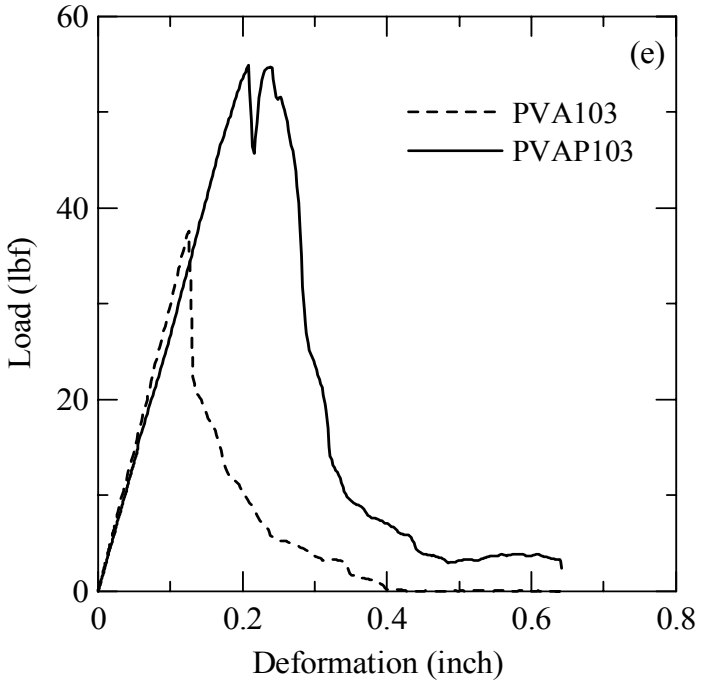

Fig. 2.13. Continued

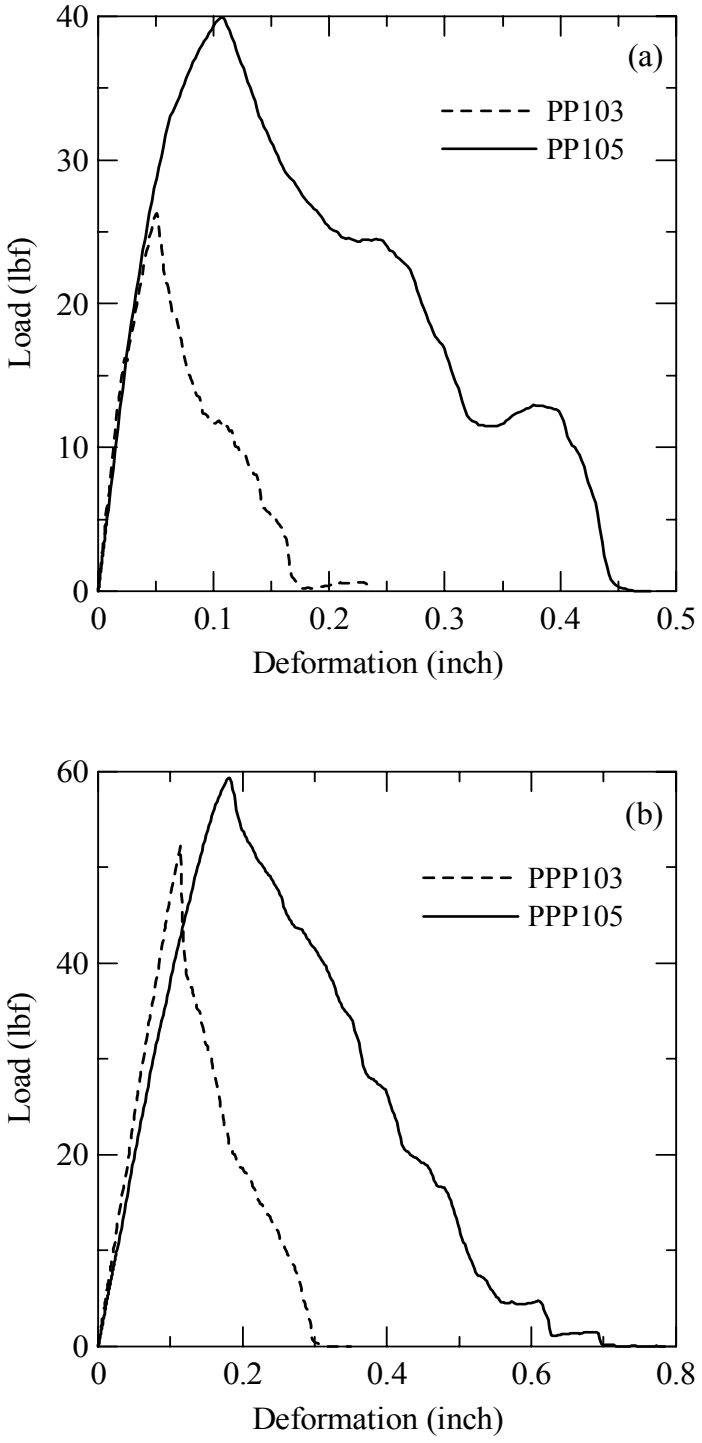

Fig. 2.14. Deformation vs. load for different embedded lengths (a) PP with cast procedure (b) PP with pultrusion procedure (c) PVA with pultrusion procedure

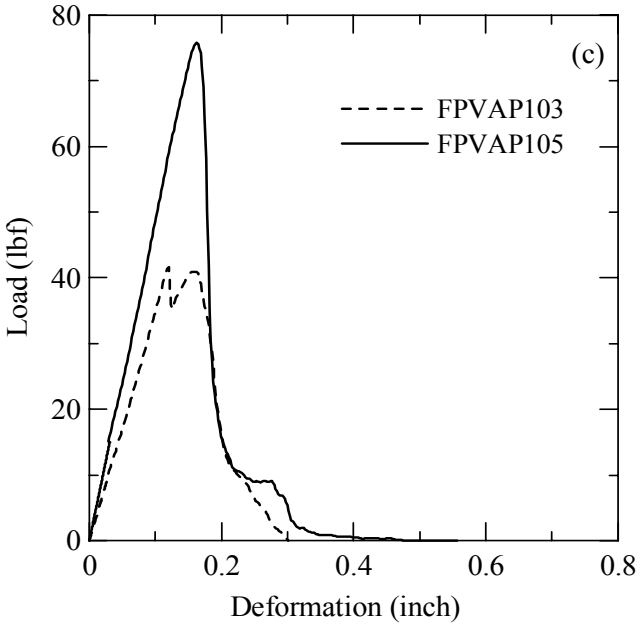

Fig. 2.14. Continued

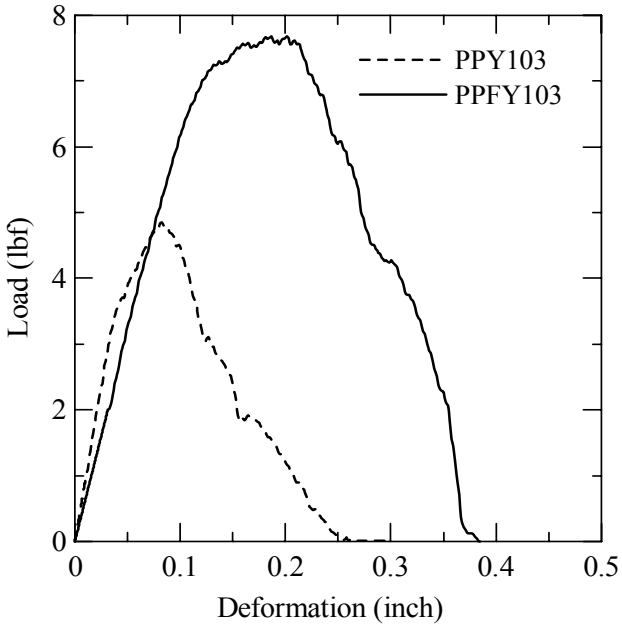

Fig. 2.15. Deformation vs. load for a yarn pullout (yarn embedded as woven or single yarn)

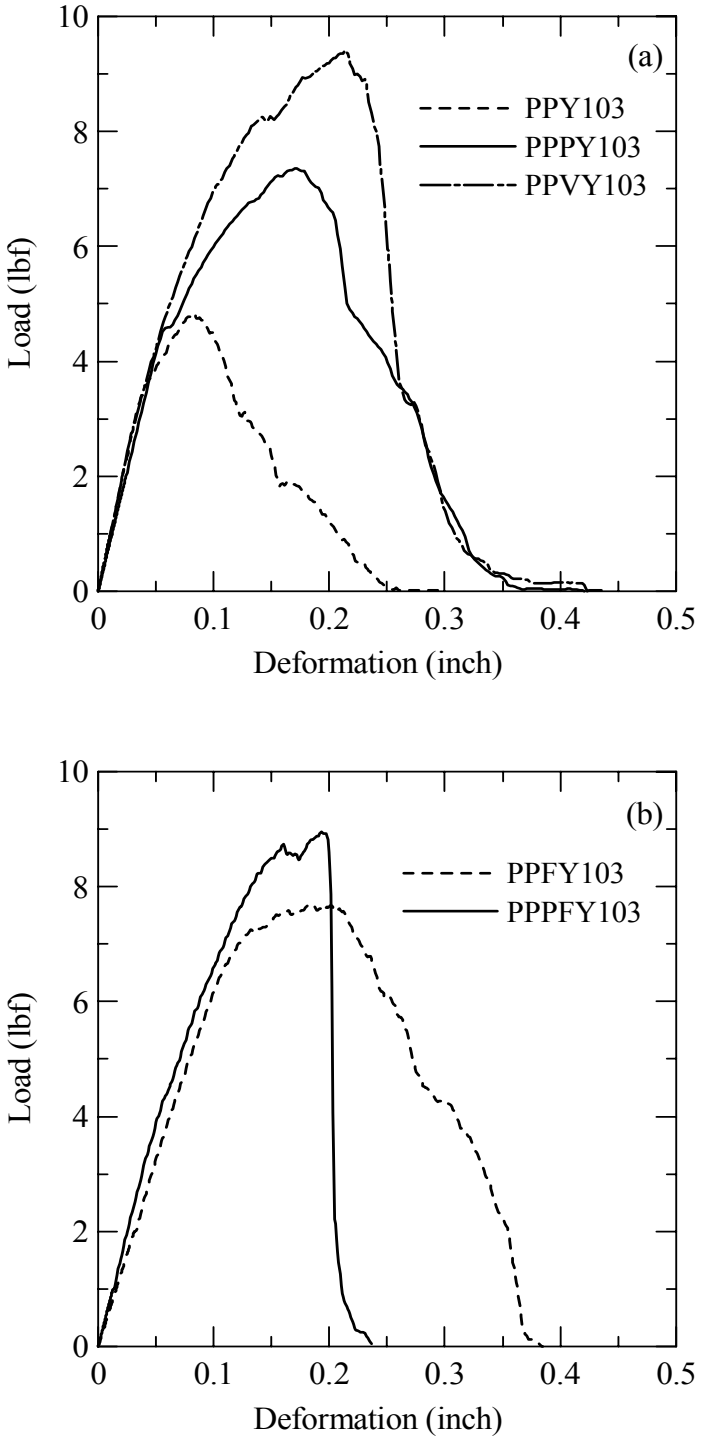

Fig. 2.16. Deformation vs. load for a yarn pullout with different procedures (a) Embedded as a yarn (b) Embedded as woven

2.2 Scanning Electron Microscope

2.2.1 Procedure

To understand the patterns of fiber debonding, and to study the surface on the specimens, the fracture surfaces of the tested specimens were examined using a scanning electron microscope. The JEOL SEM 840 scanning electron microscope was used to study the characteristic of fabric surface as well as the fabric matrix interface. Samples were conditioned in an oven at 80 degree Celsius for about one day to remove the moisture. They were then coated by gold film using a sputtering technique to make the surfaces conductive. The standard procedures for examining samples under scanning electron microscope were followed. All the observations were noted down.

2.2.2 Results

Figure 2.17 shows the surface topography of a groove where AR-glass fabric's yarn was pulled out. As it can be seen, samples with the use of pultrusion bath have a rougher surface compared to those manufactured with the cast procedure. The surface characteristics of a pulled out yarn is shown in figure 2.18. Yarns pulled from the matrix using pultrusion bath showed that the fibers had significant amount of cement attached around them. However, yarns pulled from the matrix with the cast procedure retained the polymer coating around them. Figure 2.19 represents the part of pulled out yarn where fill and warp yarns are attached (anchorage portion). The lower portion of the yarn as seen in the figure (bottom half of the yarn in figure 2.19) indicating that the coating at the anchorage zone has failed. This is possibly due to high strains at this level.

The groove left by the fabric in the matrix done with the cast procedure did not show as clearly as the groove made in the matrix of pultrusion procedure. This case is shown for the for PP fabric (Fig. 2.20). The yarn in the matrix did not get pulled out as shown in figure 2.21. The yarn in the matrix, in pultrusion bath, was covered with more cement than in cast procedure case as was the case in anchorage portion of yarn (Fig. 2.22). The surface of pulled out yarn from the matrix in cast procedure was much smoother than the one with pultrusion procedure and had less cement attached around it as shown in figure 2.23.

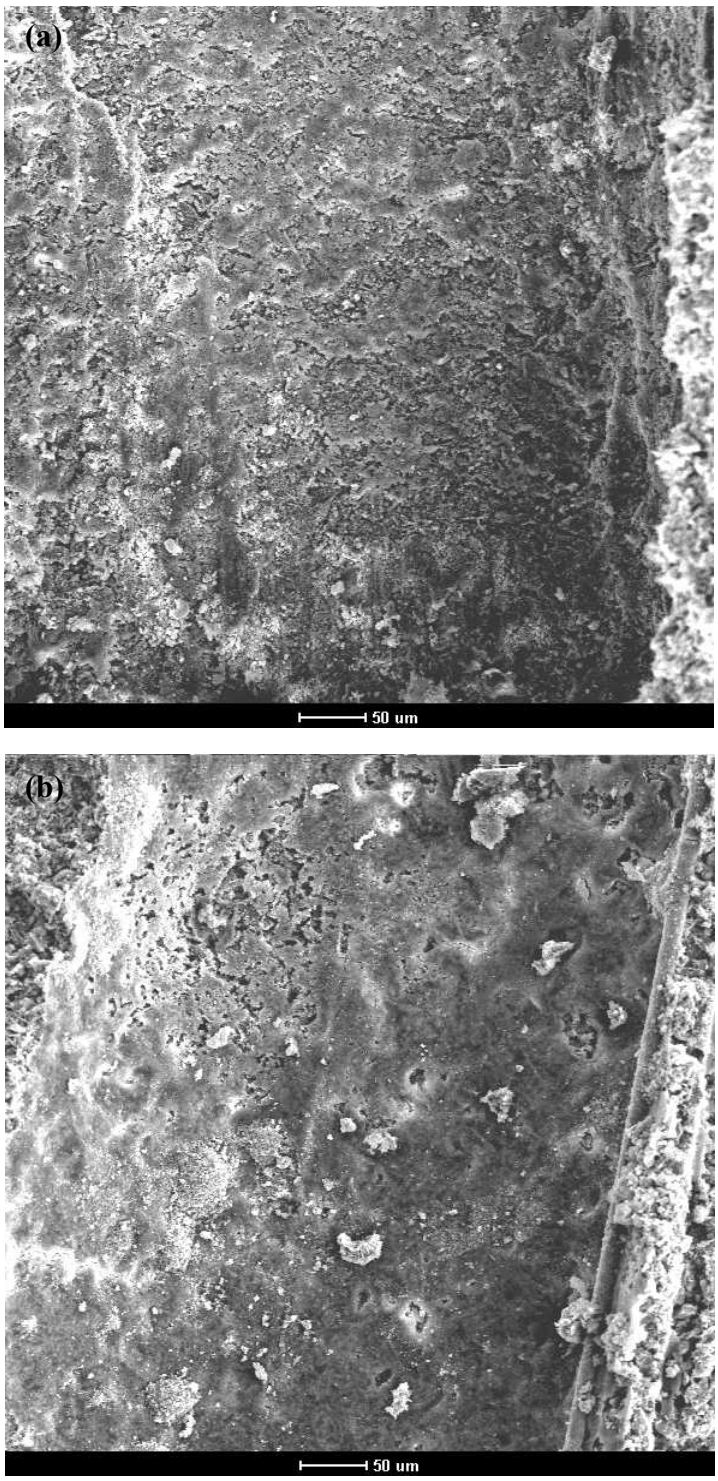

Fig. 2.17. AR-glass fiber groove near the free fiber (a) Cast procedure (x 200) (b) Pultrusion bath (x 200) (c) Cast procedure (x 1000) (d) Pultrusion bath (x 1000)

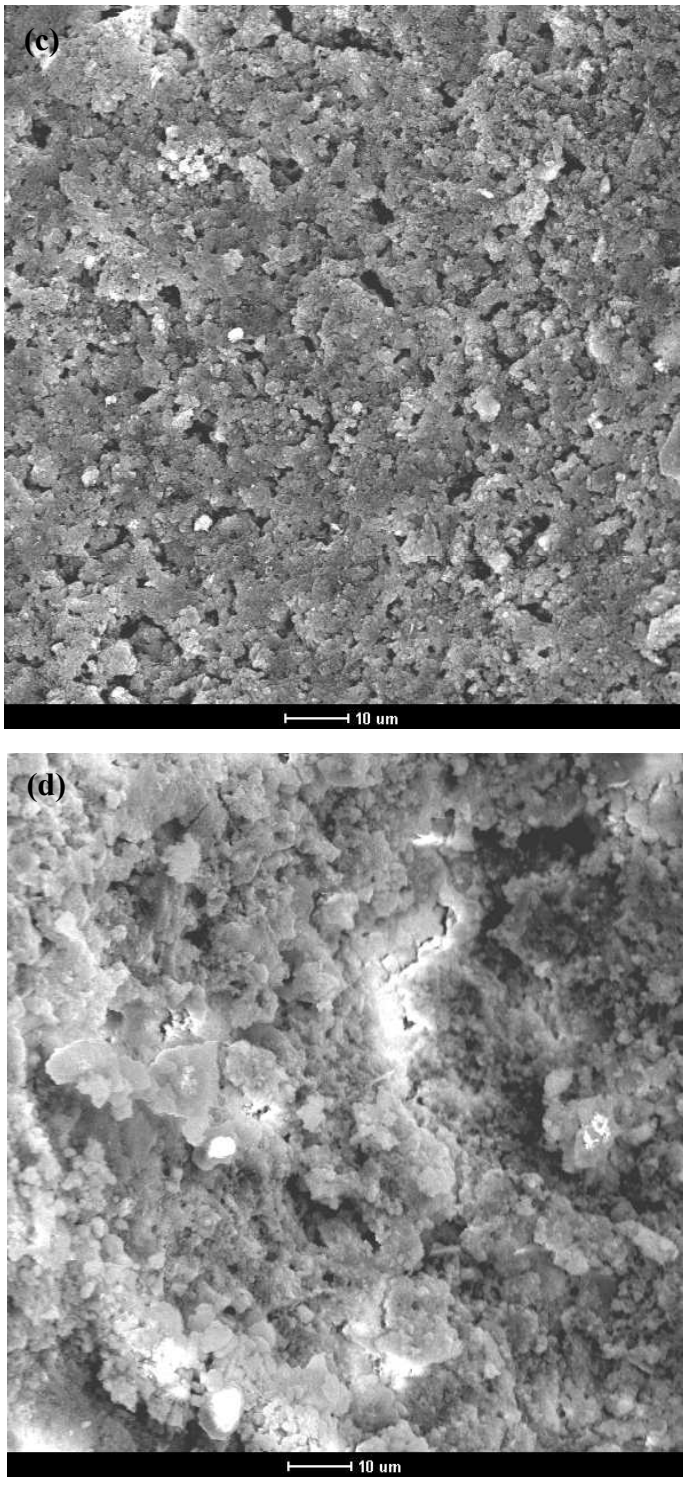

Fig. 2.17. Continued

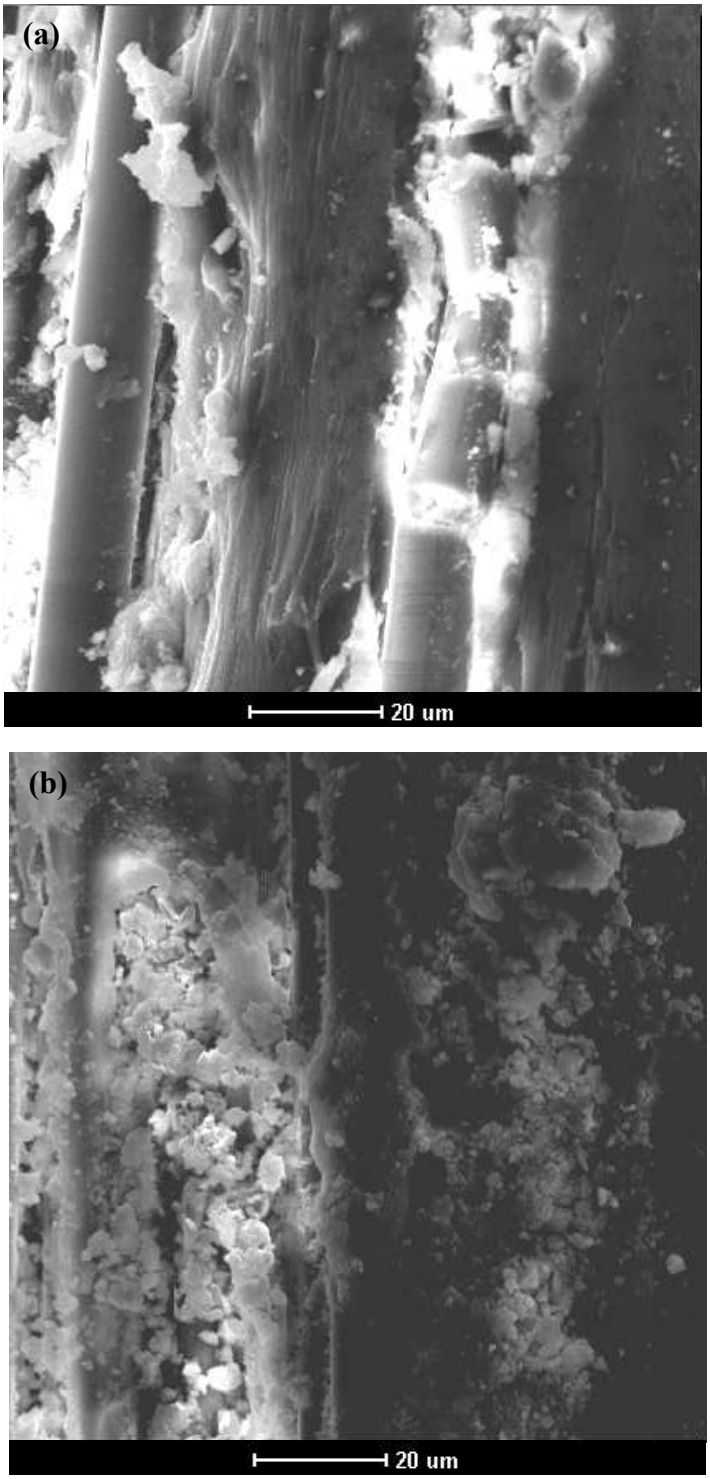

Fig. 2.18. Pulled out AR-glass fiber (x 1000) (a) Cast procedure (b) Pultrusion procedure

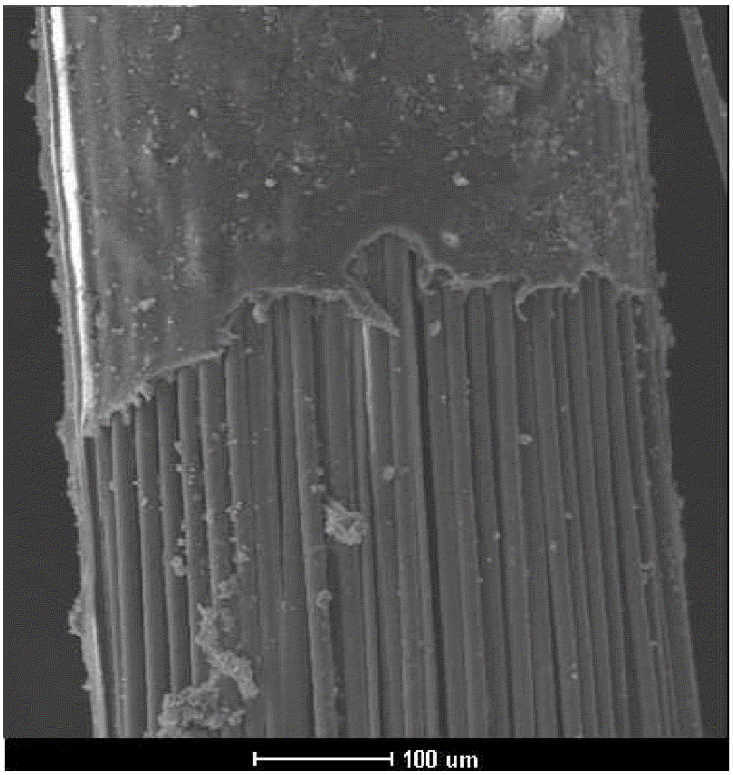

Fig. 2.19. Anchorage portion at pulled out AR-glass from cast procedure (x 200)

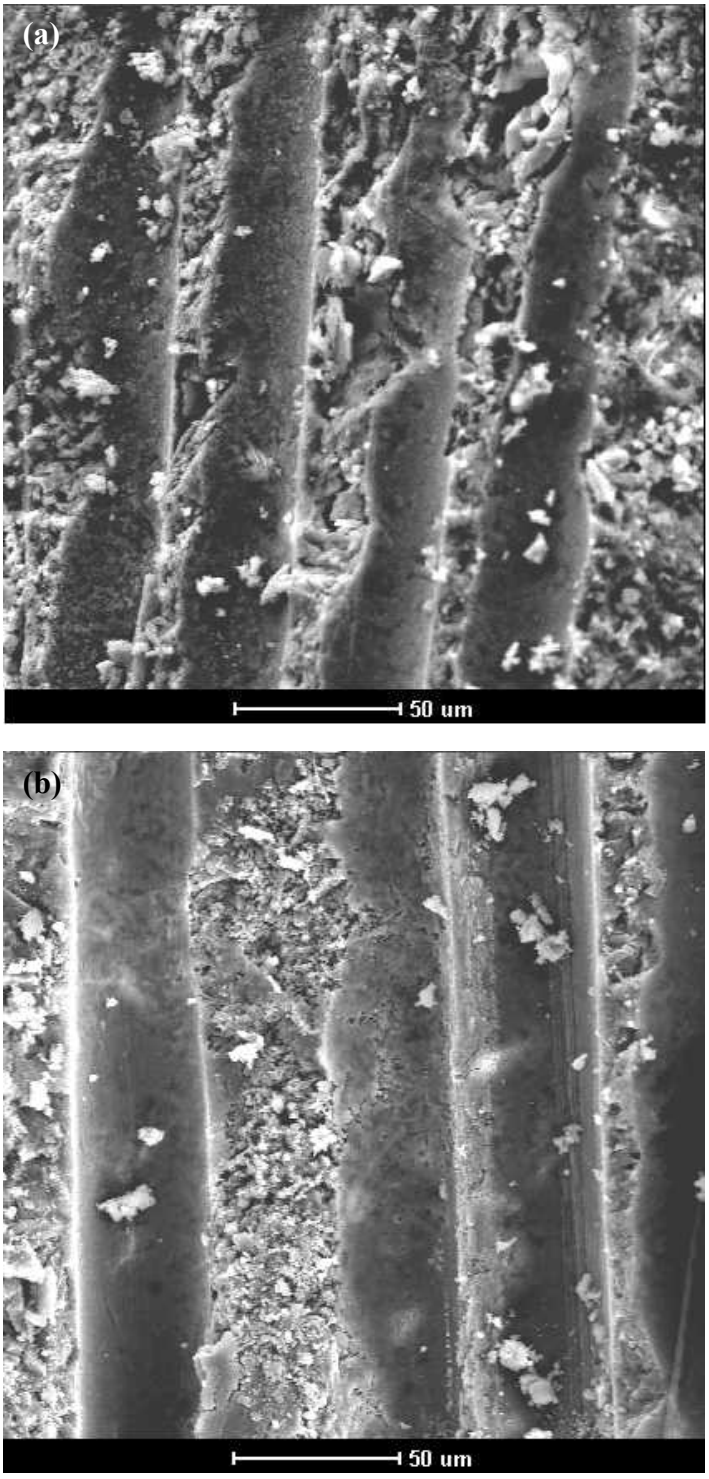

Fig. 2.20. PP fiber groove near the free fiber (x 500) (a) Cast procedure (b) Pultrusion procedure

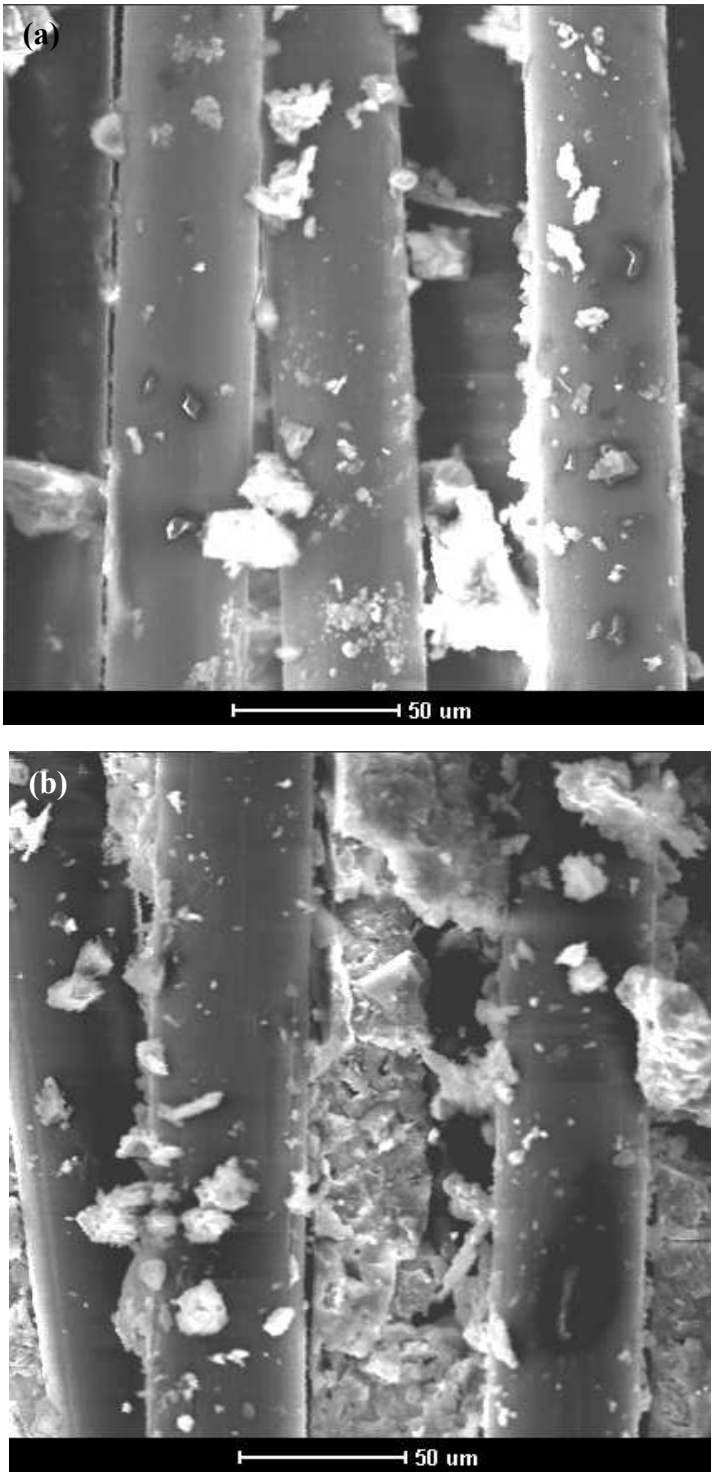

Fig. 2.21. PP fiber in matrix (x 500) (a) Cast procedure (b) Pultrusion procedure

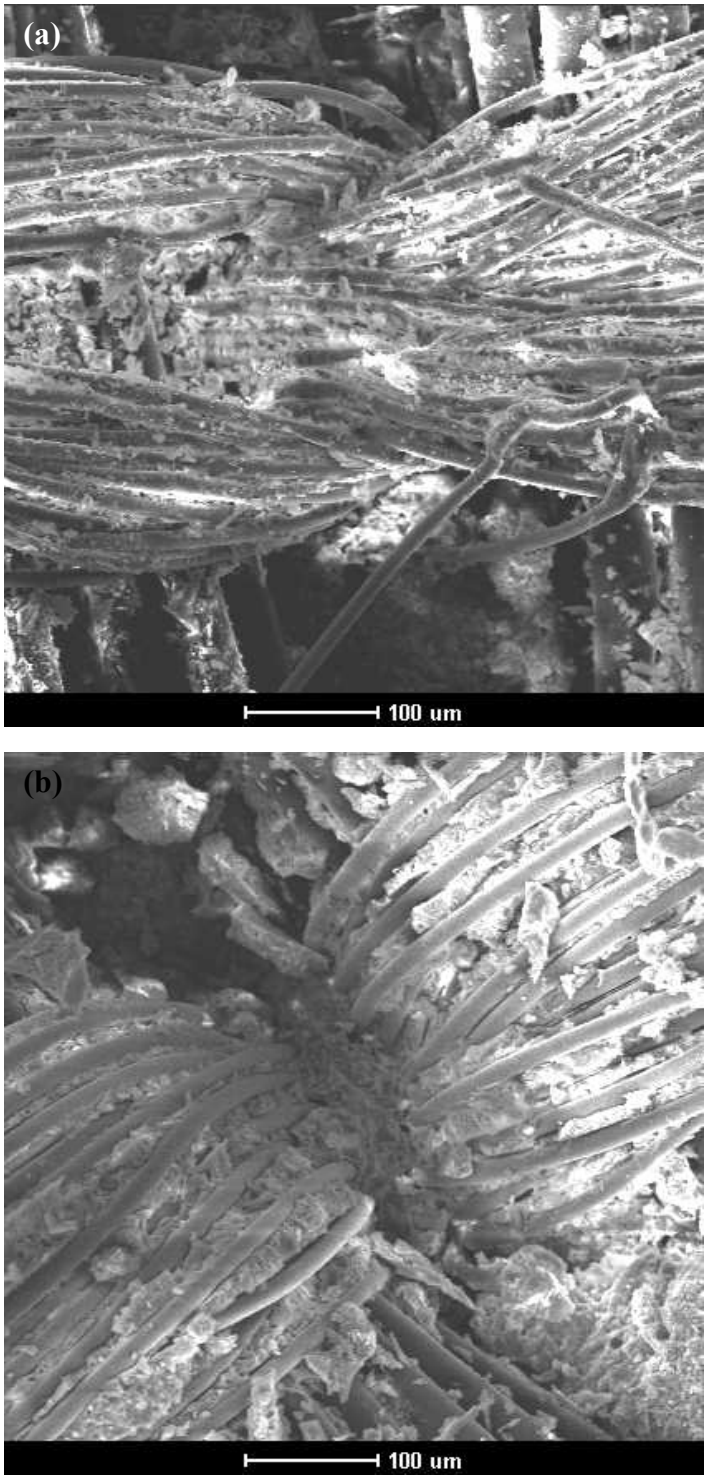

Fig. 2.22. PP Anchorage (x 200) (a) Cast procedure (b) Pultrusion procedure

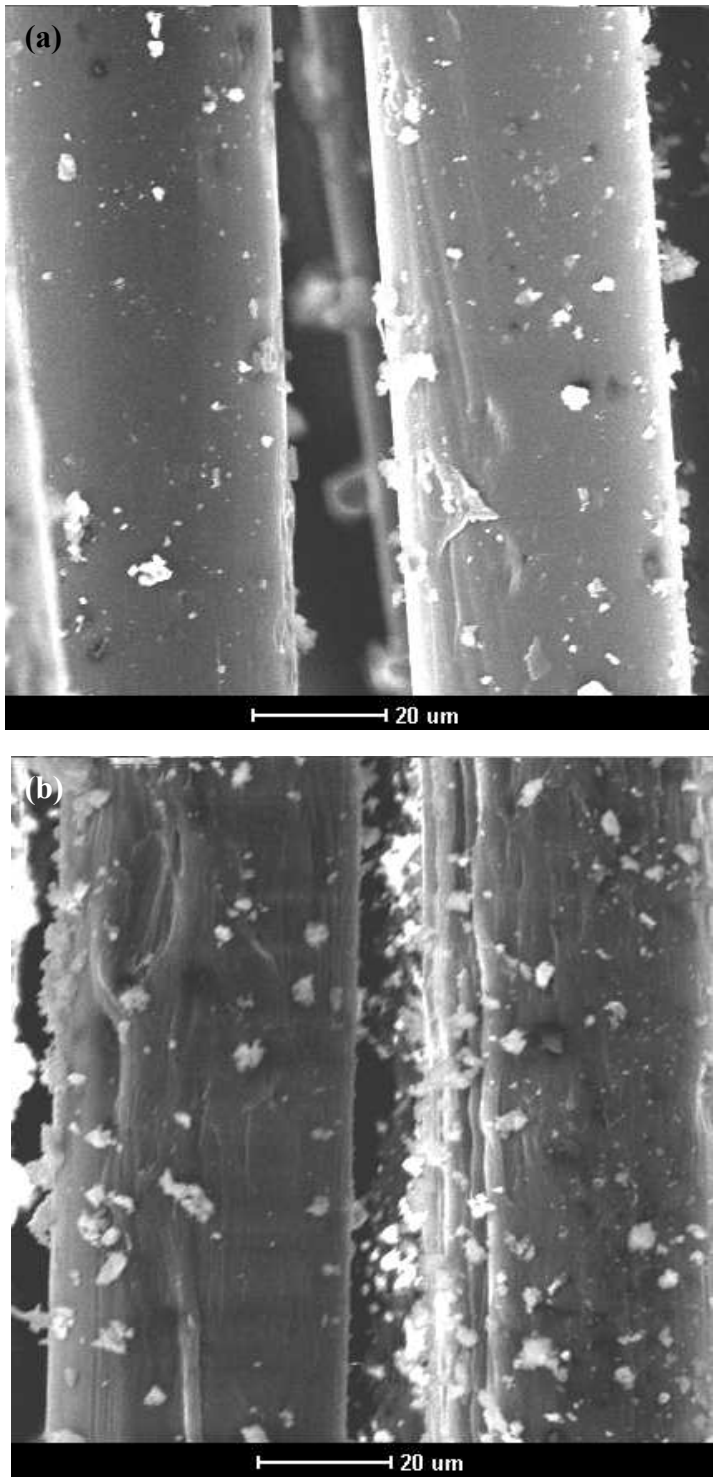

Fig. 2.23. Pulled out PP fiber (x 1000) (a) Cast procedure (b) Pultrusion procedure

2.3 Discussion

Experimental results showed that depending on the length of free fiber, stiffness changes and rate of change as a function of length is also affected by the type of fabric. This suggests that, one should be concerned in translating the results of pullout tests with free fibers to tensile tests without free fibers. However, we do think that this is possible with some modifications. The modification of pullout test results to tensile test is discussed in the following chapter.

Increase in embedded length increases the pullout load by increasing the surface area which experiences the frictional shear stress in the specimens. This explains the necessity of higher load to pullout the yarns whose embedded length is longer.

Changing the fabrication process affected the results and enabled us to compare between several possible situations. In the case of AR-glass fabrics which had the largest fabric opening, the results do not change much and use of vacuum shows the highest τ_{max}. In contract, in the case of PP (0.3" embedded length), difference is significant and use of pultrusion bath shows the highest τ_{max}. This is perhaps due to the tight knit nature of this fabric. In several cases, during the pullout test, we observed broken yarn or/and filaments which drew our attention to the nature of failure of the fabrics. For example, PP with pultrusion procedure with 0.3" embedded length does not have any broken yarn and show that the load increases significantly compared to the cast procedure case. However, AR-glass fabric case had many broken yarns for the specimens with pultrusion procedure. This might explain the significantly smaller maximum loads which would be interpreted as much smaller τ_{max} values. The case of PP fabric with pultrusion procedure

with embedded length of 0.3" did not have any broken yarns but 0.5" did have some broken yarns. As a result, specimens made under similar conditions, τ_{max} for 0.5" embedded length resulted smaller values even though maximum load was higher. However, from the SEM results, yarn in the matrix with pultrusion procedure had rough surface and had more cement attached in both, AR-glass and PP fibers. This explains that there was more friction caused in the matrix with pultrusion procedure and increase of friction might have resulted in broken yarns.

Peled and Mobasher (2003) studied the effect of addition of fly ash in the mix design and showed, addition of fly ash improves toughness and strength of the fabric reinforced concrete under tensile test. Our pullout test results showed that by adding fly ash τ_{max} can be increased. It means that fly ash does help in the improvement of interfacial shear bond as well as toughness and strength.

From the results of one yarn pullout test it was clear that pulling out a yarn from the matrix embedded as a yarn needs less load than woven conditions. This result agrees with the study of Peled et al. (1994). This, however, means pullout model needs to be modified to predict load and deformation for woven case.

CHAPTER 3

PULLOUT MODEL

Experimental results discussed in preceding chapter were verified by mathematical models of pullout. A modified shear lag approach is used to simulate the response of a fabric pullout from the matrix. The criterion for growth of the debonded fiber/matrix interface is expressed in terms of the interfacial stress, and three conditions of debonding, failure, and frictional pullout are modeled as a stress based approach. The model has been discussed in detail in this chapter and the simulated results are compared with experimentally obtained data from the pullout experiments. The model is comprised of two parts, the yarn condition and the woven condition.

3.1 Description of the model

3.1.1 Yarn Condition

The model used for predicting the pullout response for yarn condition has three stages.

a. first stage – bonded condition
b. second stage – bonded and debonded transition, and
c. third stage – frictional slip condition

In the first stage (bonded condition), it is assumed that the interface between the fabric and the matrix is perfectly bonded. In the second stage (bonded and debonded transition), debonding starts when the interfacial shear stress reaches the ultimate shear

stress τ_{max}. The shear stress over the debonded region is replaced by the frictional stress τ_f, which is assumed to be a linear function of the contact pressure p at the interface. As the load is increased, the debonding zone extends over the entire interface. The maximum load is achieved under partial debonding conditions. Once completely debonded, frictional forces are the only means of resisting the slip. In the final stage (slipping condition), the static frictional stress was replaced by a dynamic frictional stress, τ_d which was lower in magnitude. The load-slip relationship in this range is a linear descending model.

Gresczuk (1969), derived the relationship between fiber-matrix interfacial shear stress, τ, and embedded fiber length in a pullout test specimen as:

$$\tau(x) = \frac{P\alpha}{2\pi r}[sinh(\alpha x) - coth(\alpha L)cosh(\alpha x)] \tag{3.3}$$

where, $\alpha = \left(\frac{2G_i}{b_i r E_f}\right)$. In the above formula, P is the tension load applied on the fabric, r is the equivalent radius of the composite fabric, b_i is the effective width of the interface, E_f is the modulus of elasticity of filament in the fiber direction, G_i is the shear modulus of the interface layer at the interface, and L is the length of the embedded fabric in the matrix.

Mobasher et al. (2003) derived the displacement U between the interface layer and the fabric for a bonded condition by integrating the strain difference along the interface as

$$U = \frac{P(s^2 - c^2 + c)}{E_f \pi r^2 s\alpha} - \frac{P}{E_s \pi (r_s^2 - r^2)}[1 + \frac{c^2 - s^2 - c}{s\alpha}] \tag{3.4}$$

where, $s = \sinh(\alpha L)$, $c = \cosh(\alpha L)$, $r_s = b_i + r$ and E_s is the modulus of the interface layer.

Stang (1990) derived the fiber displacement for the condition of existence of both bonded and debonded zone (see figure 3.1) as

$$U(x) = \frac{P - \tau_f a}{E_f \pi r^2 \omega} \frac{\cosh(\omega x)}{\sinh\left[\omega(L - L_d)\right]}, \quad 0 \le x \le (L - L_d) \tag{3.5}$$

$$U(x) = \frac{P - \tau_f a}{E_f \pi r^2 \omega} \coth\left[\omega(L - L_d)\right] - \frac{P - \tau_f L}{E_f \pi r^2}(L - L_d) - \frac{\tau_f}{2E_f \pi r^2}(L - L_d)^2$$

$$+ \frac{P - \tau_f L}{E_f \pi r^2} x + \frac{\tau_f}{2E_f \pi r^2} x^2, \qquad (L - L_d) < x \le L \tag{3.6}$$

where, $\omega = \sqrt{\frac{G_i}{E_f \pi r^2}}$ and L_d is the length of debonding zone. In the case of the displacement at the fiber end $U(L)$ is give by

$$U(L) = \frac{P - \tau_f L_d}{E_f \pi r^2 \omega} \coth\left[\omega(L - L_d)\right] + \frac{P - \frac{1}{2}\tau_f L_d}{E_f \pi r^2} L_d \tag{3.7}$$

After debonding occurs, the debonding zone extends over the entire interface. As the load is increased τ reaches τ_{max} as expressed by the equation below

$$\tau = \left(P - \tau_f L_d\right) \omega \frac{\cosh(\omega x)}{\sinh\left[\omega(L - L_d)\right]}, \quad 0 \le x \le (L - L_d) \tag{3.8}$$

Once completely debonded, fiber starts pulling out by slipping. Pulling force is calculated by following equation:

$$P = 2\tau_d \pi r (L - L_p) \tag{3.9}$$

where, L_p is the length of pull out fiber. Using this P, deformation can be expressed as

$$U = U_0 + L_p + \frac{P}{E_f \pi r^2} L_p + \frac{P}{E_f \pi r^2} L_s - \frac{L_s^2 \tau_d}{E_f r} - \frac{r L_s^2 \tau_d}{E_s (r_s^2 - r^2)} \qquad (3.10)$$

where, U_0 is the deformation which occurred in stage 1, stage 2, L_p is the length of pull out fiber and L_s is the length of slipping fiber.

The flow chart of model is in figure 3.2. First, load is imposed. Then, interfacial shear force τ and deformation U are calculated using equation3.1 and 3.2. If τ exceeded τ_{max}, the second stage starts. Since specimen starts debonding, the debonding length L_d is imposed. Using equation 3.5 and 3.6, τ and U are calculated. If τ is over τ_{max}, L_d is increased incrementally and continue until L_d exceeds embedded length L. When all the embedded yarns are debondded, yarn starts pulling out. At this stage, pulling yarn L_p is imposed incrementally and load is calculated by equation 3.7 until yarn pulls out completely.

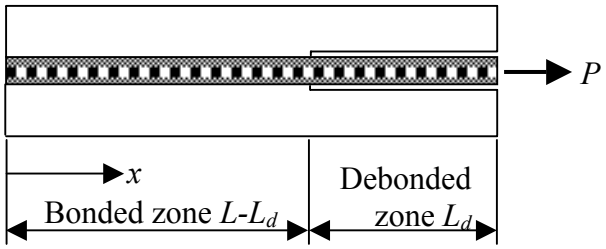

Fig. 3.1. Mathematical model at stage-2

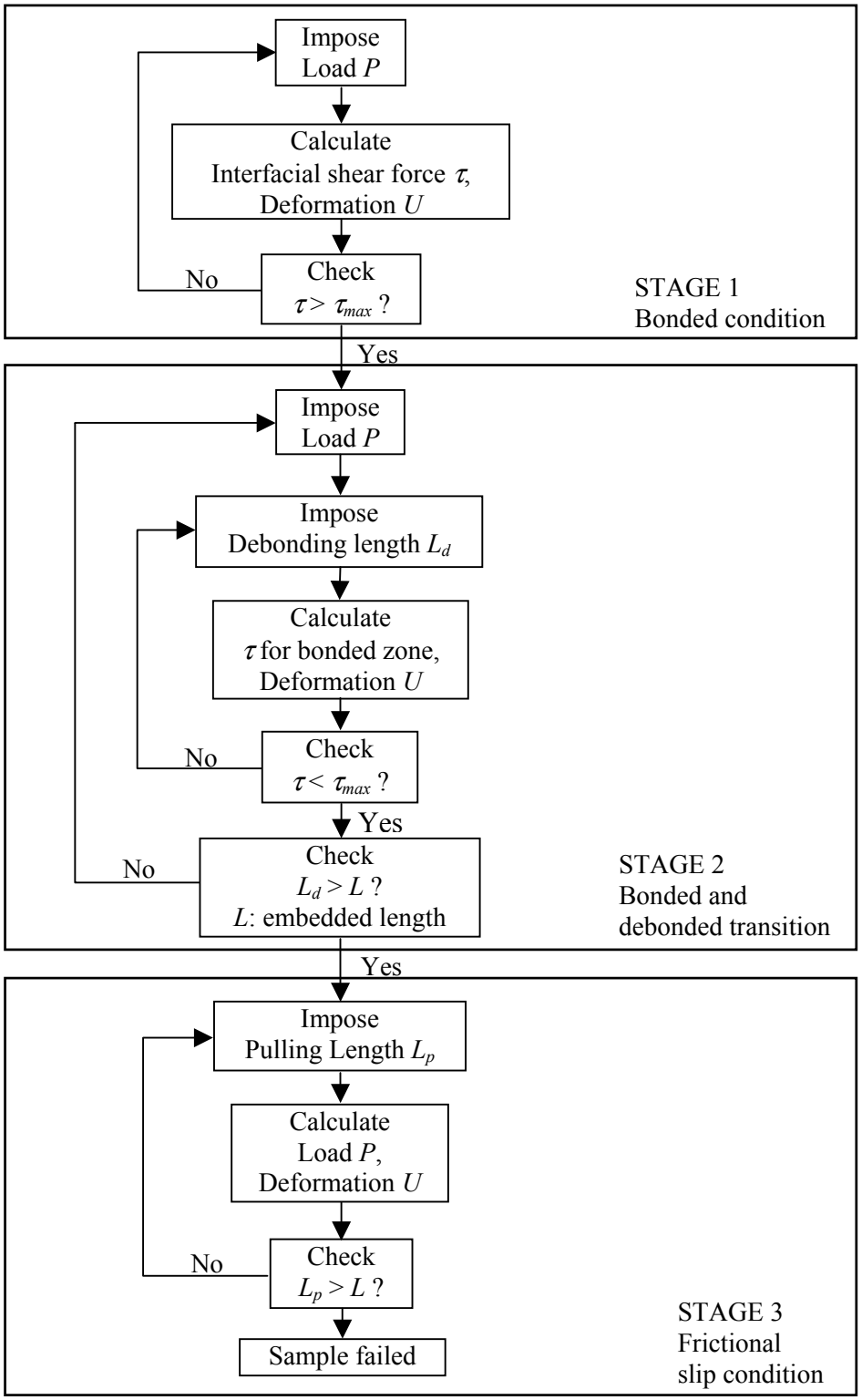

Fig. 3.2. Flowchart of yarn model

3.1.2 Woven Condition

In the case of woven or bonded fabrics, the main flow (three stages of the model) is same as that of yarn condition. However, the second stage has been modified to incorporate the additional load carrying capacity associated with the restraint due to the fill-yarns. It is expected that the mode of failure in these composites is governed by sequential stages of debonding and failure of anchoring points as the crack propagates from each junction of warp and fill to the next.

It is understood that during debonding the following sequence of events take place as the load increases:

a. Debonding along the length of yarn until a fill-warp junction is reached.
b. Load transfer to the fill yarn at the junction. In the woven fabrics this may be due to the curvature of the warp yarn causing additional anchorage. In the case of the bonded fabrics, this strength is due to the strength of the interface. In both cases, there is s certain degree of support offered by the fill yarn in carrying the load through bending.
c. Failure of the joint, followed by extension of the debonding to the next fill yarn.

The approach proposed here is to model the fill yarns as a beam on elastic foundation subjected to a concentrated load (Fig.3.3). The deflection at the middle for the condition can be expressed as

$$\delta = \frac{P\lambda}{2k}\frac{\cosh(\lambda l)+\cos(\lambda l)-2}{\sinh(\lambda l)+\sin(\lambda l)} \tag{3.11}$$

where, $\lambda = \sqrt[4]{\frac{k}{4EI}}$ and $k = bk_0$. k_0 is the modulus of foundation in lbs./in^3, b is the constant width of the beam in contact with the foundation and EI is the flexural rigidity of the beam. In the present approach, b is considered as thickness of yarn and I is calculated from fill-yarn geometry (Hetényi, 1983). k_0 and E are considered as the values related to matrix and fiber interface, respectively. The above equation can be rewritten as

$$P = \frac{2k\delta}{\lambda} \frac{\sinh(\lambda l) + \sin(\lambda l)}{\cosh(\lambda l) + \cos(\lambda l) - 2} \tag{3.12}$$

When length of debondding exceeds spacing of the fill yarns, P is calculated and added as the force needed to overcome the restraining of fill-yarns at the stage 2. However, anchorage can not exceed certain load condition. When load transferred through the anchorage zone exceeds the strength, anchorage fails, and debonding is allowed to extend to the next joint. The flowchart of stage 2 is in figure 3.4.

The strength of anchorage was obtained experimentally. Figure 3.5 was obtained by pulling out the yarn whose sides were clipped as seen in the figure 3.6. The strength

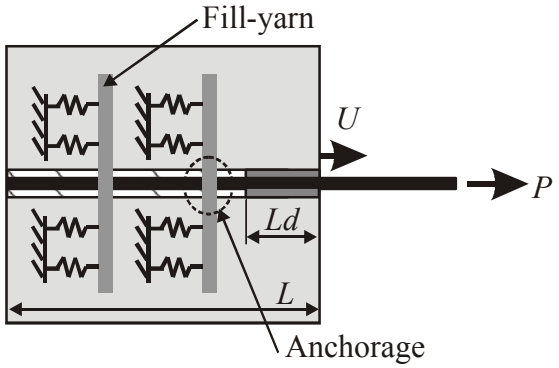

Fig. 3.3. Mathematical model for woven condition

of anchorage has been indicated in the figure 3.5. Experiments were conducted using similar equipment as for the pullout test. However, the bottom grip was changed to grip the plate as shown in figure 3.7.

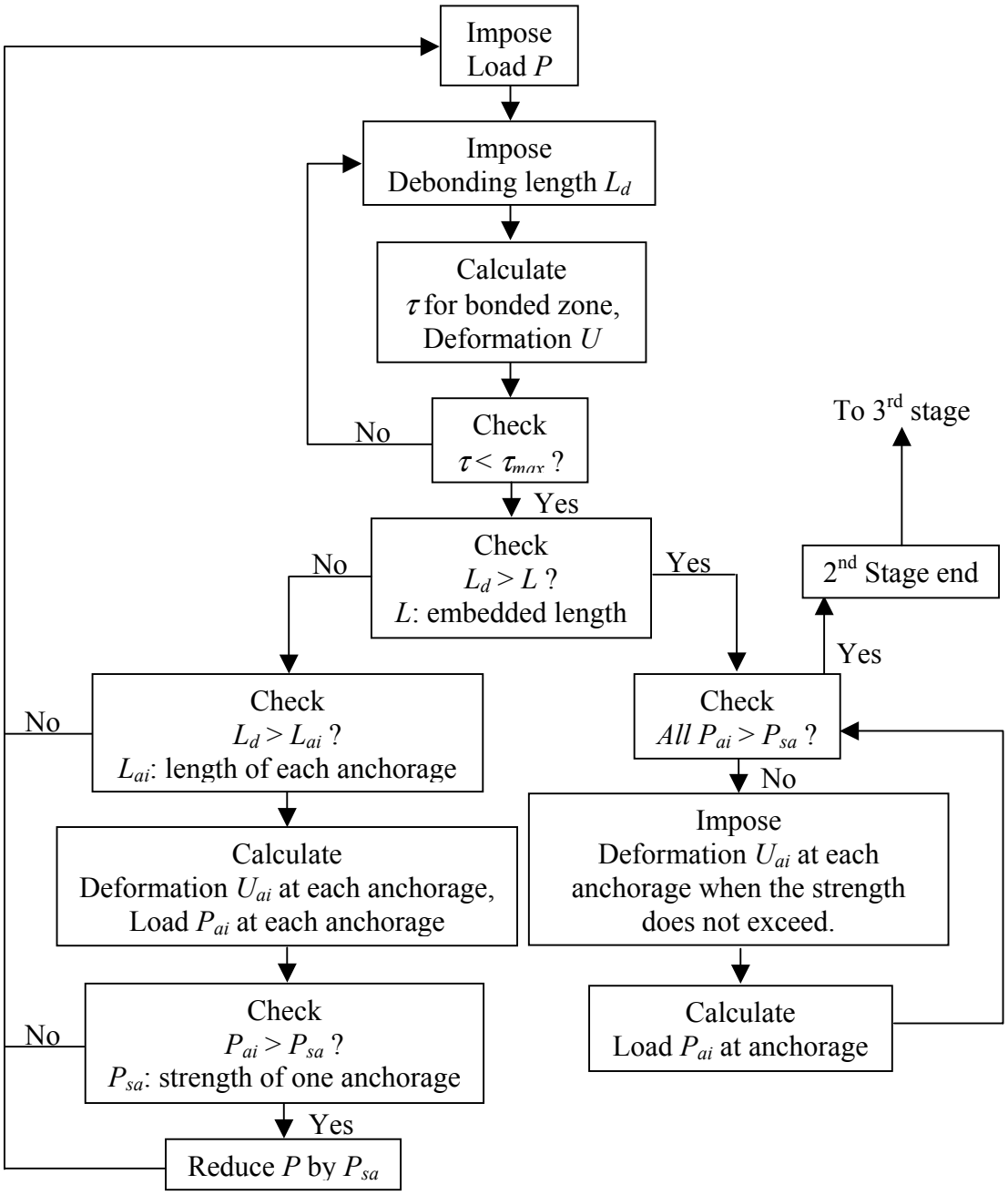

Fig. 3.4. Flowchart of woven model at stage-2

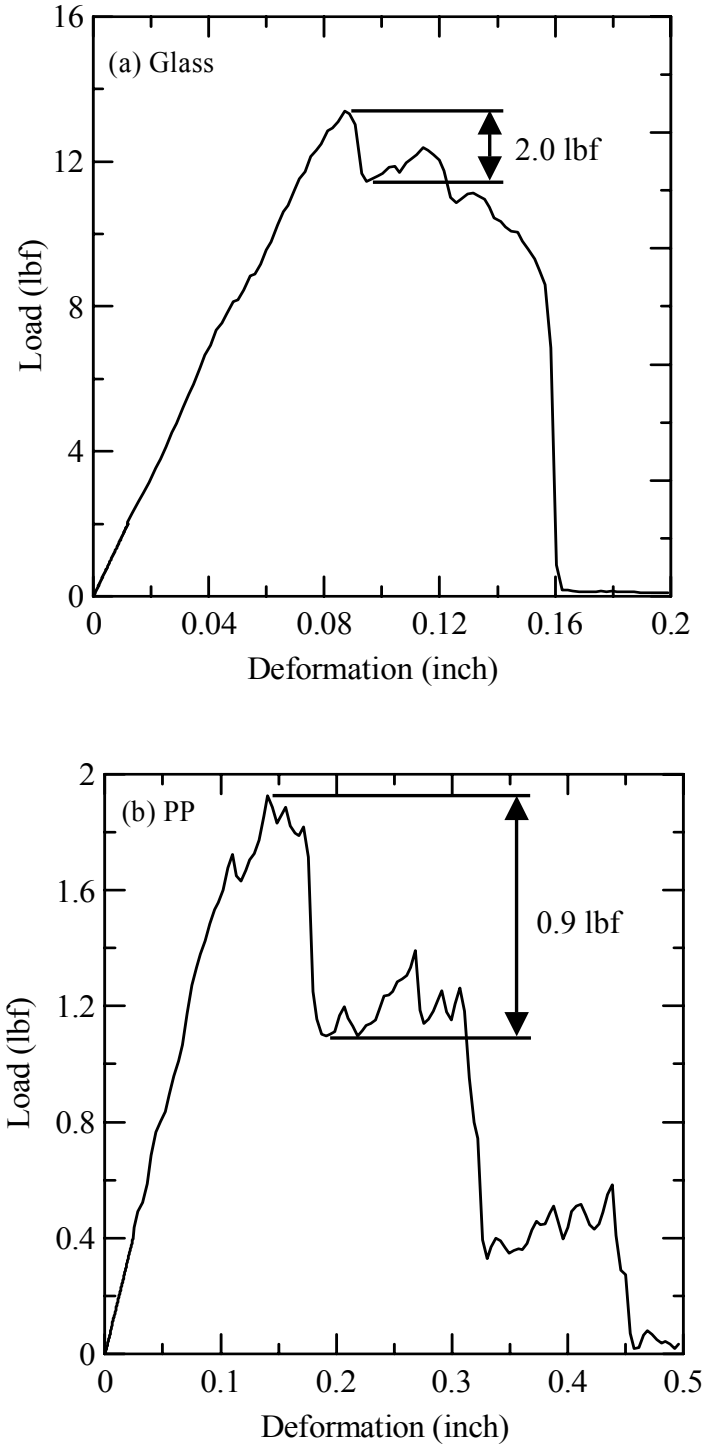

Fig. 3.5. Strength of anchorage (a) AR-glass (b) PP

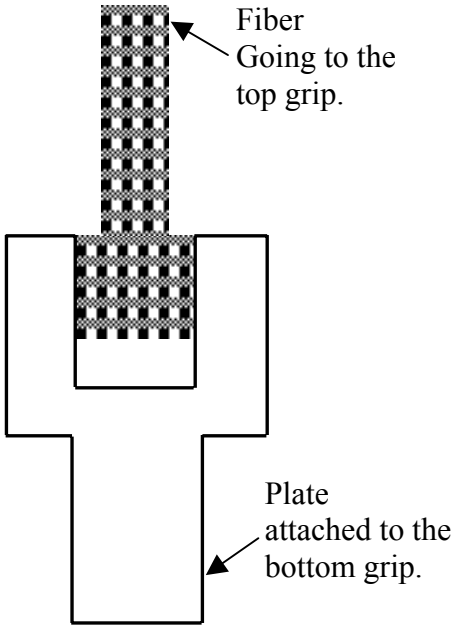

Fig. 3.6. Schematic drawing of specimen

Fig. 3.7. Setup for pullout test

3.2 Modification of Experimental Results

Before comparing the experiment results with calculated results from the models, experimental results were modified to correct for the stiffness of the free length of the fabrics. This modification is due to the consideration of geometrical difference between pullout and tensile tests. The samples for pullout test have free fiber portions that do not exist in tensile samples. However, the length of free fiber affects the results of pullout test as shown in chapter 2. Proper accounting for this difference is necessary to extend the pullout to tensile results.

To modify the results of pullout test, the following steps have been applied. First, the fiber length versus the slope of deformation-load, $1/K$, was plotted as shown in figure 3.8 and trend line was obtained. Using the slope of the trend line, $1/K_l$, the intercept of the curve was obtained and considered as the stiffness of the fabric with a zero free length condition by the following equation,

$$d_2 = d - P\frac{l_f}{K_l} \tag{3.13}$$

where, d_2 is the displacement for zero free fiber length, d and P are the displacement and load from the experimental results respectively and l_f is the free fiber length used for the experiment.

Derivation of this equation is provided below. A Pullout sample has two parts, free fiber and matrix which have different stiffness K_1 and K_2 and deformations d_1 and d_2, respectively. This condition is expressed by the generalized stiffness formulation as:

$$P = K_1 d_1 \qquad d_1 = \frac{P}{K_1} \tag{3.14}$$

$$P = K_2 d_2 \qquad d_2 = \frac{P}{K_2} \tag{3.15}$$

where, K_1 and d_1 differ depending on the length of free fiber. The relationship between K_1 and free fiber length is obtained experimentally as the slope, $1/K_l$. The plot of $1/K$ as the function of free fiber length as shown in figure 3.8. If free fiber length is l_f, then $1/K_1$ can be expressed as

$$\frac{1}{K_1} = \frac{l_f}{K_l} \tag{3.16}$$

Let summation of deformation, d_1 and d_2, equal to d which is the obtained from the experiment. d_2 is the deformation of no free fiber condition. Since $1/K_l$ can be obtained experimentally by taking different free fiber lengths, d_1 can be obtained by calculation. Therefore, d_2 is expressed as

$$d_2 = d - d_1 = d - P\frac{l_f}{K_l} \tag{3.17}$$

$1/K_l$ for glass, PP and PE are obtained using the experimental results as shown in Figure 3.1. $1/K_l$ for glass, PP and PE are 1.118e-5 lbf^{-1}, 8.986e-4 lbf^{-1} and 1.211e-2 lbf^{-1}, respectively. Using these values, each free fiber length (1, 2 and 3 inches) for each fabric is modified to reflect the zero free fiber length. As seen in figure 2.10 in Chapter 2, different free fiber lengths returned different stiffness values. However, by modifying the results, the different stiffness values could be modified as that from the free fiber length at zero (figure 3.9), indicating that the stiffness values are relatively the same for these specimens.

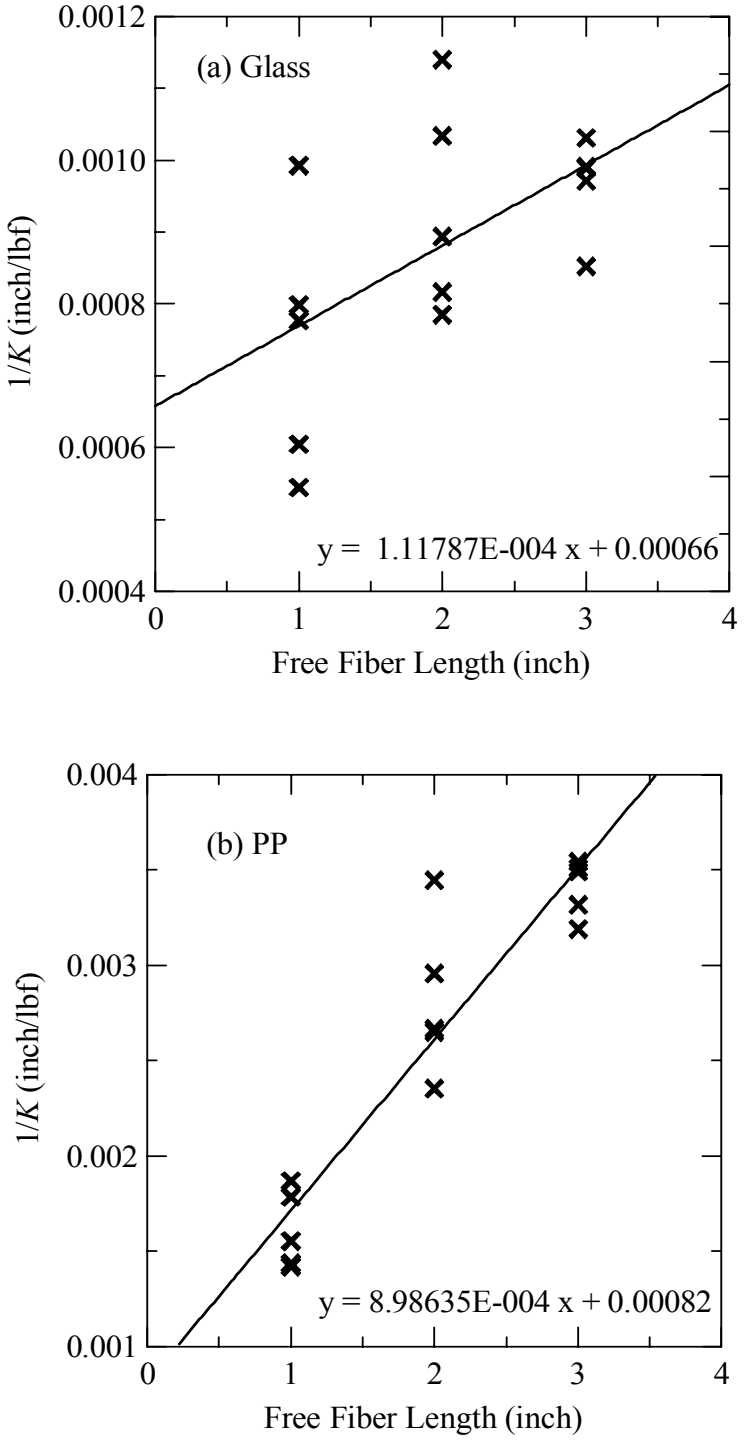

Fig. 3.8. Free fiber length vs. 1/*K* (a) AR-glass (slope: 1.118e-4 lbf^{-1}) (b) PP (slope: 8.986e-4 lbf^{-1}) (c) PE (slope: 1.211e-2 lbf^{-1})

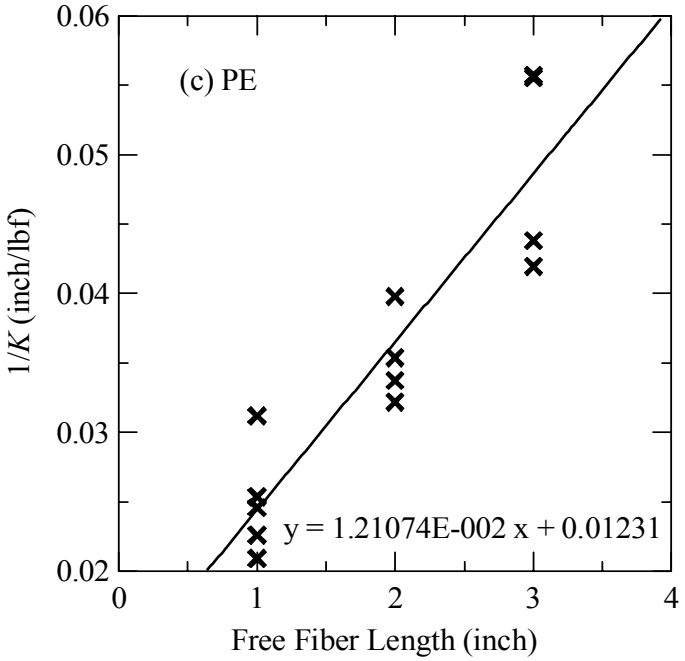

Fig. 3.8. Continued

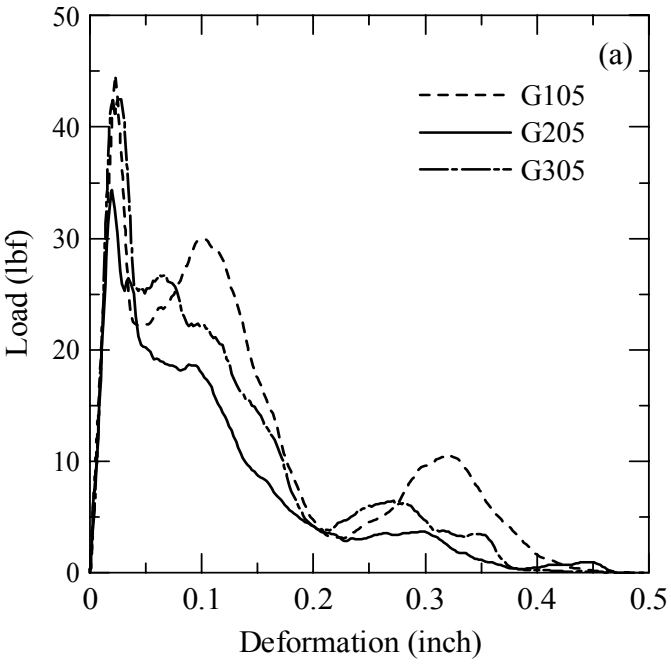

Fig. 3.9. Modified deformation vs. load (a) AR-glass (b) PP (c) PE

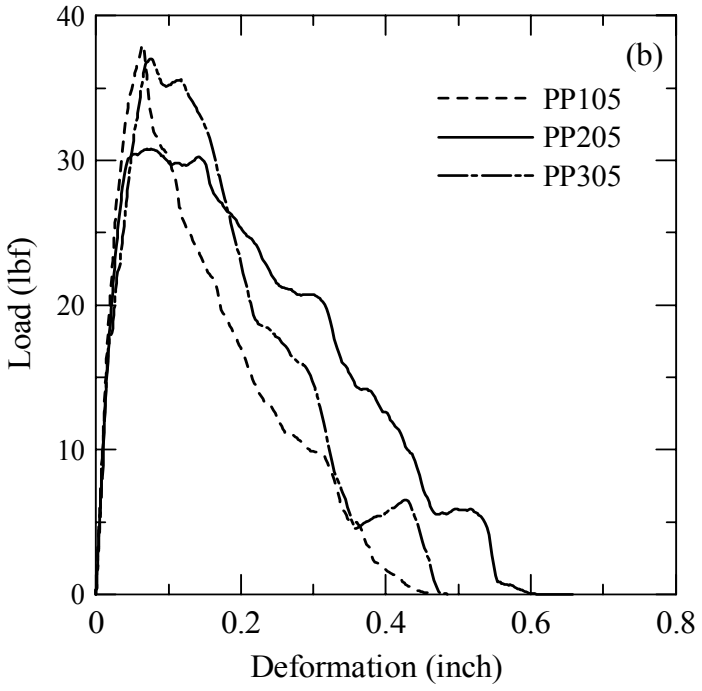

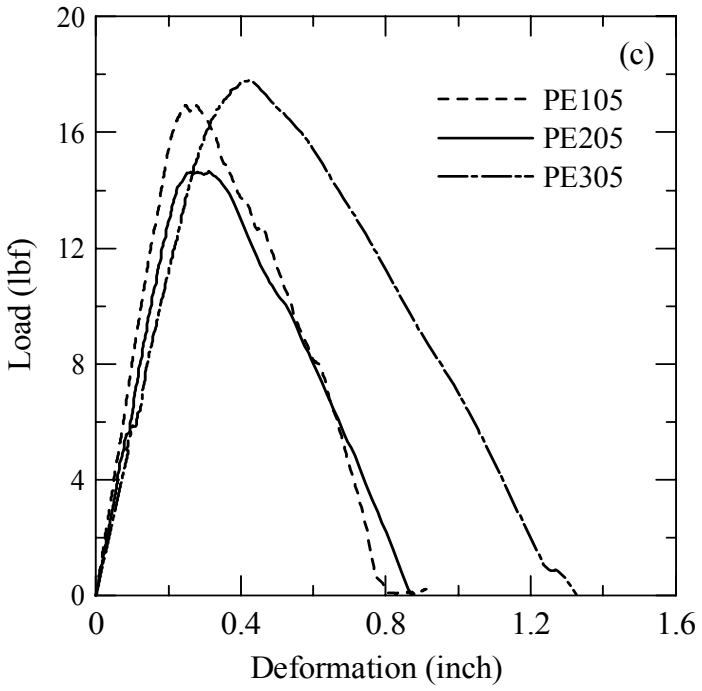

Fig. 3.9. Continued

3. 3 Results

The geometrical values used to calculate the load and deformation are given in table 3.1 and 3.2. The values in table 3.2 were obtained by curve fitting the calculation results with experimental results except for the strength for anchorage. Strength of the anchorage zone is obtained by using the experimental results as described in section 3.2 and shown in figure 3.5. The value for τ_{max} was obtained from the experimental results by dividing the maximum force by the nominal area in shear and is given in table 2.4. Figure 3.10 is comparison of experimental and mathematical results for glass, PP and PE fabrics. Figure 3.10 shows two mathematical results obtained from yarn and woven models. As clearly seen in the figure, model for a yarn predicted less pullout load than

Table 3.1

Geometry of Fabrics

Fabric	Height of Fill Yarn (inch)	Thickness of Fill Yarn (inch)	Distance between Yarns (inch)	Number of Fill Yarn per 1 inch
Glass	0.070	0.014	0.150	5
PE	0.010	0.014	0.010	16
PP	0.015	0.010	0.015	7

Table 3.2

Values for Mathematical Calculation

Fabric	E for Matrix (MPa)	E for Fiber (MPa)	E for Beam (MPa)	E for Foundation (N/m^3)	Strength for Anchorage (N)
Glass	4000	78600x0.04	2000	4000	9
PE		1760x0.1	0.1		1
PP		6900x0.2	3.5		4

woven fibers. The yarn model calculated the maximum load of nearly 30 lbf for glass fabric compared to the woven model, 45 lbf, that was nearly identical with the experimental results. Similarly, for PP fabric, the yarn model calculated approximately 20 lbf of maximum load and the woven model was more than 35 lbf. For PE fabric, the yarn model calculated ≈ 14 lbf and the woven model calculated ≈ 17 lbf.

Based on these results, we were able to find the parameters for beam on elastic foundation presented in table 3.2. Using these values, the sensitivity of the model to the embedded length was studied as seen in figure 3.11. PP fabric with normal procedure showed high sensitivity of fiber embedded length but PP fabric with pultrusion bath predicted less than the experimental result (by ≈ 10 lbf). Since there were some differences in τ_{max} between 0.3" and 0.5" embedded length for PP with pultrusion bath as seen in table 2.4, using the experimental result of τ_{max}, the load and deformation were calculated (Figure 3.12). The result showed that the use of experimental result of τ_{max} (= 2.91) improved the maximum load to nearly 50 lbf that was nearly identical with the experimental result.

To get the effects of different procedures, based on the normal condition, pultrusion bath procedure was calculated by changing τ_{max} obtained from the experiment. These results returned much smaller values than experimental results as see in figure 3.13. For PP with both 0.3" and 0.5" embedded lengths, the maximum load obtained was nearly 15 lbf less than the experimental result. To fit the calculation results with the experimental results, strength of anchorage was changed since this was the most sensitive parameter in increasing the load. In figure 3.14, the calculation results could fit with the

experimental data by increasing the strength of anchorage from 0.9 lbf (4 N) to 1.6 lbf (7 N). Figure 3.15 shows the data for PP with the vacuum and the strength of anchorage was increased from 0.9 lbf (4 N) to 1.2 lbf (5.5 N). When 0.9 lbf was used, the calculated maximum load was ≈ 27 lbf that nearly 5 lbf less than the experimental result.

Figures 3.15 and 3.16 are for glass fabric case. In the case of glass fabrics, mathematical calculation and experimental results fitted well without changing the strength of anchorage. The different results obtained by changing the mix design in the experiments were also simulated well by the models using the appropriate τ_{max} as seen in figure 3.16.

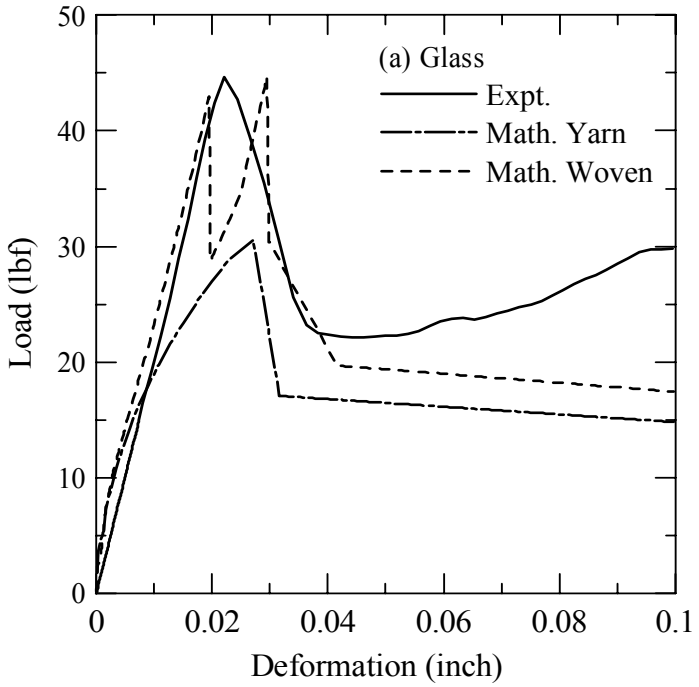

Fig. 3.10. Comparison of experimental and mathematical results (a) AR-glass (b) PP (c) PE (Expt. - experimental results, Math. Yarn - mathematically simulated result using one yarn concept, Math. Woven - mathematically simulated using woven concept)

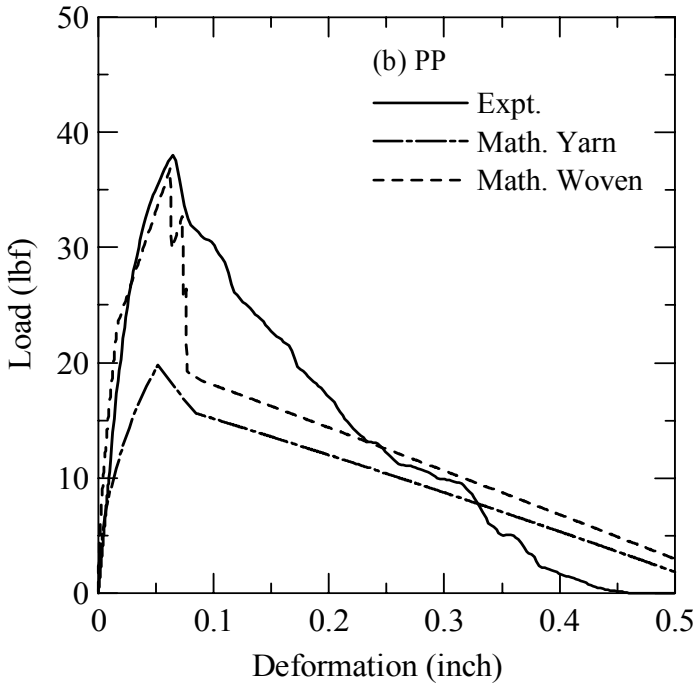

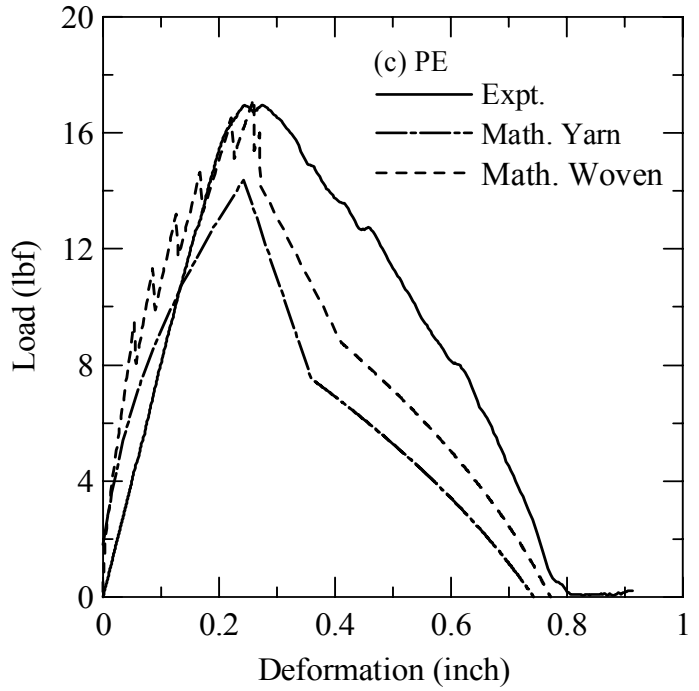

Fig. 3.10. Continued

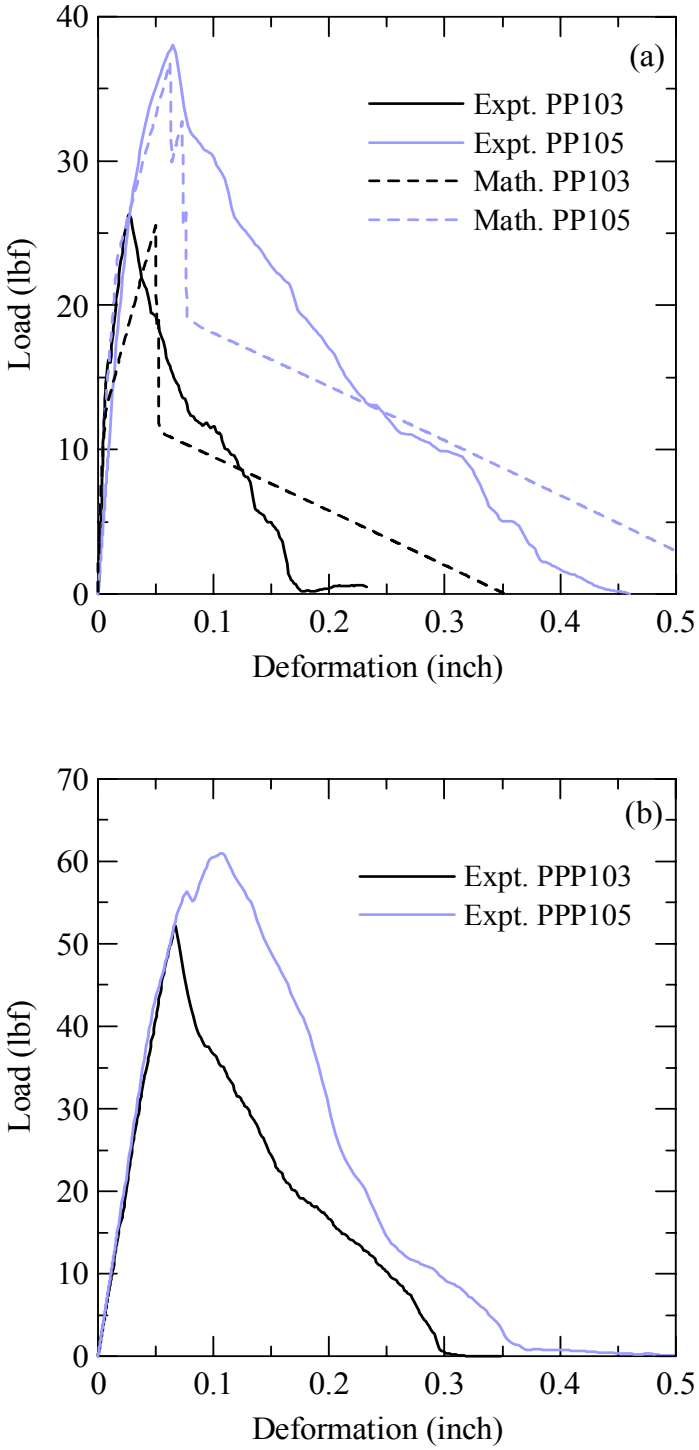

Fig. 3.11. Sensitivity of the woven model for embedded length (a) PP with cast procedure (b) PP with pultrusion procedure

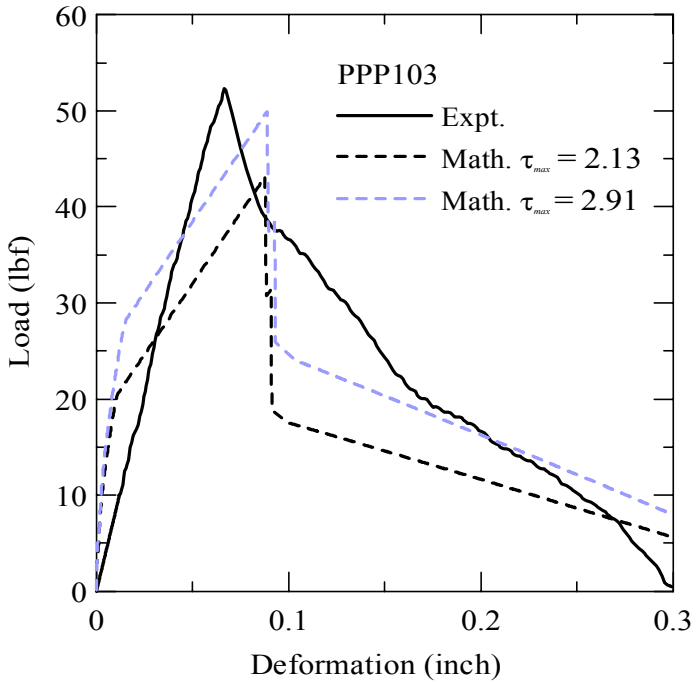

Fig. 3.12. Using experimentally obtained τ_{max} for mathematical calculation (experimental results: PPP103 - $\tau_{max} = 2.91$, PPP105 - $\tau_{max} = 2.13$)

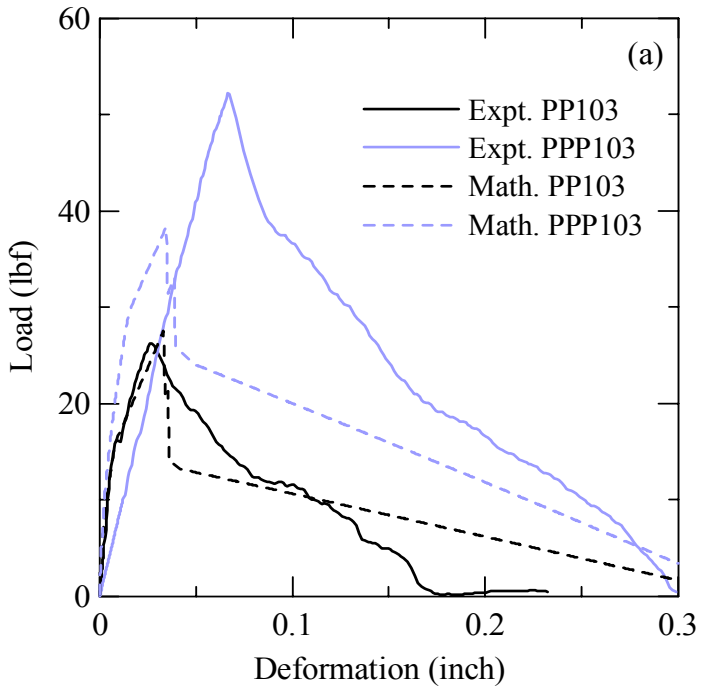

Fig. 3.13. Effect of different procedures for PP (a) Pultrusion bath, embedded length – 0.3”, E (beam) – 5.5 MPa (b) Pultrusion bath, embedded length – 0.5” (c) Vacuum, embedded length – 0.5”

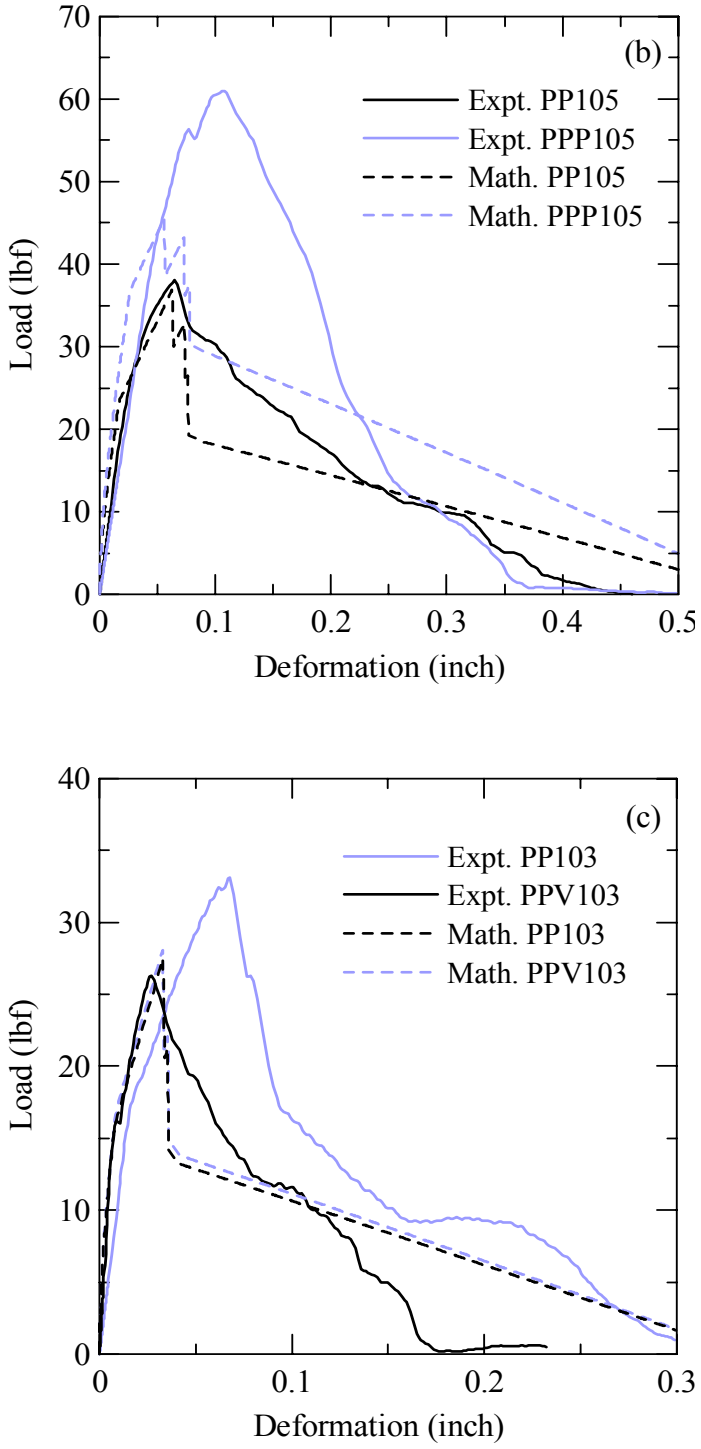

Fig. 3.13. Continued

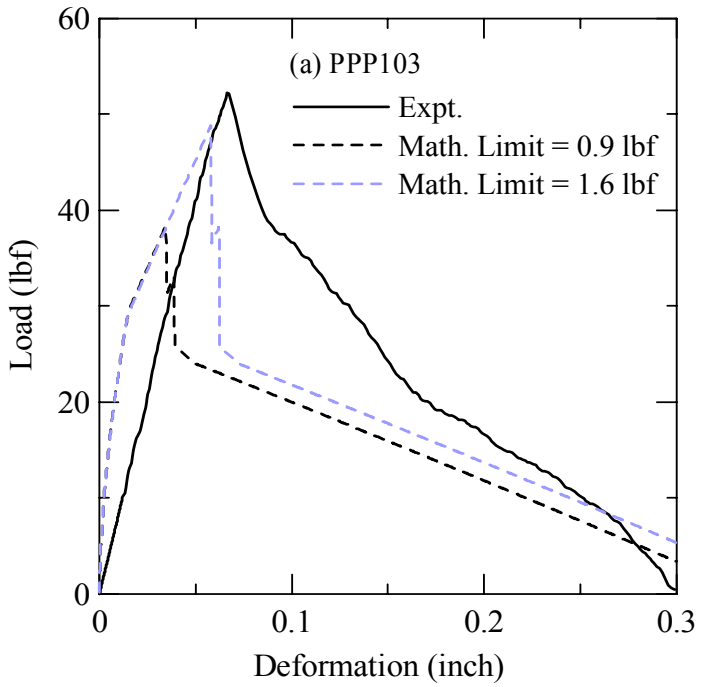

Fig. 3.14. Fitting the mathematical results to experimental results by changing the strength of anchorage (a) Pultrusion bath, embedded length – 0.3”, E, beam – 5.5 MPa (b) Pultrusion bath, embedded length – 0.5” (c) Vacuum Procedure E (beam) – 5.5 MPa (Limit - the strength of anchorage)

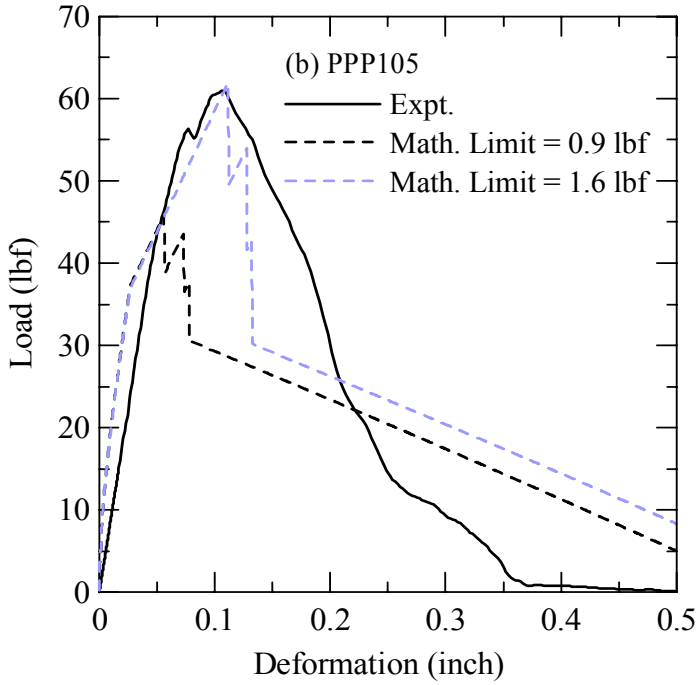

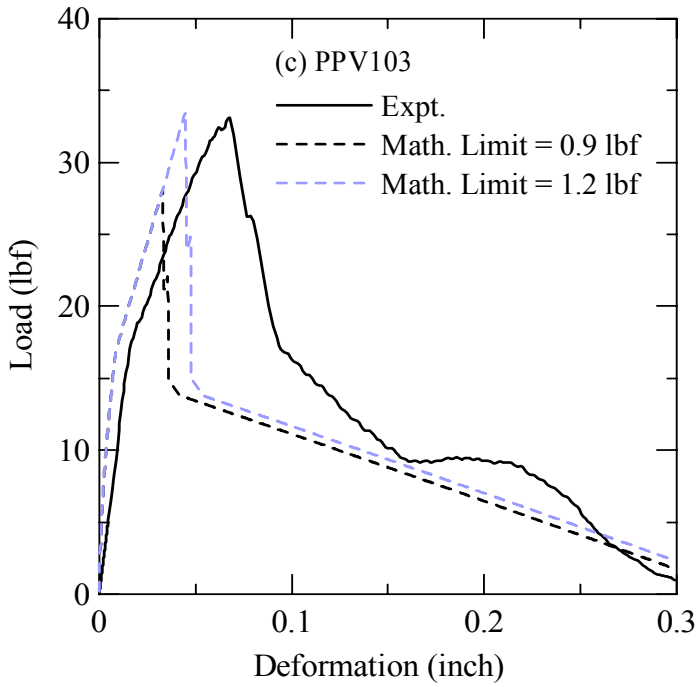

Fig. 3.14. Continued

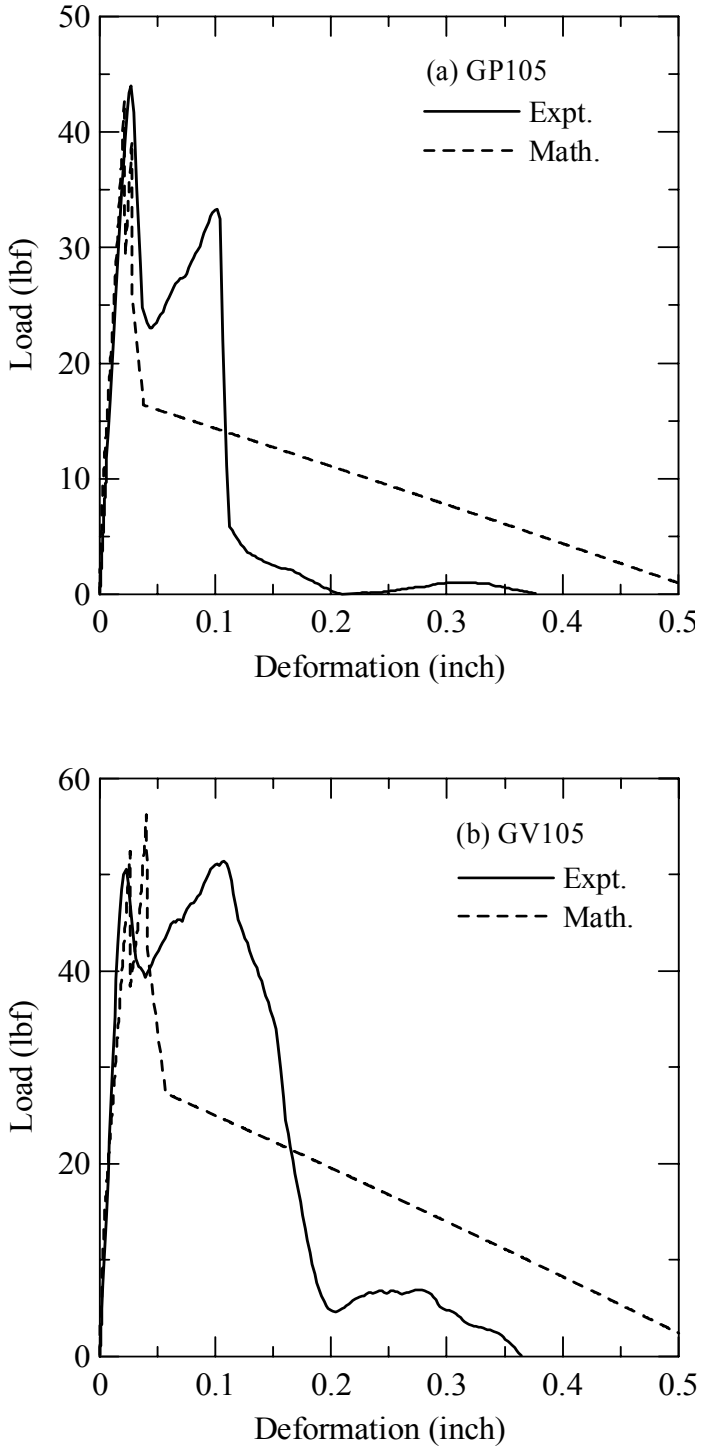

Fig. 3.15. Effect of different procedures for AR-glass (a) Pultrusion (b) Vacuum

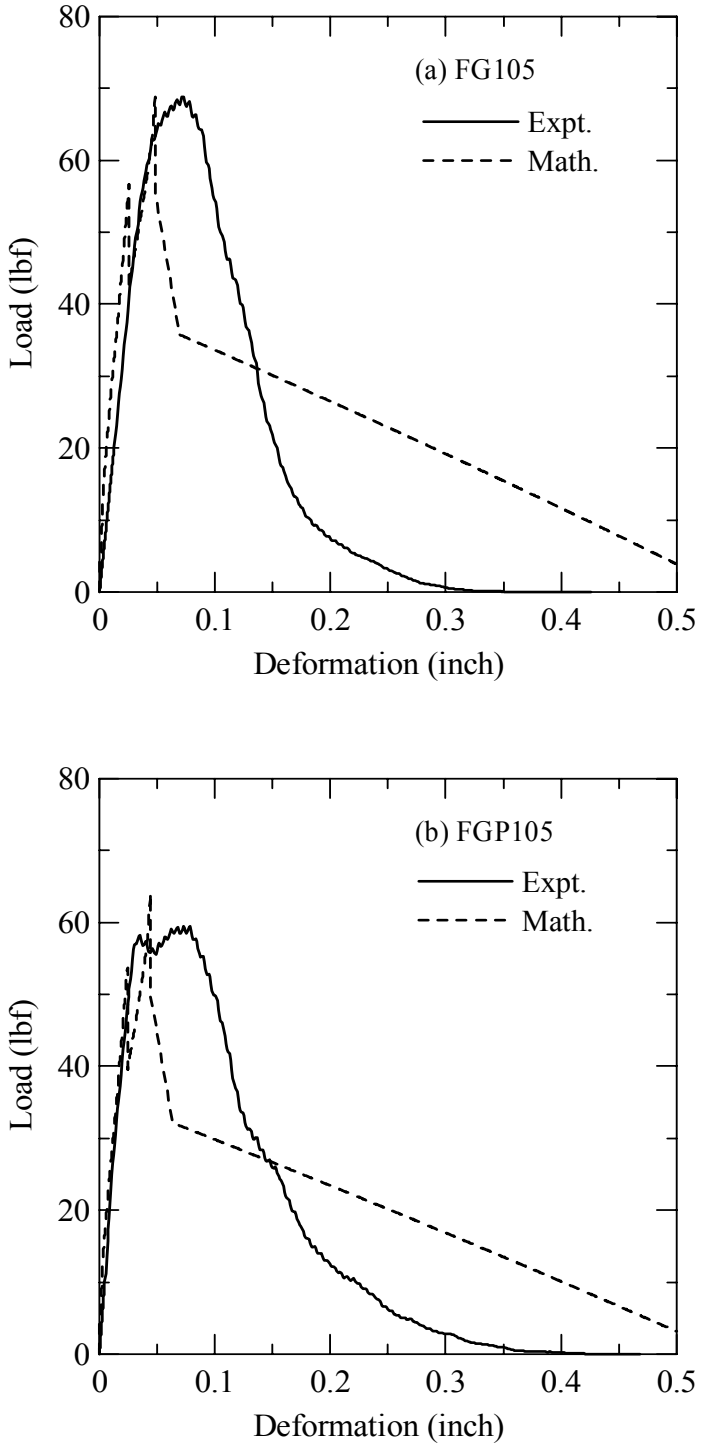

Fig. 3.16. Experimental and simulation results for mix design 2 (a) Cast procedure (b) Pultrusion procedure

3.4 Discussion

In the case of woven fabrics, there was a significant effect of fill-yarn as shown by the experimental results. This can be explained by the calculation results computed by both straight yarn and woven yarn models. Using the straight yarn model, the maximum load was predicted much lower. However, by adding the fill-yarn condition as an elastic beam, maximum load fitted well with the experimental results as shown in figure 3. 3.

Since specimen under tensile test starts cracking from the center and cracks increase as load increases, embedded length (between crack to crack) changes while the free length of the fabric is nearly zero for all the cases. To implement the pullout model into tensile model, it is important that the pullout model is sensitive to the embedded length. Figure 3.4 shows that the woven model corresponded well to the embedded length similar to the experimental results. From this, we can argue that the sensitivity of woven model for the embedded length was quite high. However, as we saw in figure 3.4b, the simulation result of PP with pultrusion bath did not match well with experimental data. When τ_{max} was changed to match the experimental result, the simulation result was at similar range with the experimental result. This suggests that it is important to use appropriate τ_{max} in models.

The simulation results for load and deformation for vacuum and pultrusion based on normal procedure did not match well with the experimental results. To fit with the experimental results, it was necessary to increase the strength of anchorage to reflect the importance of this parameter in transferring the load to the matrix. Evaluation of the micrographs based on the SEM study showed that use of pultrusion bath increased the

penetration of paste between the yarns, hence it is possible that the procedure positively affects the strength of the anchorage zone. As seen in figure 3.10, the calculation result of glass fabric with pultrusion bath agreed well with experimental results without increasing the strength of anchorage. This might also be explained by the condition of anchorage. Fill-yarns of PP fabrics loop around yarns and the penetration of the matrix in this zone affect the strength significantly as explained by figure 2.22. In contrast, fill-yarns of glass fabric are bonded to the yarns and the penetration of cement does not change the strength of this zone significantly. The stiffness of the anchorage zone is only affected by the proper packing of the paste in the local vicinity of the anchorage zone. That may explain why it was not necessary to modify the strength of anchorage to correlate the experimental and theoretical results of AR Glass fabrics.

CHAPTER 4

SHEAR MODEL

It is important to understand the mechanical properties of fiber reinforced concrete properly since there has been a rapid increase in the production of fiber reinforced concrete within the last fifty years. Main mechanical properties of any fiber reinforced cement concrete are shear, tensile, compressive, fractures, and interfacial bonding between the cement and fiber etc. One way to better understand such mechanical properties is by simulating the composite responses mathematically.

In this chapter, we will discuss about a mathematical model we developed to calculate the shear force and deformation and will attempt to compare our simulation data with an experimental study done previously by Haupt (1997) and presented as a MS thesis under Dr. Barzin Mobasher at Arizona State University.

4.1 Model

As shown in figure 4.1, there are three major failure conditions for the fiber reinforced concrete. The first failure is the initiation of matrix failure in the presence of fiber. Concrete starts cracking from this point. The second failure is the final failure of matrix in the presence of fiber. At this point, concrete completely cracks and fiber alone carries the load. Ultimately when fiber reaches its maximum strength, both concrete and fibers fail and composite material is no longer carrying the load.

After the first failure, the stiffness of the concrete decreases while stress increases. After crack starts, concrete can carry the load until concrete cracks completely. However

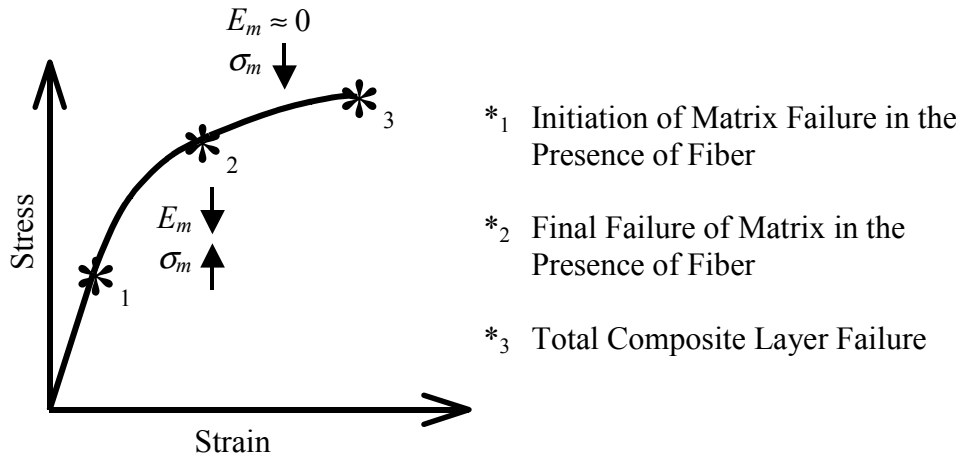

Fig. 4.1. Failure condition of composite material

because of cracks, stiffness starts reducing. In the case of shear load, reduction in the shear modulus causes degradation in the stiffness, since concrete and fiber are propagated by shear load.

After the second failure, stiffness of the concrete reaches nearly zero and stress in the concrete starts reducing since concrete can no longer carry the load. From this point, depending on the fiber direction, fiber starts carrying the load.

The approach used in this study is the classical laminate theory that was extended by the first order approximations that overestimate the ply discount method (Talreja 1986, Allen et. al. 1987). A single ply is defined as a lamina and modeled as an orthotropic sheet in plane stress. The principal material axis are longitudinal to the fiber (denoted as 1), transverse to the fiber direction (denoted as 2), and normal to the lamina surface (denoted as 3) as shown for an "n" layer laminate in figure 4.2. Geometrical axis are denoted as x, y and z in shown in figure 4.2. Strain values are imposed and stress is

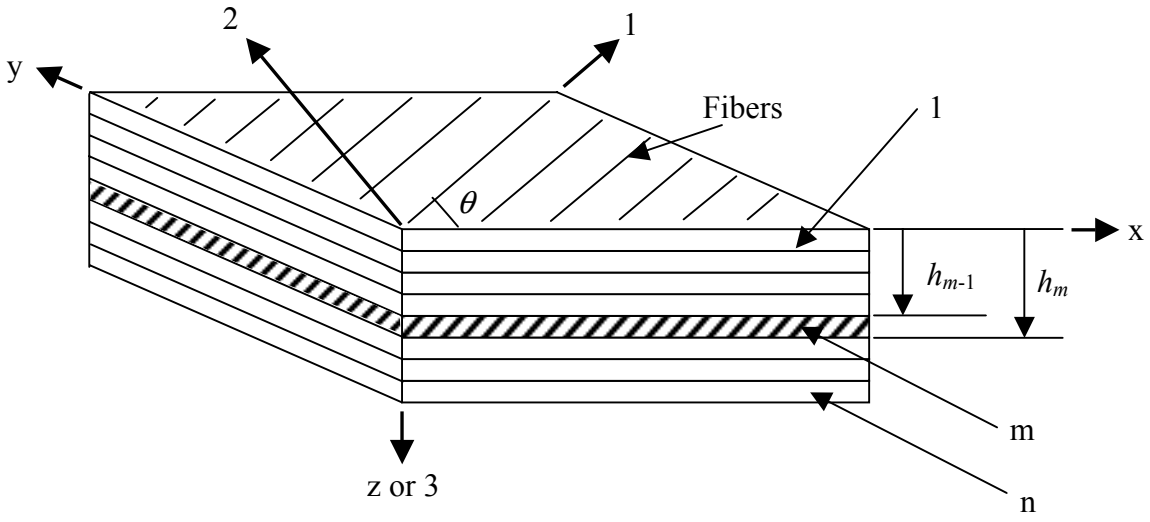

Fig. 4.2. Definition of axes and plies

calculated using the stress-strain relationship (the constitutive relation) incrementally. The constitutive relations for a general orthotropic material include the compliance matrix, *S*, or the stiffness matrix, *Q*, and relate the stress and strain within a lamina loaded in its principal directions (Jones, 1999). Since the present model updates the elastic stiffness of the matrix due to propagation of laminates, an elastically equivalent compliance matrix $\overline{S}$ is defined where the bar indicates use of updated elastic properties. In the term $\overline{S}^i_{jk}$, parameter *i* represents the load increment, *j* is the direction of applied strain, and *k* is the observed stress. The stress-strain relationship is represented in incremental form for each loading increment *i*, as following:

$$\Delta\varepsilon^i_j = \overline{S}^i_{jk}\,\Delta\sigma^i_k \tag{4.18}$$

$$\sigma^i_k = \left(\overline{S}^i_{jk}\right)^{-1}\Delta\varepsilon^i_j + \sigma^{i-1}_k \tag{4.19}$$

In matrix form,

$$\sigma_k^i = \begin{bmatrix} \sigma_1 \\ \sigma_2 \\ \tau_{12} \end{bmatrix}_k^i = \begin{bmatrix} \overline{S}_{11} & \overline{S}_{12} & 0 \\ \overline{S}_{21} & \overline{S}_{22} & 0 \\ 0 & 0 & \overline{S}_{66} \end{bmatrix}^{-1} \begin{bmatrix} \Delta\varepsilon_1 \\ \Delta\varepsilon_2 \\ \Delta\gamma_{12} \end{bmatrix}_k^i + \begin{bmatrix} \sigma_1 \\ \sigma_2 \\ \tau_{12} \end{bmatrix}_k^{i-1} \tag{4.20}$$

$$\overline{S}_{11} = \frac{1}{E_{1(\omega)}} \qquad \overline{S}_{12} = -\frac{\upsilon_{12}}{E_{1(\omega)}} \qquad \overline{S}_{22} = \frac{1}{E_{2(\omega)}} \qquad \overline{S}_{66} = \frac{1}{G_{12(\omega)}} \tag{4.21}$$

where, $E_1(\omega)$ and $E_2(\omega)$ are the elastic modulus corresponding to the propagation damage at loading increment *i* in direction 1 and 2, respectively, $G_{12}(\omega)$ is the shear modulus in the 1-2 plane, and ν_{12} is the major Poission's ratio. The elastic stiffness of the lamina, $E_1(\omega)$, is obtained using "Rule of Mixtures", the sum of the contributions from each phase to the overall stiffness, as given by following equation:

$$E_1(\omega) = E_f V_f + E_m(\omega)(1 - V_f) \tag{4.22}$$

where, E_f is the elastic modulus for fiber and $E_m(\omega)$ is the elastic modulus of matrix corresponding to the damage and V_f is the volume fraction of fibers. Due to low volume fraction of fibers (normally less than 10%), the stiffness of the lamina is dominated by matrix properties in the direction transverse to the fiber. A general observation is that the transverse stiffness (and strength) of an aligned composites are poor, especially in the low fiber fractions studied here. Calculation of the transverse modulus E_2 and ν_{12} are obtained using the Halpin-Tsai equations (Agarwal and Broutman 1990) as shown in equation 4.6. A value of $\xi = 0.2$ is used in the present study.

$$E_2(\omega) = \frac{E_m(\omega)\xi(1 + \xi\,\eta V_f)}{1 - \eta V_f} \qquad \eta = \frac{E_f - E_m(\omega)}{E_f + \xi\, E_m(\omega)} \tag{4.23}$$

If the stress (from equation 4.3) reaches the ultimate strength of concrete, concrete starts cracking and propagating between the concrete and fibers. Because of crack and

propagation, shear modulus and ultimately the modulus of elasticity of concrete are reduced using the equation,

$$E_m(\omega) = 2\left(1+\nu_m\right)G_m\beta \tag{4.24}$$

where, ν_m is the Poission's ratio, G_m is the shear modulus, and β is reduction factor which reduces exponentially based on the strain values. In the present study, β is calculated using the following equation,

$$\beta = \exp(-\alpha\left|\varepsilon_{xy}\right|) \tag{4.25}$$

where, α is used as an adjustable parameter and a value of 3000 is used in this study. At this condition, stress is calculated by using this reduced modulus of elasticity until concrete completely cracks.

Once the concrete is completely cracked, concrete cannot carry any more load and stress starts reducing. The stress is reduced exponentially based on the strain values at this condition. However, if fiber is at appropriate position, it continues to carry the load. As a result, stress in composite is calculated by

$$\sigma_c = V_f E_f \varepsilon_f + \sigma_m \tag{4.26}$$

where, V_f is the volume of fiber, E_f is the modulus of elasticity of fiber, ε_f is the strain in fiber and σ_m is the stress in concrete.

After calculating the stress, force per unit length of cross section, N, is calculated by calculating the lamina stiffness components using the following equations

$$N = \varepsilon^0 \overline{A}_{ij} \tag{4.27}$$

$$\overline{A}_{ij} = \sum_{m=1}^{n} \bar{Q}_{ij}^{m} (h_m - h_{m-1}) \tag{4.28}$$

where, ε^{0} is the midplane axial strain, $\bar{Q}_{ij}^{m}$ is the stiffness along an arbitrary orientation θ at m^{th} ply at i^{th} incremental load in the j direction of applied strain, and h_m and h_{m-1} are the hight of m^{th} and m-1^{th} ply respectively (Fig. 4.2). $\bar{Q}_{ij}^{m}$ is then obtained using the coordinate transformation and compliance matrix using the following equation,

$$\overline{Q}_{ij} = T_{ij}^{-1} \overline{S}_{ij}^{-1} R T R^{-1} \tag{4.29}$$

where, T is transformation matrix and R is Reuter matrix as shown below.

$$T = \begin{bmatrix} m^2 & n^2 & 2mn \\ n^2 & m^2 & -2mn \\ -mn & mn & \left(m^2 - n^2\right) \end{bmatrix} \tag{4.30}$$

$$m = \cos\theta \qquad n = \sin\theta \tag{4.31}$$

$$R = \begin{bmatrix} 1 & 0 & 0 \\ 0 & 1 & 0 \\ 0 & 0 & 2 \end{bmatrix} \tag{4.32}$$

Since $\overline{S}_{ij}$ is calculated by considering the matrix damage, $\overline{A}_{ij}$ also takes into account the fact that some of the layers have cracked or propagated.

The flowchart of the model is given in figure 4.3. The first failure (initiation of matrix failure) is checked using Tsai-Wu criteria defined in the following equations,

$$F_1\sigma_1 + F_2\sigma_2 + F_{11}\sigma_1^2 + F_{22}\sigma_2^2 + F_{66}\tau_{12}^2 - \sqrt{F_{11}F_{22}}\sigma_1\sigma_2 = 1 \tag{4.33}$$

$$F_1 = \left(\frac{1}{\sigma_1^T} + \frac{1}{\sigma_1^C}\right) \qquad F_2 = \left(\frac{1}{\sigma_2^T} + \frac{1}{\sigma_2^C}\right)$$
$$F_{11} = -\frac{1}{\sigma_1^T \sigma_1^C} \qquad F_{22} = -\frac{1}{\sigma_2^T \sigma_2^C} \qquad F_{66} = \left(\frac{1}{\tau_{12}^F}\right)^2 \tag{4.34}$$

where, σ_1^T and σ_2^T are the maximum tensile strength at direction 1 and 2 respectively, σ_1^C and σ_2^C are the maximum compressive strength in direction 1 and 2 respectively, and τ_{12}^F is the maximum shear strength in 1-2 plane. Tsai-Wu criteria is called "interactive criteria" that takes into account the stress interactions. This means that the failure loads with multi-axial stress in the material may well differ from those with a uniaxial stress. The second (the final failure of matrix in the presence of fiber) and third (total composite layer) failures are checked by the maximum stress criterion. The maximum stress criterion consist of fiber sub-criteria, corresponding to the strength in each of the five fundamental failure modes. If any one of these limits or criterion is exceeded by the corresponding stress expressed in the principal material axes, the material is deemed to have failed. Since this criteria allows us to know which direction failed, stresses are updated considering the effect of fibers at the failure direction. For the tensile failure at direction 1 at the second failure, ACK method is used to check the termination of the cracked matrix zone. If the strain calculated by following equation, is more than the current iteration strain, cracked matrix is terminated and softening matrix zone started.

$$\varepsilon_{um} = \left[\frac{12\tau\gamma E_f V_f^2}{E_c E_m^2 r V_m}\right]^{\frac{1}{3}} \tag{4.35}$$

where, γ is the fractural fraction and r is the fiber radius. In the current study, $\gamma = 0.5$ has been used.

The deformation is calculated by taking the differences in strain at each incremental load in diagonal direction. Strains are transformed to the diagonal directions using the transformation matrix (Equation 4.13) and θ is obtained using the following equation,

$$\theta = \tan^{-1}(\frac{l}{h}) \tag{4.36}$$

where, l and h are the length and height of the specimens.

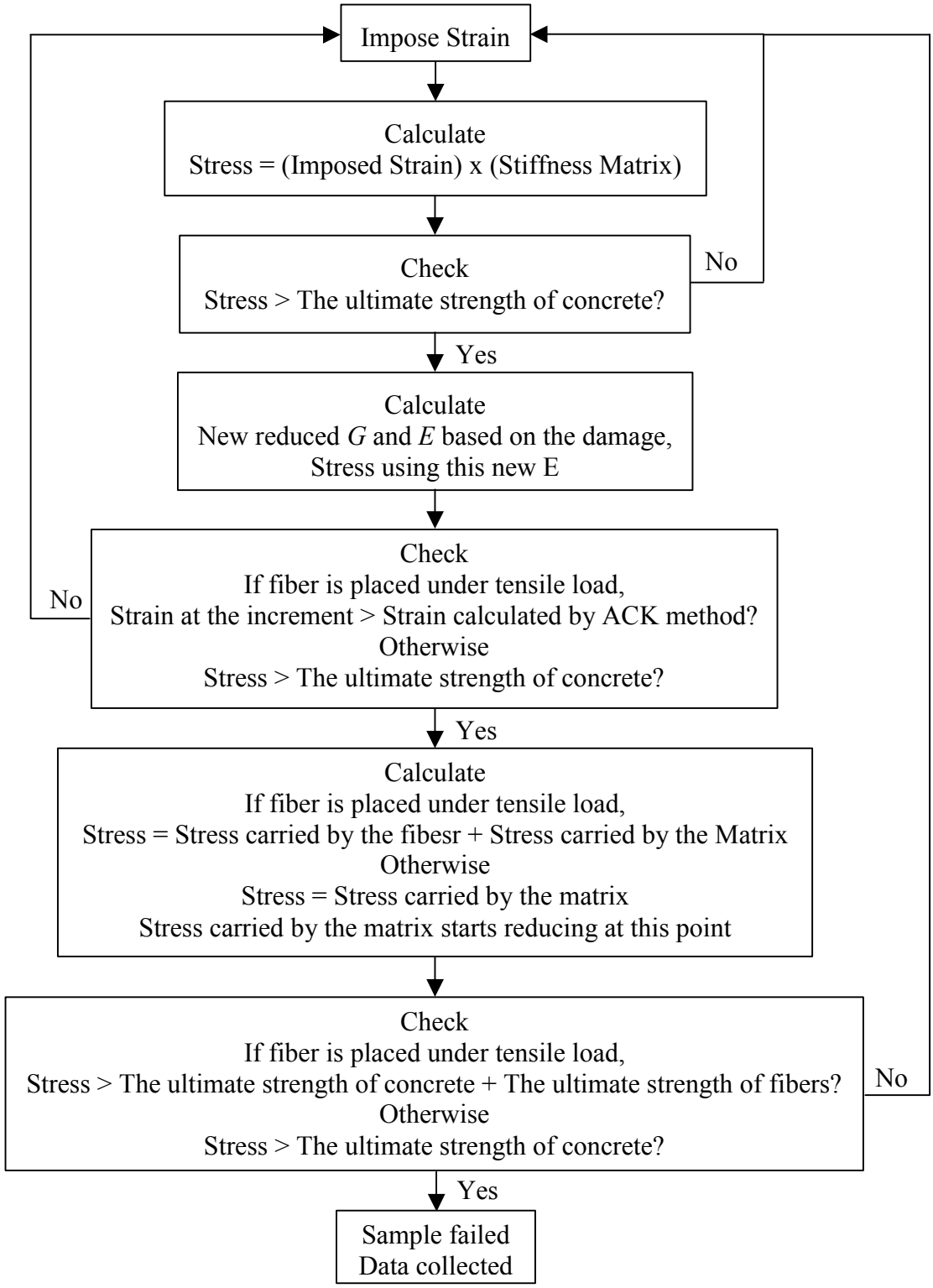

Fig. 4.3. Flowchart of shear model

4.2 Experimental Data

To verify the model, simulation results are compared with experimental data obtained from the study by Haupt (1997). In the experiement continuous alkali-resistant (AR) glass fibers were used in the manufacture of composites using the filament winding technique. The fibers have a Young's modulus of 70 GPa with a single fiber tensile strength of 3600MPa and a strain at failure of 2%. Mixture has 0.35 water to cementious solids ratio and 15% silica fume. After specimens were made, they were cured for 28 days in a calcium hydroxide water bath. Then, they were cut into 16" long and 8" wide by the diamond blade saw as an individual specimen. Pieces of U-channel steel were glued by epoxy along the 16" length on the top and bottom. After at least 24 hours of curing, tests were performed under actuator stroke control (rate of 0.005 in/sec). Experiment set up is as shown in figure 4.4. Data for stroke, force and deformation across the two diagonals were obtained. To measure the specimen deformation across the two diagonals, two LVDTs were glued on each specimen. The specimen lay ups were [0/90]s, [45/-45]s, [0/45/90]s, [0/-45/90]s, [0/45/-45]s,[0/-45/45/90]s.

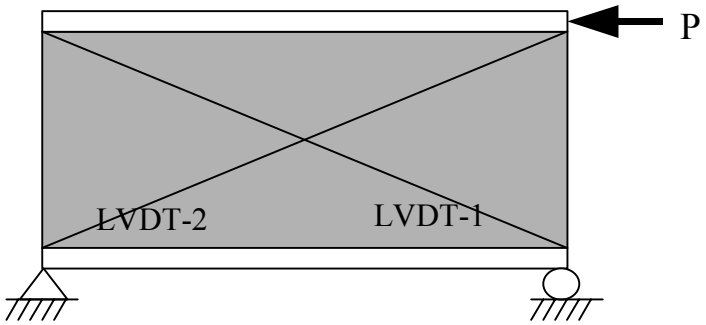

Fig. 4.4. Experiment set up

4.3 Results

Table 4.1 lists the properties of the materials used for calculations. The properties for AR glass fibers were used.

Figures 4.5 to 4.10 compare the experimental and mathematical results for deformation versus load. Over all, the mathematical results returned slightly smaller load than the experimental results however model simulated the trend well.

Figure 4.5 shows [0/90]s lay up results. There was a significant difference in the stiffness (Fig. 4.5). The Strain at the maximum load was ≈ 0.06 in the experiment compared to about 0.01 in the simulation. However, the results of maximum load differed only slightly. Maximum load in the experiment was approximately 2250 lbf and in the simulation was nearly 1750 lbf.

[45/-45]s lay up results matched quite well the experiment data until concrete starts cracking (Fig. 4.6). The load when matrix failed was approximately 3000 lbf for both experimental and mathematical data. However, after matrix failed, load continuously increased with decreased Young's modulus in the mathematical results that

Table 4.1

Constant Values for Calculation

	Concrete	AR Glass Fiber
Modulus of Elasticity	1.5E6 psi	11.5E6 psi
Poisson's Ratio	0.17	0.25
Ultimate Compressive Strength	5000 psi	-
Ultimate Tensile Strength	700 psi	522000 psi

was not seen in the experiment. After matrix failed, load became nearly constant in the experiment.

Figure 4.7 shows a good match between experimental and simulation results for [0/45/90]s lay up. Both results showed that matrix failed at nearly 2000 lbf and after this point, load slowly increased.

The simulation result for [0/-45/90]s was much smaller (< 2500 lbf) at the matrix failure than the experimental results (> 4000 .lbf) as seen in figure 4.8.

The both simulaiton and experimental results for [0/45/-45]s lay up showed similar trends considering the slope of plots in figure 4.9. However, simulation showed matrix failure at lower load (< 2500 lbf) than that of experimental (≈ 6000 lbf) case.

Figure 4.10, [0/-45/45/90]s lay up, also showed similar results as [0/45/-45] lay up. The loads in experiments were ≈ 4000 lbf to 6000 lbf at matrix failure which were larger than the calculated result of < 3000 lbf.

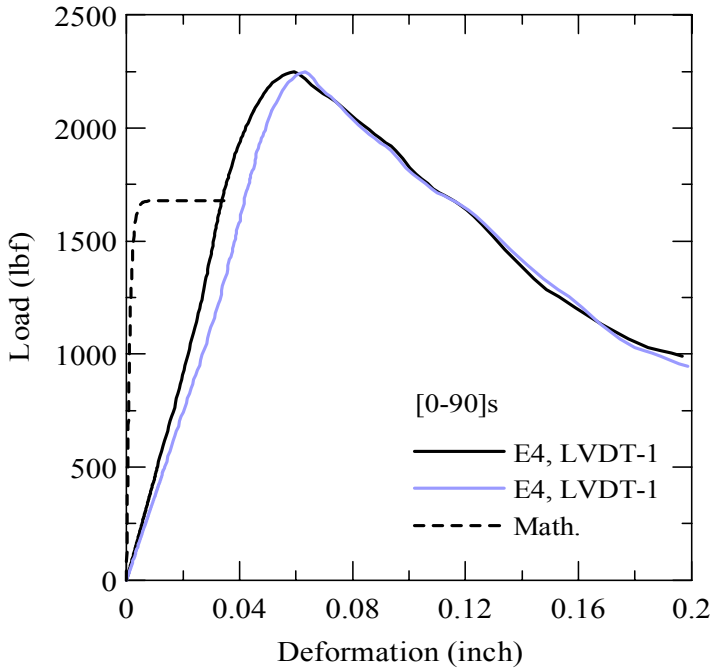

Fig. 4.5. Experimental and simulation results for [0/90]s lay up

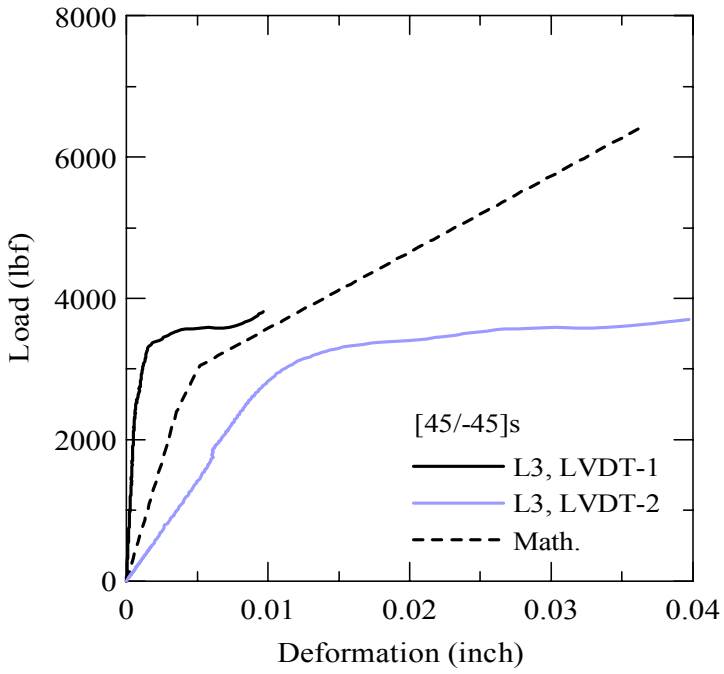

Fig. 4.6. Experimental and simulation results for [45/-45]s lay up

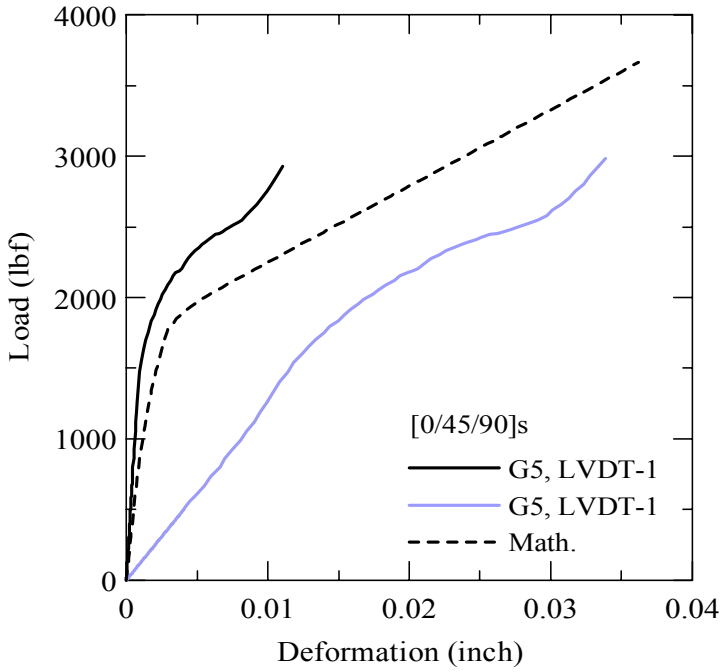

Fig. 4.7. Experimental and simulation results for [0/45/90]s lay up

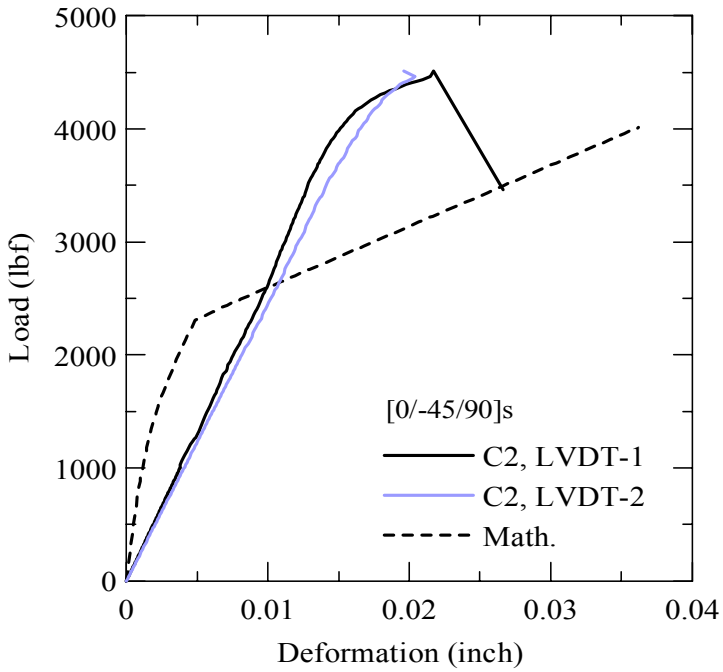

Fig. 4.8. Experimental and simulation results for [0/-45/90]s lay up

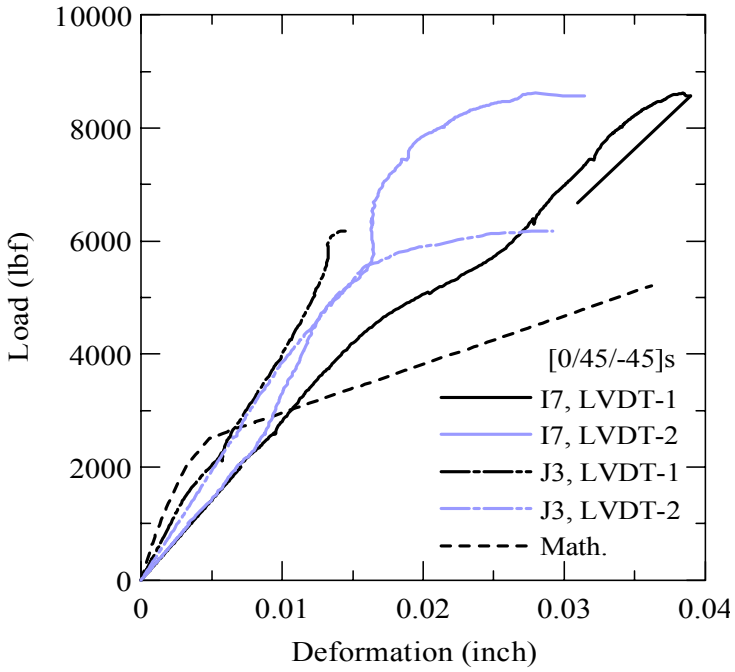

Fig. 4.9. Experimental and simulation results for [0/45/-45]s lay up

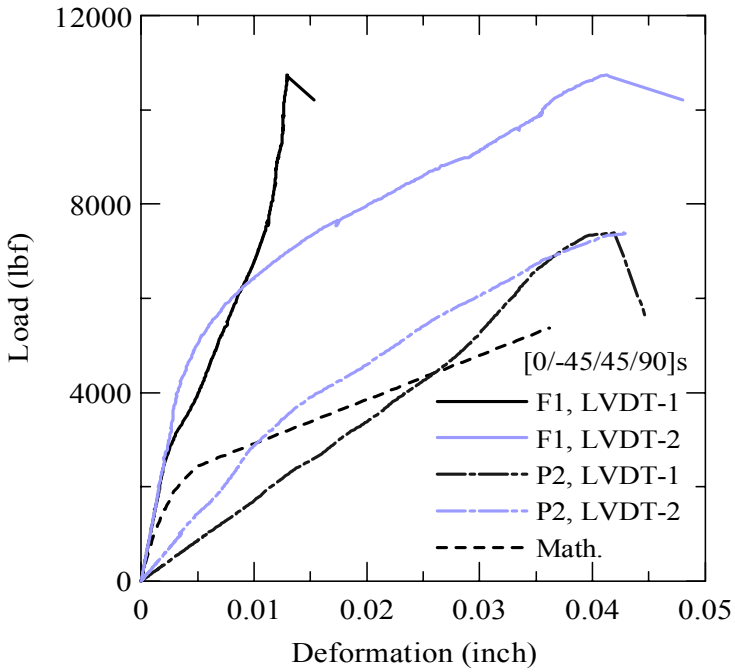

Fig. 4.10. Experimental and simulation results for [0/-45/45/90]s lay up

4.5 Discussion

As shown by Figure 4.5, [0/90]s, calculated stiffness was slightly higher than the experimental and was opposite for the loads . As seen in figure 4.11, when fiber is placed in -45 degree, fiber is under tensile load as tensile load is in fiber direction fiber is able to withstand the load. This effect has been considered in the model. However, when fiber is in angle other than -45, fiber effect is not considered. Therefore, the calculated result for [0/90]s is governed by the concrete.

Over all, mathematical results return slightly smaller load than the experimental results. In this study, the effect of fiber is pronounced only when fiber is placed under tensile load. This may have resulted in a smaller load, since fiber in other degree might help to redistribute the load throughout the matrix. In contrast, when [45/-45] lay up is calculated, results matched well since there is no 0 or 90 degree layer, the fiber effects were well simulated.

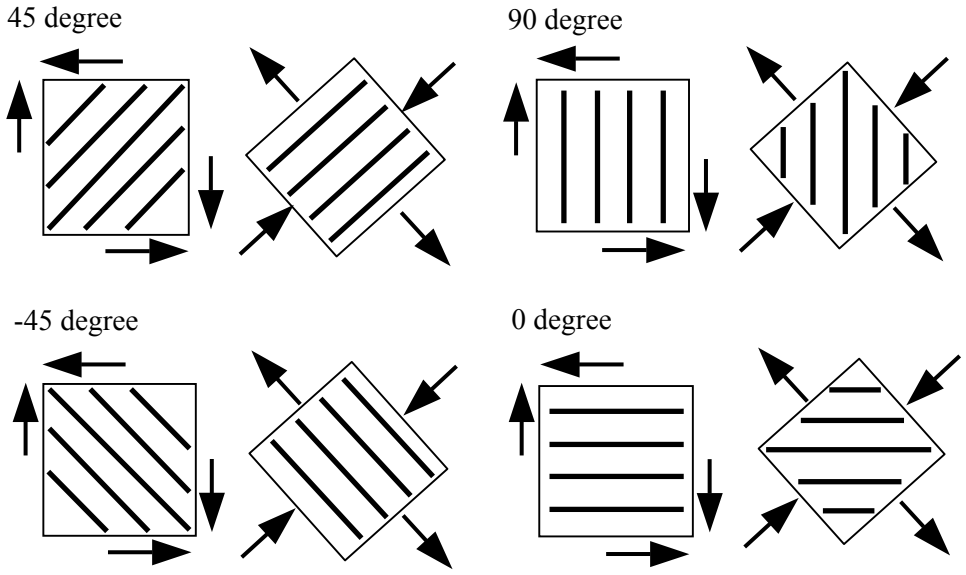

Figure 4.11. Fiber direction and load direction

CHAPTER 5

CONCLUSION

The first part of this study primarily focuses on understanding the interfacial condition for the fabric reinforced composite materials and developing the model for a fiber and fabric reinforced concrete. The second part, shear model, studies the behavior of composite material when fiber reinforced concrete is considered as laminated materials.

Pullout

To know the interfacial condition between fibers and cement, pullout test was conducted. Pullout test provided the load and deformation data for different fabrics, procedures and mix designs. In addition to the pullout experiments, mathematical models (yarn and woven conditions) were also constructed to verify the experimental data. Based on the experimental results, the yarn model was expanded to the woven model. Both models can also be implemented in the tensile model to predict the crack opening.

The main results from the experiments are summarized below.

a. Different fabric types have different effects. AR-glass fabric increased the strength of composite material, however, PE increased the toughness.
b. Woven fiber provides higher interfacial bonding than unidirectional yarn. This is caused by the restraint of fill yarns.
c. Different procedures (normal, pultrusion and vacuum) used in making the specimen caused significant differences in results depending on the fabric type

(AR-glass, PP, PE and PVA). When pultrusion bath was used, cement adsorption and penetration increased. As a result, maximum load also increased, specially, for the fabric that did not have coating around.

d. The addition of fly ash in cement mix increased the maximum load and interfacial shear bond. This supports the previous study done by Peled and Mobasher (2003) where they found the fabric reinforced concrete when mixed with fly ash increased tensile strength and toughness.

Similarly, the results from the woven model are summarized below.

a. The results of woven fiber pullout test matched well with the model data where a fill yarn condition was implemented as a beam in elastic foundation in the yarn model.
b. The sensitivity of embedded length in the model was high. The model predicted well for all the embedded length conditions.
c. In pultrusion bath with PP fabric case, it was necessarily to change the strength of anchorage to estimate accurately the load and deformation to mach to the experimental data. This shows that using pultrusion bath with PP fabrics changes the anchorage condition since cement can penetrate the fabrics.

Shear

For better understanding of material properties of fiber reinforced concrete under shear load, the model was developed to calculate the deformation and load. As our

results suggest, simulation is not perfect but working well to predict the failure load and deformation at various lay ups and conditions.

The results of shear model are summarized below.

a. When fiber is placed in appropriate position (similar direction with tensile load), the model can calculate the similar results as in the experiments.
b. Calculated results for [0/90]s lay up did not show good match with experimental results. This explains that when fiber is not placed in the tensile load direction, fiber does improve the load that can be carried by the composite.

Further Work

Pullout: Data obtained in this thesis are valuable to understand the use of fabrics (glass, PP, PE and PVA) with cement concrete as a composite construction material. However, we can achieve further improvement by extending more work in future.

a. To refine the model, it is important to collect more experimental data so that model parameters for the pulled out condition could be enhanced. In our experiment, some yarns and/or filaments or matrix for the specific sample broke instead of being pulled out. This caused in increase of standard deviation significantly. In order to understand interfacial bonding, it would be desirable that the exact number of yarns are pulled out from the matrix in all sample conditions.
b. Pull out is only one part of tensile and flexure test conditions. The next logical step would be to implement the pullout model into these different test.

c. In the model, there is no expression for the ratio of fabric to cement. In order to implement the pullout model as crack opening for tensile and flexure model, it would be important to have fabric to cement ratio defined.

Shear: To understand the response of fiber reinforced composite material, this study is valuable. However, this work can be extended for further understanding in future work.

a. In many instances it was hard to interpret the experimental data as they were not clear. A much clearer data would enable us to compare the experimental and mathematical results better. Since there was some problem in translating the experimental results, in many cases, raw data were used to compare with mathematical results which may have caused some discrepancies.

b. As seen in results, fiber does help to carry the load even if fiber is not placed in the direction of tensile load. If this condition can be implement in the model, this will help more to understand the mechanical properties of fiber reinforced composite materials.

REFERENCES

Agarwal, Bhagwan D., and Lawrence J. Broutman. Analysis and Performance of Fiber Composite. New York: Wiley-Interscience Publication, 1990.

Allen, D. H., C. E. Harris, and S. E. Groves. "A Thermomechanical Constitutive Theory For Elastic Composites with Distributed Damage – I. Theoretical Development." International Journal of Solids and Structures. 23 (1987) 1301-18.

Allen, D. H., C. E. Harris, and S. E. Groves. "A Thermomechanical Constitutive Theory For Elastic Composites with Distributed Damage – II. Application to Matrix Cracking in Laminated Composites." International Journal of Solids and Structures. 23 (1987) 1319-38.

Aveston, J., and A. Kelly. "Theory of Multiple Fracture of Fibrous Composites." Journal of Materials Science. 8 (1973) 352-62.

Greszczuk, L. B. "Theoretical Studies of the Mechanics of the Fiber-Matrix Interface in Composites" ASTM STP 452, American Society for Testing and Materials. (1969) 42-58.

Gurney, C., and J. Hunt. "Quasi-Static Crack Propagation." Proceedings of the Royal Society of London Series A – Mathematical and Physical Sciences. 299 (1967) 508-24

Haupt, Garrett James. Study of Cement Based Composites Manufactured by Extrusion, Compression molding and Filament Winding. MS Thesis. Tempe: Arizona State University, 1997

Hetényi, M. Beam on Elastic Foundation. Ann Arbor: University of Michigan Press, 1983.

Hull, Derek. An introduction to composite materials. New York: Cambridge University Press, 1981.

Jones, Robert M. Mechanics of Composites Materials. 2nd ed. Philadelphia: Taylor & Francis, 1999.

Kelly, A., and W. R. Tyson. "Fiber-Strengthened Materials." High-Strength Materials ; Proceedings of the Second Berkeley International Materials Conference: High-Strength Materials – Present Status and Anticipated Developments. Held at the University of California, Berkeley, June 15-18, 1964. Ed. Victor F. Zackay. 1965. 578-602.

Lawrence, P. J. "Some Theoretical Considerations of Fiber Pull-Out from an Elastic Matrix." Journal of Material Schience. 7 (1972) 1-6.

Mobasher, B., and Cheng Yu Li. "Effect of Interfacial Properties on the Crack Propagation in Cementitious Composites." Journal of Advanced Cement Based Materials. 4 (1996): 93-105.

Mobasher, B., D. Kingsbury, J. Montesinos, and R. S. Gorur. "Mechanical Aspects of Crimped Glass Reinforced Plastic (GRP) Rods." IEEE Transactions on Power Delivery. 18 (2003): 852-8.

Peled, A., A. Benture, and D. Yankelevsky. "Woven Fabric Reinforcement of Concrete Matrix." Journal of Advanced Cement Based Materials. 1 (1994): 216-23.

Peled, Alva, and Barzin Mobasher. "The Pultrusion Technology for the Production of Fabric-Cement Composites." Brittle Matrix Composites 7 – Proceedings of the 7th International Symposium. Ed. Brandt, A. M., V. C. Li, and I. H. Marshall.

Cambridge: Woodhead Publ. Ltd.; Warsaw: ZTUREK Research-Scientific Institute, 2003. 505-14.

Stang, H., Z. Li, and S. P. Shah. "Pullout Problem: Stress Versus Fracture Mechanical Approach." Journal of Engineering Mechanics. 116 (1990): 2136-50.

Talreja, R. "Stiffness Properties of Composite Laminates with Matrix Cracking and Interior Delamination." Engineering Fracture Mechnics. 25 (1986): 751-62.

APPENDIX A

CALCULATION RESULTS

Table A-1

Calculation Results for AR-Glass Fiber Samples

Sample ID	K (lbf/inch)	Max load (lbf)	Toughness (lbf-inch)	τ_{max} (psi)	Comments
G105-1	1836.84	44.10	4.90	356.32	
G105-2	1252.13	43.74	8.29	330.93	
G105-3	1007.54	35.88	2.75	307.36	
G105-4	1287.32	37.96	4.55	306.40	
G105-5	1654.28	44.68	5.62	352.79	
G205-1	967.31	41.56	6.96	346.67	
G205-2	1224.86	38.12	4.44	316.05	
G205-3	1118.90	27.57	2.89	230.35	
G205-4	877.29	26.60	4.82	219.31	1 yarn broke.
G205-5	1274.19	34.49	3.58	264.29	
G305-1	1011.02	47.91	6.34	366.70	1 yarn broke.
G305-2	1173.41	40.11	5.12	313.77	
G305-3	1009.08	31.01	3.33	265.04	
G305-4	969.84	34.61	2.11	279.63	
G305-5	1029.53	42.50	4.81	356.72	
GP105-1	1459.61	33.15	2.67	251.79	2 yarns broke.
GP105-2	1157.73	18.31	1.67	149.98	5 yarns broke, filament of 2 yarns broke.
GP105-3	892.67	34.44	5.02	265.69	3 yarns broke.
GP105-4	1289.67	44.72	3.69	366.89	
GP105-5	1132.70	24.24	2.86	181.17	3 yarns broke, filament of 4 yarns broke.
GP105-6	1551.77	41.40	3.66	317.07	2 yarns broke, filament of 1 yarn broke.
GV105-1	2181.59	67.26	6.28	483.93	Matrix split into two.
GV105-2	1529.11	55.47	9.31	448.65	
GV105-3	1593.58	56.10	7.23	393.21	3 yarns broke.
GV105-4	2075.51	53.31	8.77	380.45	1 yarn broke.
GV105-5	2050.54	66.81	9.88	473.88	2 yarns broke.
GV105-6	1859.06	50.74	6.76	379.82	2 yarns broke.
FG105-1	1159.76	32.59	4.23	262.75	Filament of 6 yarns broke.
FG105-2	1265.11	32.57	5.07	290.29	
FG105-3	1345.38	68.93	8.00	558.20	
FG105-4	1460.35	71.09	8.45	616.00	Filament of 1 yarn broke.
FG105-5	1709.21	69.45	2.69	550.74	Matrix split into two.
FG105-6	1238.91	52.71	6.98	462.36	
FGP105-1	1794.41	25.67	2.90	204.03	
FGP105-2	1571.97	32.35	3.51	289.33	1 yarn broke.
FGP105-3	1329.49	55.61	2.77	449.78	Matrix split into two.
FGP105-4	1076.26	59.89	7.29	499.26	1 yarn broke.
FGP105-5	1355.55	40.78	1.80	338.04	Matrix split into two.
FGP105-6	1778.90	59.56	8.42	502.11	

Table A-2

Calculation Results for PP Fiber Samples

Sample ID	K (lbf/inch)	Max load (lbf)	Toughness (lbf-inch)	τ_{max} (psi)	Comments
PP103-1	335.58	22.45	2.58	194.57	
PP103-2	335.09	28.49	4.90	250.11	
PP103-3	661.80	27.21	2.43	221.75	
PP103-4	152.82	9.72	1.08	91.52	Matrix broke.
PP103-5	565.53	26.38	3.92	218.01	
PP103-6	719.47	44.56	6.96	368.80	
PP105-1	704.33	36.67	5.49	199.24	
PP105-2	643.62	40.01	9.63	217.77	
PP105-3	696.09	48.38	7.22	244.21	
PP105-4	560.16	37.84	6.98	215.43	
PP105-5	535.10	33.17	8.14	169.91	
PP205-1	375.05	27.84	6.88	150.05	
PP205-2	424.82	39.40	9.64	203.67	
PP205-3	377.37	30.88	10.36	170.25	
PP205-4	338.09	37.13	8.91	186.70	
PP205-5	290.15	36.43	7.22	195.65	
PP305-1	301.42	54.39	12.78	276.07	
PP305-2	282.22	37.45	8.89	200.25	
PP305-3	284.96	36.81	8.56	183.25	
PP305-4	286.50	27.20	6.41	159.46	
PP305-5	313.50	26.12	5.72	133.37	
PPP103-1	475.60	52.56	6.77	418.91	
PPP103-2	430.58	38.12	7.82	311.41	1 yarn slipped.
PPP103-3	351.68	76.71	15.92	519.93	
PPP103-4	631.34	35.12	6.98	294.81	1 yarn broke.
PPP103-5	553.24	60.25	11.95	455.42	
PPP103-6	645.81	44.55	5.52	402.67	Matrix broke.
PPP103-7	650.49	69.34	9.61	551.77	
PPP105-1	512.15	79.66	19.65	389.29	Matrix cracked.
PPP105-2	621.09	36.73	5.52	189.76	Matrix broke.
PPP105-3	519.90	78.19	12.59	356.74	
PPP105-4	595.73	49.84	4.77	266.91	
PPP105-5	404.57	59.57	18.05	319.71	
PPP105-6	471.71	61.01	10.84	341.23	Matrix broke.
PPV103-1	781.95	29.66	2.55	263.43	
PPV103-2	608.72	31.61	3.74	260.54	
PPV103-3	583.28	19.50	2.19	150.19	
PPV103-4	625.97	32.02	6.66	286.88	Matrix cracked.
PPV103-5	559.02	33.14	3.94	293.78	
PPV103-6	670.07	22.88	3.51	202.69	

Table A-3

Calculation Results for PE Fiber Samples

Sample ID	K (lbf/inch)	Max load (lbf)	Toughness (lbf-inch)	τ_{max} (psi)	Comments
PE105-1	32.07	16.57	9.37	145.02	
PE105-2	39.45	16.97	7.91	149.48	
PE105-3	47.85	15.67	5.48	142.01	
PE105-4	44.27	19.12	11.62	153.95	
PE105-5	40.70	16.88	7.19	143.85	
PE205-1	28.27	10.92	3.85	94.68	
PE205-2	31.07	18.54	9.67	163.00	
PE205-3	29.65	19.85	11.49	165.98	
PE205-4	25.14	14.81	7.50	129.58	
PE305-1	17.95	19.12	16.30	168.59	
PE305-2	22.82	19.42	12.02	174.26	
PE305-3	23.83	13.62	4.48	122.86	Matrix broke.
PE305-4	18.00	17.93	13.28	163.70	

Table A-4

Calculation Results for PVA Fiber Samples

Sample ID	K (lbf/inch)	Max load (lbf)	Toughness (lbf-inch)	τ_{max} (psi)	Comments
PVA103-1	325.21	40.48	4.21	305.30	
PVA103-2	279.43	36.97	4.49	258.20	
PVA103-3	228.76	25.04	3.22	199.14	
PVA103-4	340.58	43.49	5.32	222.56	
PVA103-5	232.48	26.68	4.17	188.30	3 yarns broke.
PVA103-6	236.03	24.16	3.94	169.81	
PVAP103-1	205.00	62.69	19.48	523.64	8 yarns broke.
PVAP103-2	261.74	60.52	11.23	438.45	5 yarns broke.
PVAP103-3	244.49	54.68	12.24	414.22	
PVAP103-4	302.64	63.29	14.06	458.85	5 yarns broke.
PVAP103-5	227.18	62.33	13.52	463.21	All (8) yarns broke.
PVAP103-6	341.39	64.37	11.25	486.54	All (8) yarns broke.
FPVAP103-1	316.09	42.48	6.27	393.17	
FPVAP103-2	379.58	54.59	7.20	560.15	2 yarns broke.
FPVAP103-3	361.19	55.50	7.82	374.05	1 yarn broke.
FPVAP105-1	412.43	74.10	13.05	374.05	Filaments of 2 yarns broke.
FPVAP105-2	430.80	70.12	15.11	369.28	1 yarn broke.
FPVAP105-3	381.60	69.17	14.79	338.03	1 yarn broke.
FPVAP105-4	487.13	77.89	12.42	410.42	All (8) yarns broke.
FPVAP105-5	461.45	76.11	9.41	381.90	

Table A-5

Calculation Results for PP Yarn Samples

Sample ID	K (lbf/inch)	Max load (lbf)	Toughness (lbf-inch)	τ_{max} (psi)	Comments
PPY103-1	88.81	4.92	0.85	302.45	
PPY103-2	46.39	12.14	2.54	786.60	
PPY103-3	109.40	4.52	0.94	275.65	
PPY103-4	103.39	2.81	0.59	182.15	Filaments broke.
PPY103-5	78.49	2.36	0.54	147.00	
PPY103-6	84.55	3.27	0.44	234.08	
PPY103-7	100.21	9.37	2.25	600.12	Yarn broke.
PPY103-8	97.67	4.95	0.65	396.62	
PPPY103-1	99.78	5.39	1.46	327.41	
PPPY103-2	118.36	4.95	0.70	320.76	
PPPY103-3	99.70	8.05	1.20	594.81	Filaments broke.
PPPY103-4	109.44	4.54	0.97	309.55	
PPPY103-5	96.40	10.27	1.76	786.67	Filaments broke.
PPPY103-6	137.82	4.90	1.32	279.27	
PPPY103-7	100.45	3.81	0.73	249.52	
PPPY103-8	96.81	7.44	1.52	443.04	
PPVY103-1	94.31	9.42	1.86	608.53	Few filaments did not pull out.
PPVY103-2	98.72	6.89	1.49	494.62	Few filaments broke or did not pull out.
PPVY103-3	82.57	11.48	2.19	643.65	Few filaments did not pull out.
PPVY103-4	80.10	12.17	2.15	872.11	Few filaments did not pull out.
PPVY103-5	87.65	7.18	1.60	459.80	Few filaments did not pull out.
PPVY103-6	131.62	6.50	1.26	459.21	Few filaments did not pull out.
PPVY103-1	94.31	9.42	1.86	326.35	Few filaments did not pull out.
PPFY103-1	111.32	5.23	0.94	449.70	
PPFY103-2	120.19	7.72	1.84	183.14	
PPFY103-3	133.54	2.75	0.40	334.99	Broken matrix at bottom.
PPFY103-4	63.50	5.29	1.39	495.78	
PPFY103-5	110.73	7.36	1.52	588.96	
PPFY103-6	81.97	9.25	1.71	486.21	
PPPFY103-1	64.40	7.17	1.33	458.54	Yarn broke.
PPPFY103-2	75.76	6.97	1.48	518.52	
PPPFY103-3	63.70	9.56	2.05	753.19	Yarn broke.
PPPFY103-4	79.27	9.55	1.39	554.09	
PPPFY103-5	68.60	7.90	1.25	684.71	
PPPFY103-6	63.18	10.30	1.71	906.94	Yarn broke.
PPPFY103-7	82.18	12.34	2.37	302.45	Yarn broke.

Table A-6

Calculation Results for Fiber Pullout Samples

Sample ID	K (lbf/inch)	Max Load (lbf)	Slip at Max Load (inch)	Comments
FiG105-1	137.24	10.44	0.117	
FiG105-2	121.38	8.75	0.105	
FiG105-3	166.57	13.40	0.087	
FiG105-4	66.27	4.51	0.167	Fiber came out from the plate.
FiG105-5	106.80	9.20	0.104	
FiPP103-1	16.75	3.33	0.247	
FiPP103-2	15.56	2.33	0.195	
FiPP103-3	16.43	1.97	0.144	
FiPP103-4	16.53	1.93	0.141	
FiPVA103-1	10.63	0.50	0.072	
FiPVA103-2	8.65	0.61	0.076	
FiPVA103-3	9.03	0.48	0.075	
FiPVA103-4	6.09	0.50	0.072	
FiPVA103-5	6.20	0.47	0.063	
FiPVA103-6	10.74	0.58	0.072	

APPENDIX B

GRAPHS FOR ALL THE TESTED SAMPLES

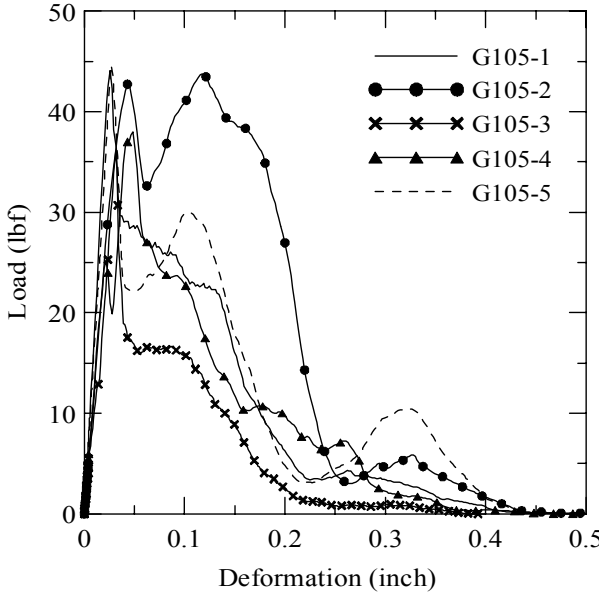

Fig. B-1. AR-glass fiber with mix design 1, cast procedure, 0.5” embedded and 1” free fiber length

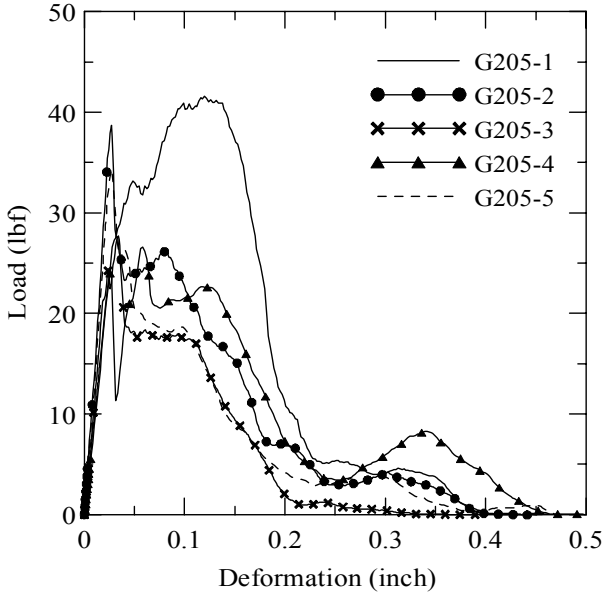

Fig. B-2. AR-glass fiber with mix design 1, cast procedure, 0.5” embedded and 2” free fiber length

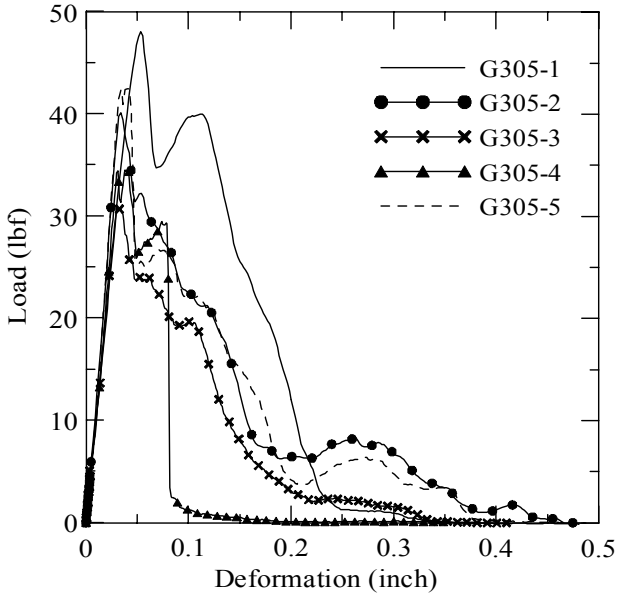

Fig. B-3. AR-glass fiber with mix design 1, cast procedure, 0.5” embedded and 3” free fiber length

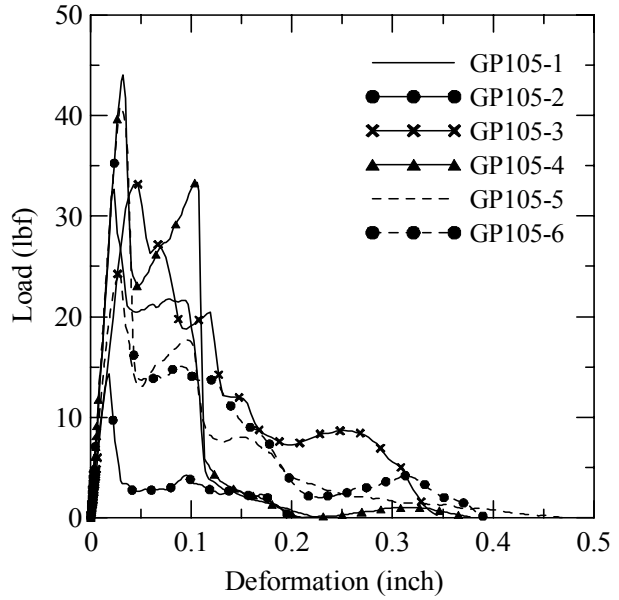

Fig. B-4. AR-glass fiber with mix design 1, pultrusion procedure, 0.5” embedded and 1” free fiber length

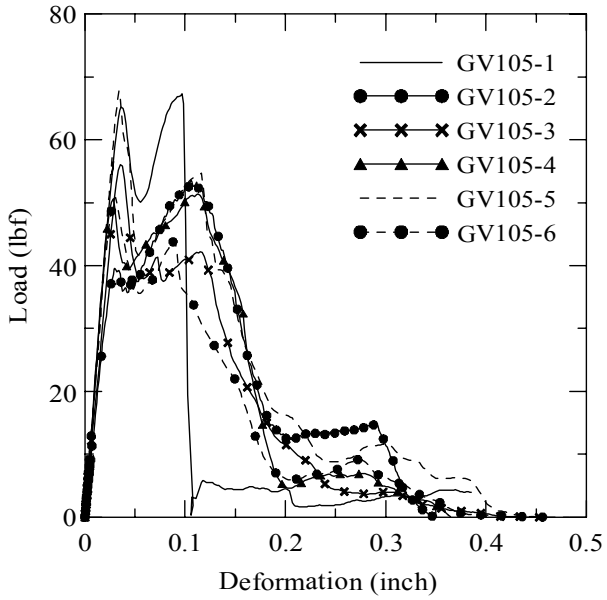

Fig. B-5. AR-glass fiber with mix design 1, vacuum procedure, 0.5” embedded and 1” free fiber length

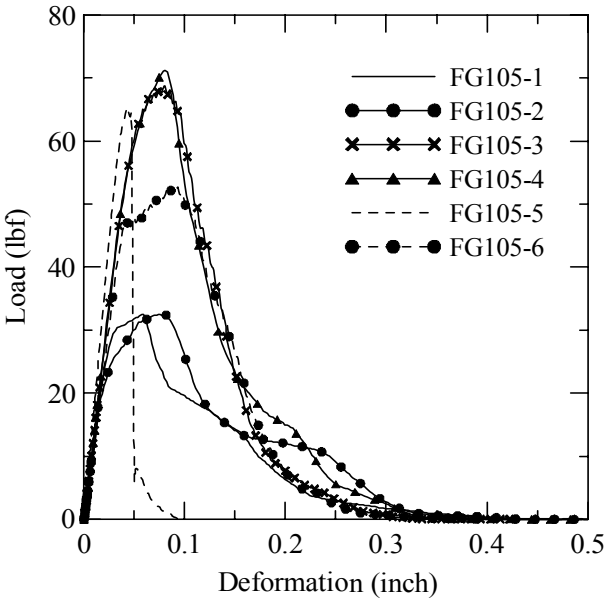

Fig. B-6. AR-glass fiber with mix design 2, cast procedure, 0.5” embedded and 1” free fiber length

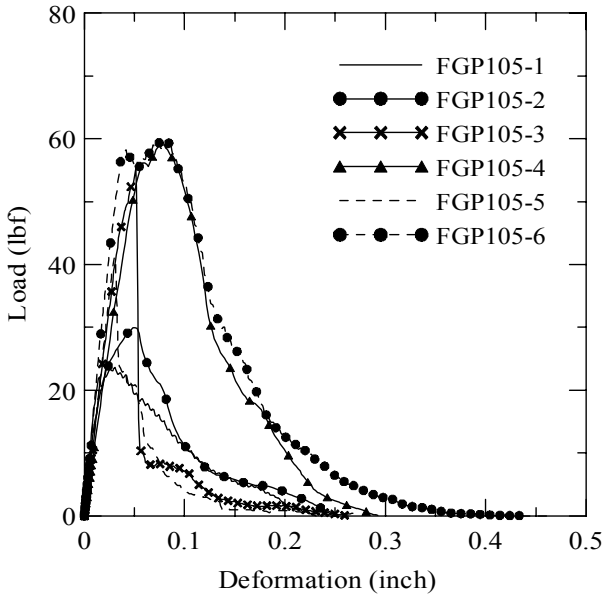

Fig. B-7. AR-glass fiber with mix design 2, pultrusion procedure, 0.5” embedded and 1” free fiber length

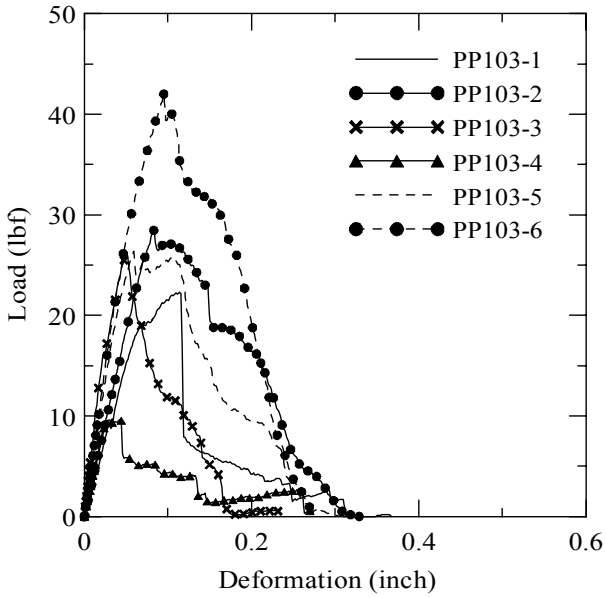

Fig. B-8. PP fiber with mix design 1, cast procedure, 0.3” embedded and 1” free fiber length

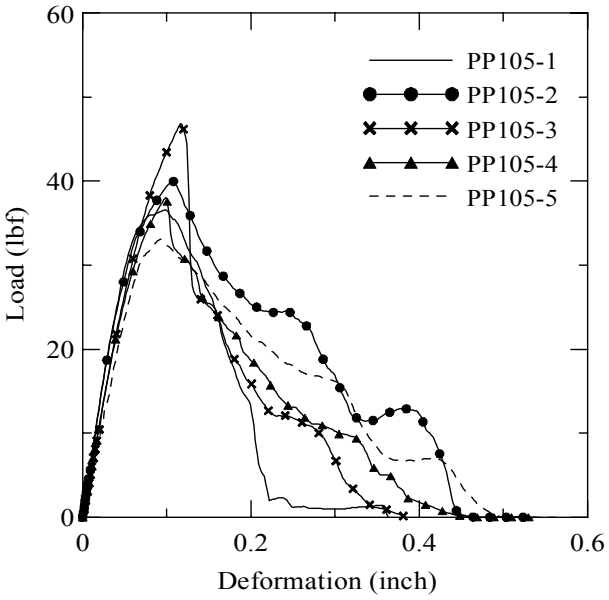

Fig. B-9. PP fiber with mix design 1, cast procedure, 0.5” embedded and 1” free fiber length

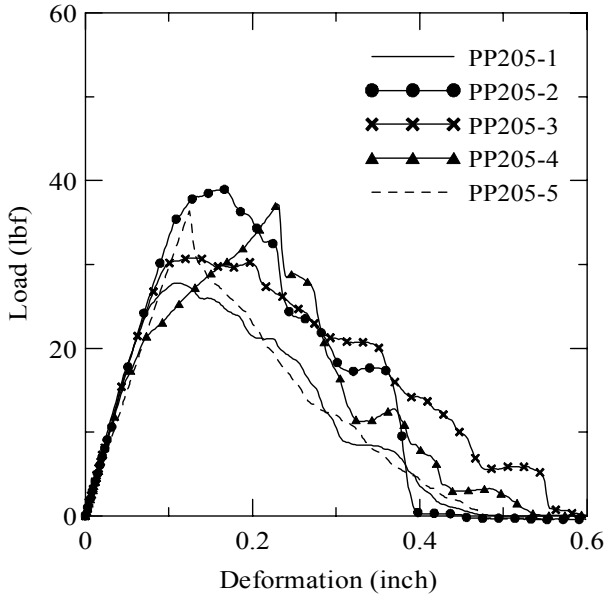

Fig. B-10. PP fiber with mix design 1, cast procedure, 0.5” embedded and 2” free fiber length

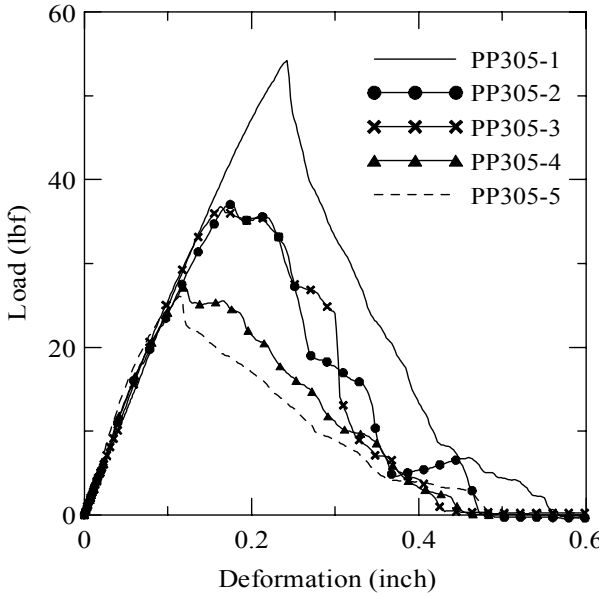

Fig. B-11. PP fiber with mix design 1, cast procedure, 0.5” embedded and 3” free fiber length

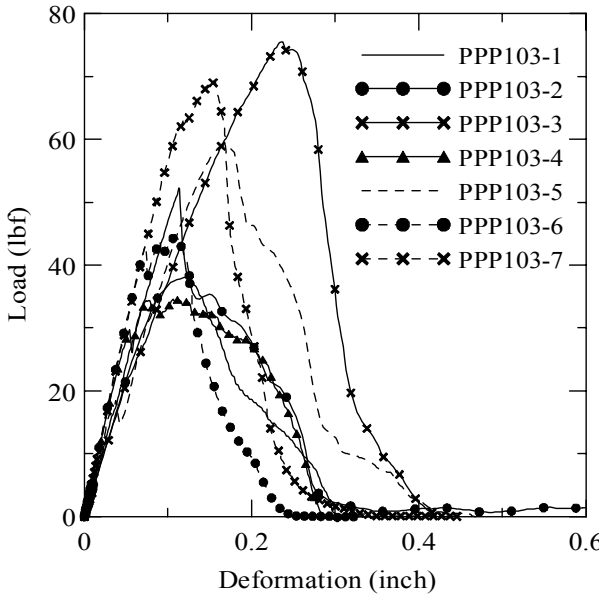

Fig. B-12. PP fiber with mix design 1, pultrusion procedure, 0.3” embedded and 1” free fiber length

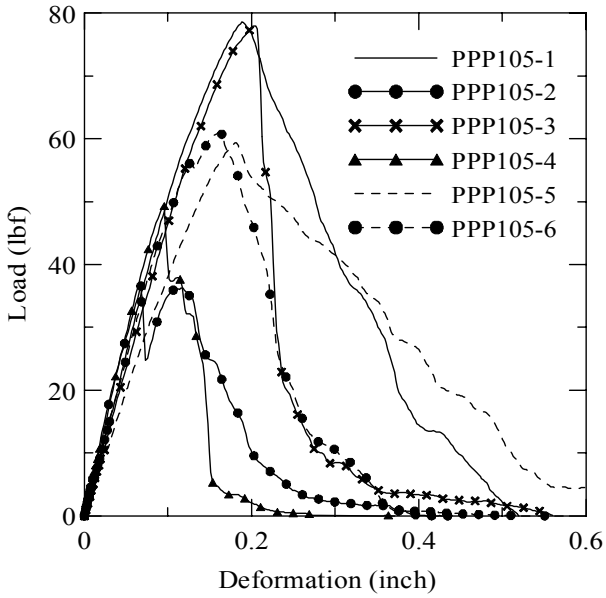

Fig. B-13. PP fiber with mix design 1, pultrusion procedure, 0.5” embedded length and 1” free length

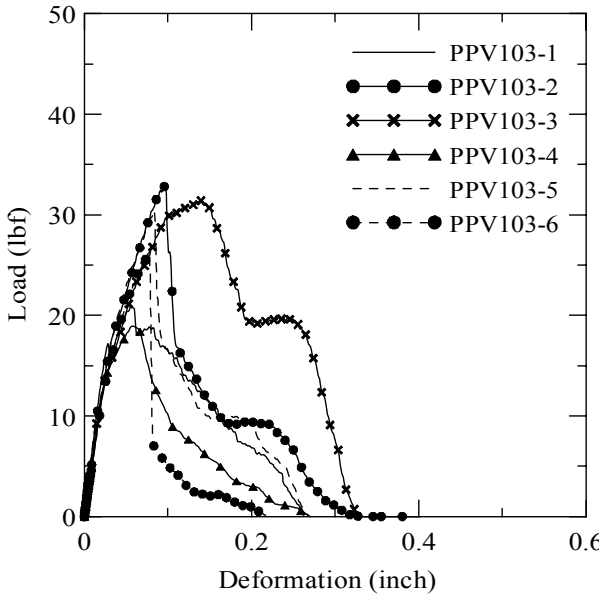

Fig. B-14. PP fiber with mix design 1, vacuum procedure, 0.3” embedded and 1” free fiber length

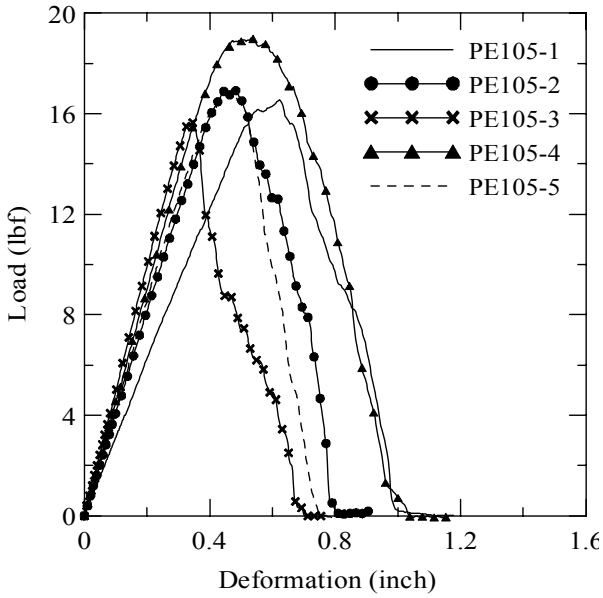

Fig. B-15. PE fiber with mix design 1, cast procedure, 0.5” embedded and 1” free fiber length

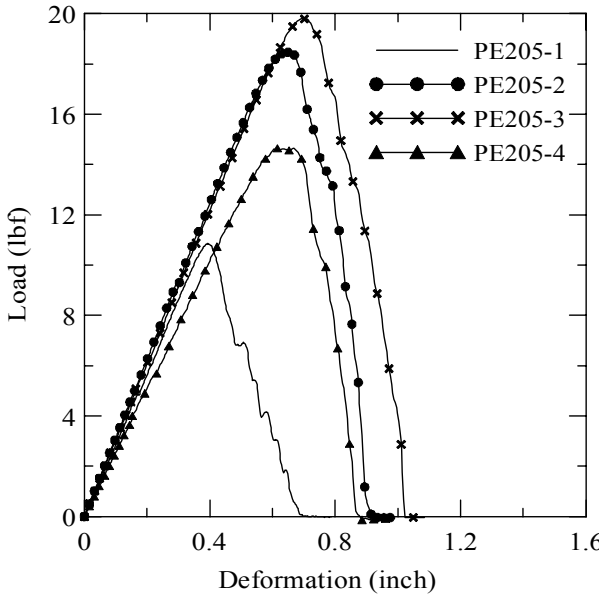

Fig. B-16. PE fiber with mix design 1, cast procedure, 0.5” embedded and 2” free fiber length

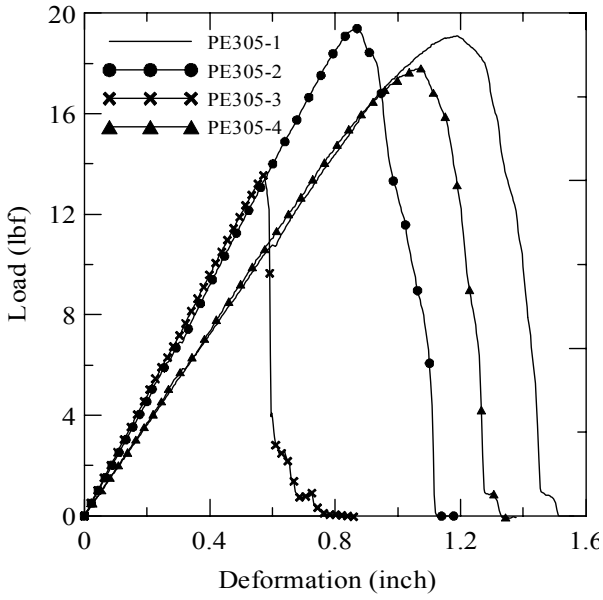

Fig. B-17. PE fiber with mix design 1, cast procedure, 0.5” embedded and 3” free fiber length

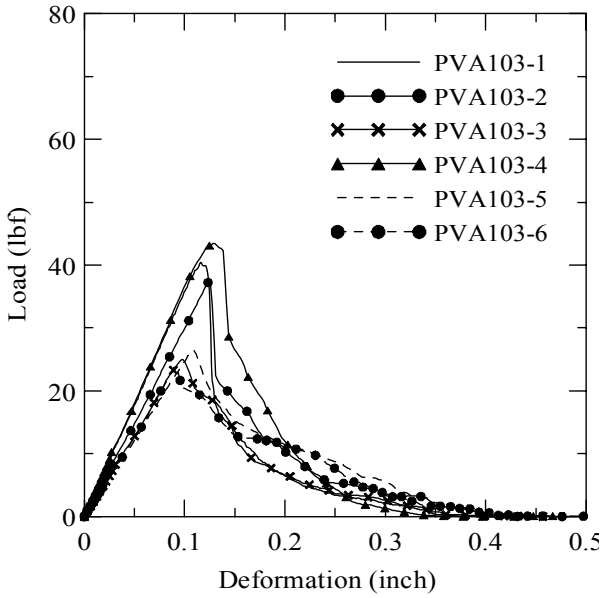

Fig. B-18. PVA fiber with mix design 1, cast procedure, 0.3” embedded and 1” free fiber length

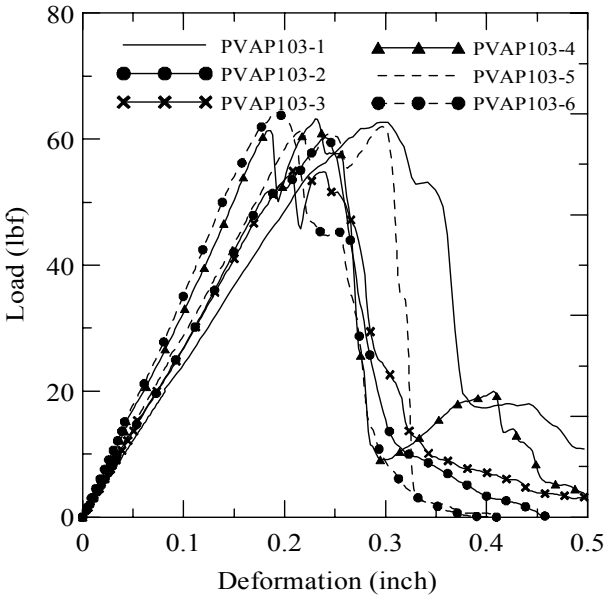

Fig. B-19. PVA fiber with mix design 1, pultrusion procedure, 0.3” embedded and 1” free fiber length

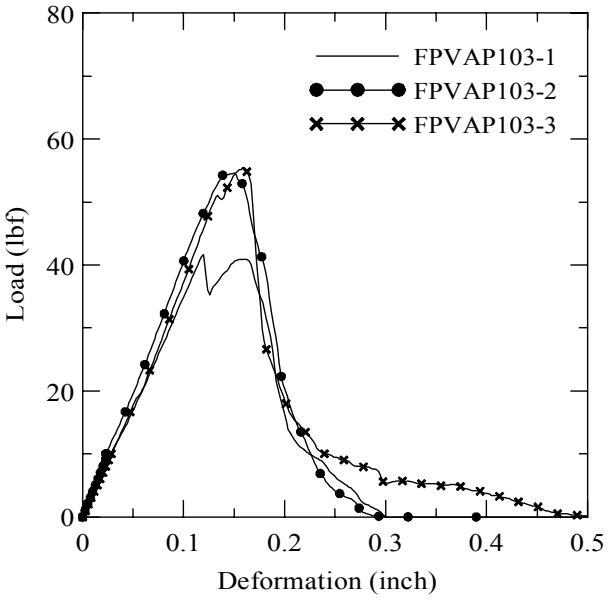

Fig. B-20. PVA fiber with mix design 2, pultrusion procedure, 0.3” embedded and 1” free fiber length

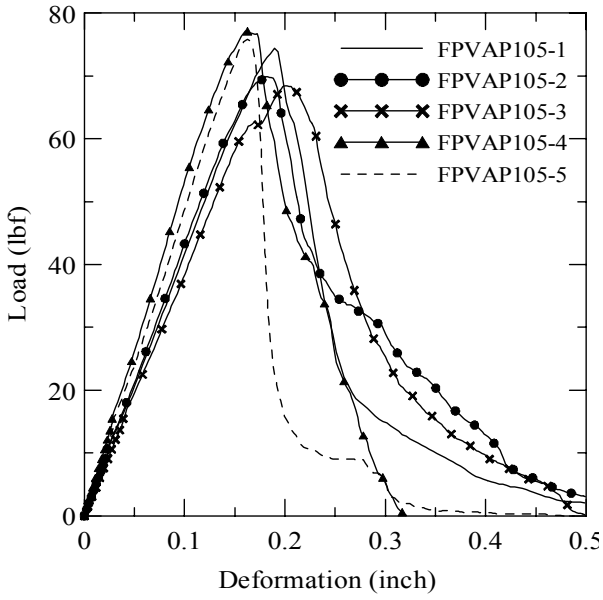

Fig. B-21. PVA fiber with mix design 2, pultrusion procedure, 0.5” embedded and 1” free fiber length

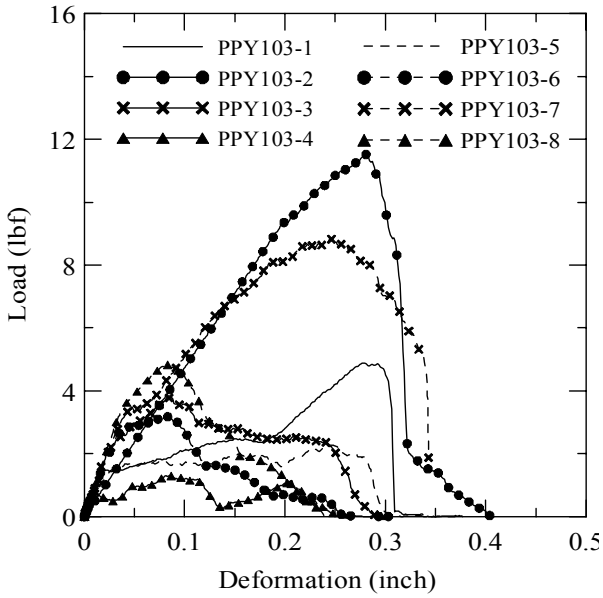

Fig. B-22. PP yarn embedded as single yarn with mix design 1, cast procedure, 0.3” embedded and 1” free length

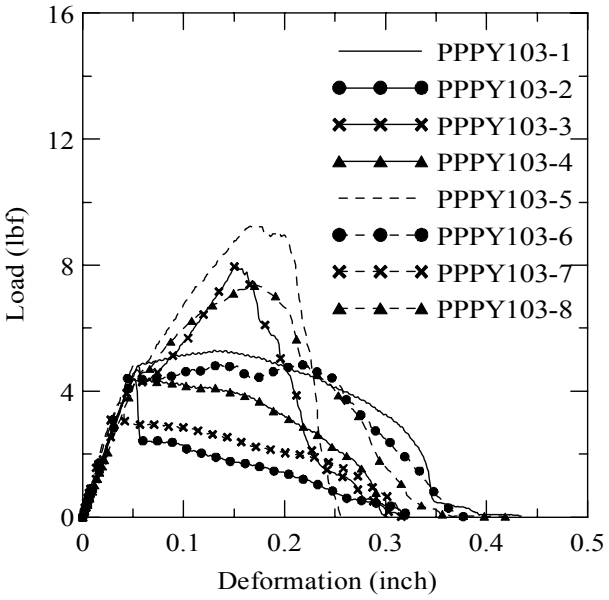

Fig. B-23. PP yarn embedded as single yarn with mix design 1, pultrusion procedure, 0.3” embedded and 1” free fiber length

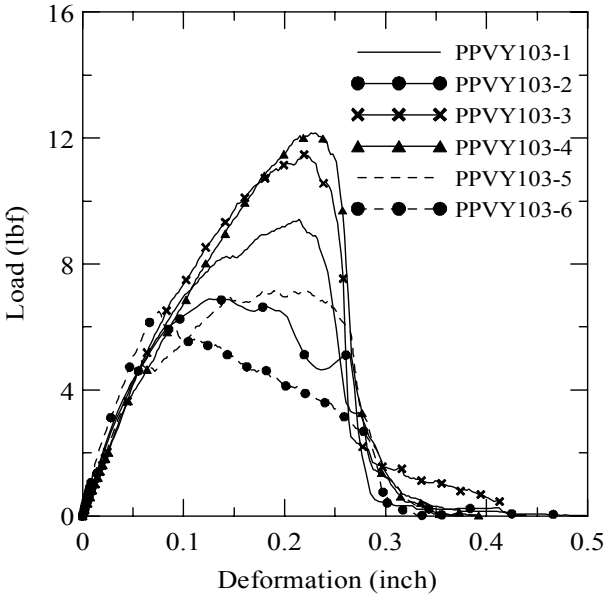

Fig. B-24. PP yarn embedded as single yarn with mix design 1, vacuum procedure, 0.3” embedded and 1” free fiber length

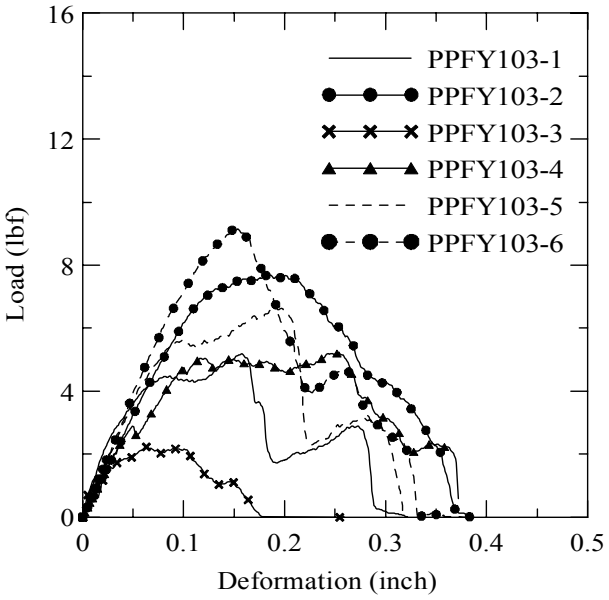

Fig. B-25. PP yarn embedded as fiber with mix design 1, cast procedure, 0.3” embedded and 1” free fiber length

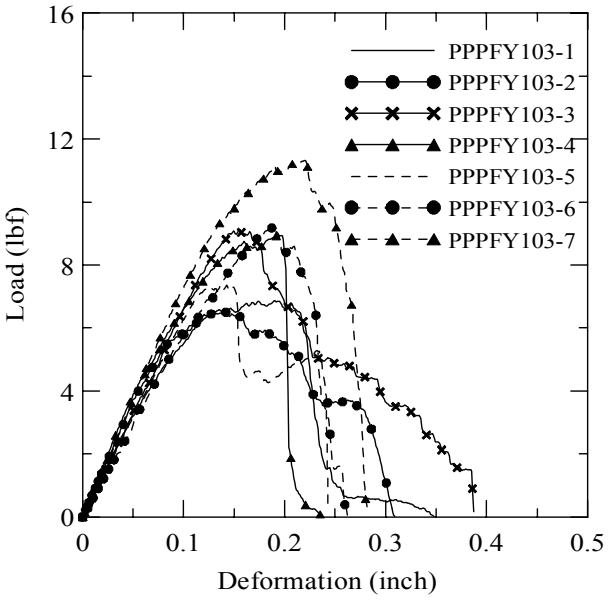

Fig. B-26. PP yarnr embedded as fiber with mix design 1, pultrusion procedure, 0.3” embedded and 1” free fiber length

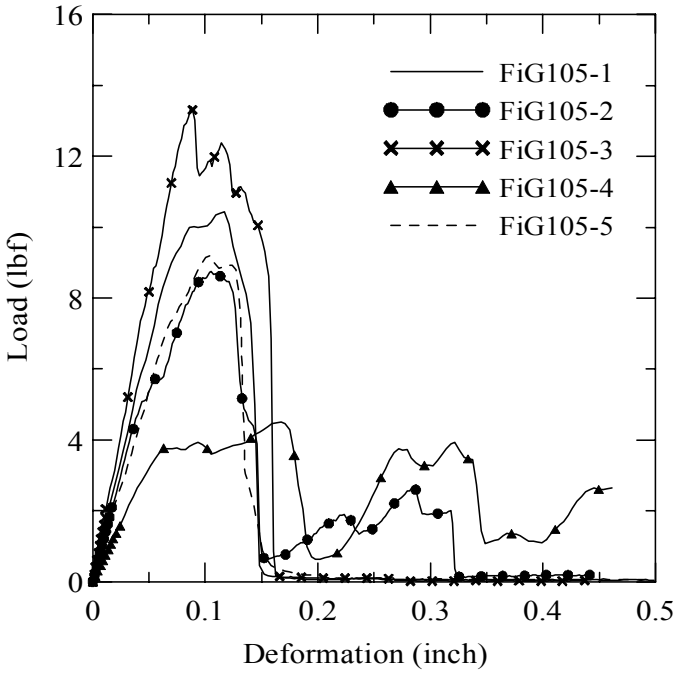

Fig. B-27. AR-glass fiber pullout for anchorage strength

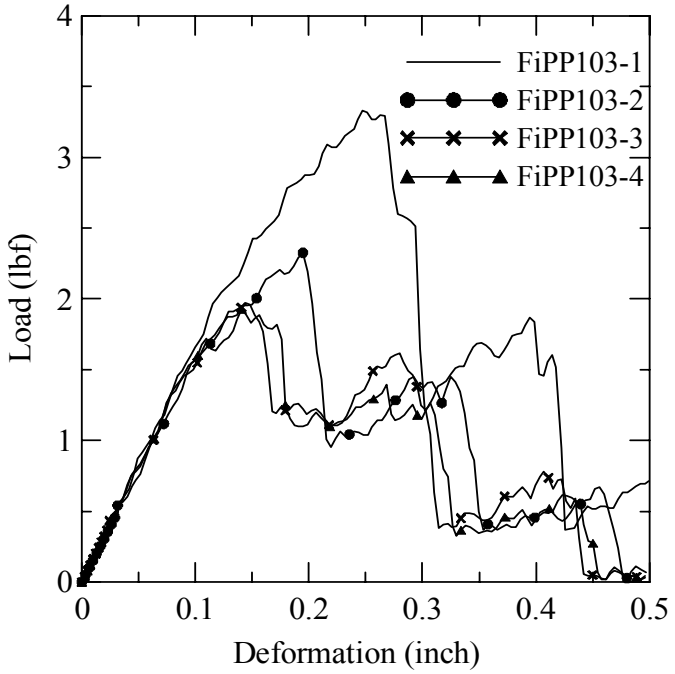

Fig. B-28. AR-glass fiber pullout for anchorage strength

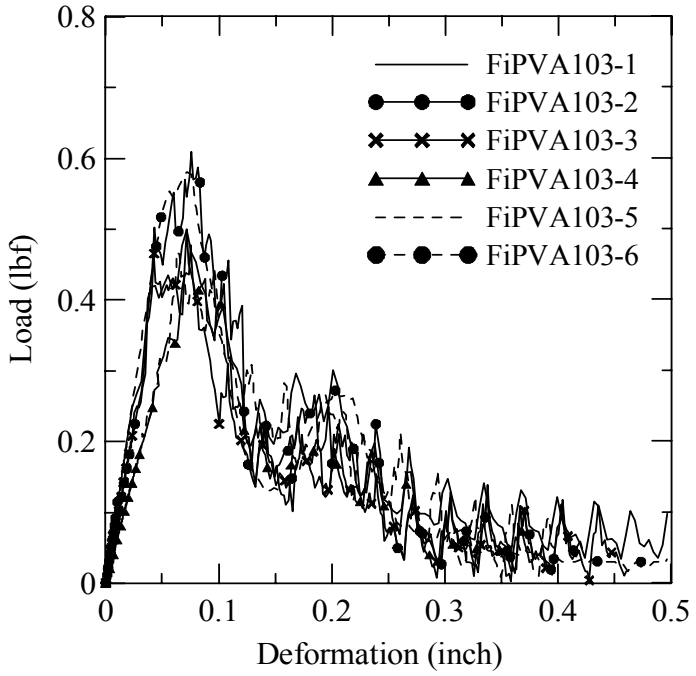

Fig. B-29. PVA fiber pullout for anchorage strength

APPENDIX C

GRAPHS FOR COMPARISONES

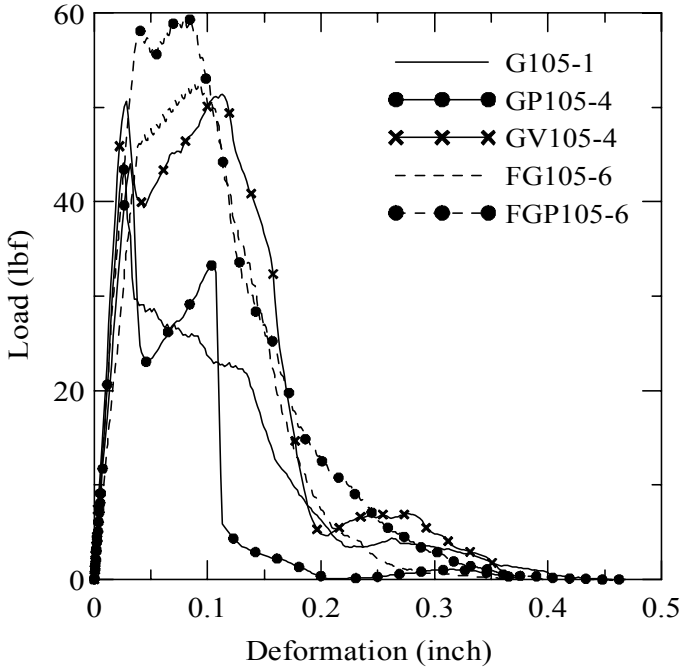

Fig. C-1. AR-glass fiber samples for various conditions

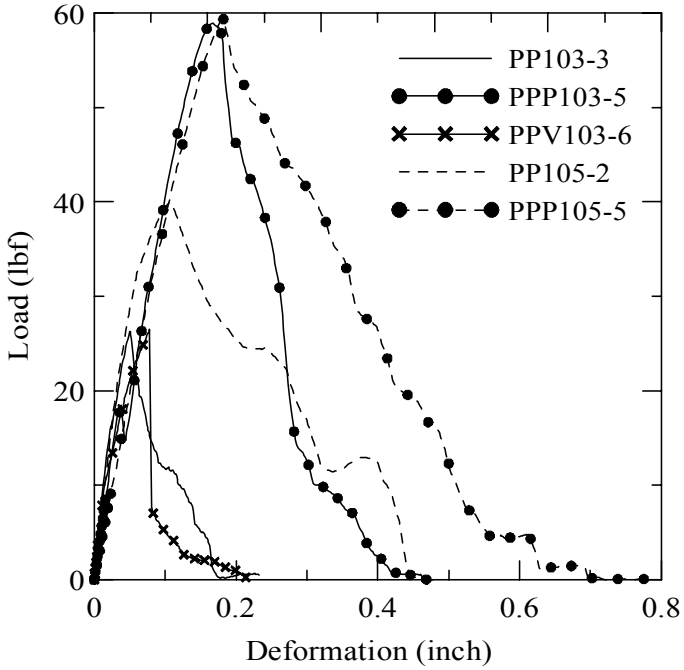

Fig. C-2. PP fiber samples for various conditions

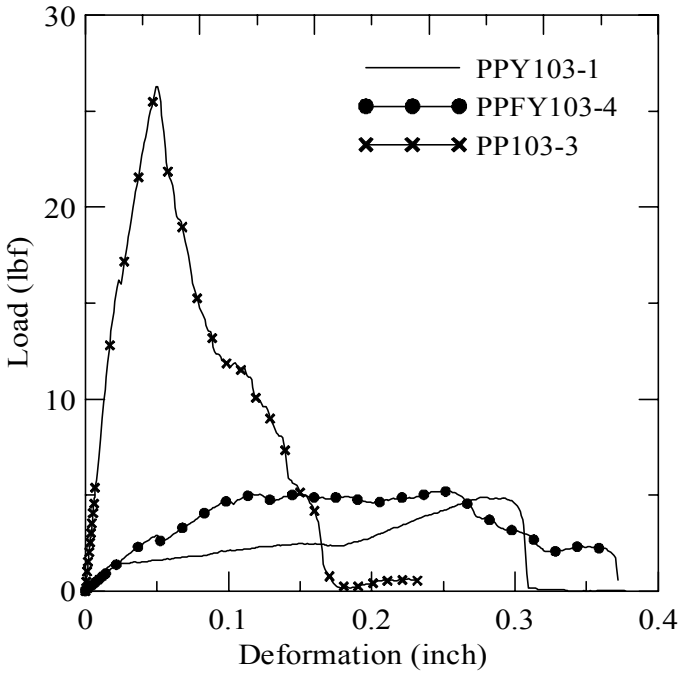

Fig. C-3. 1 and 8 yarns results for PP fiber with control procedure

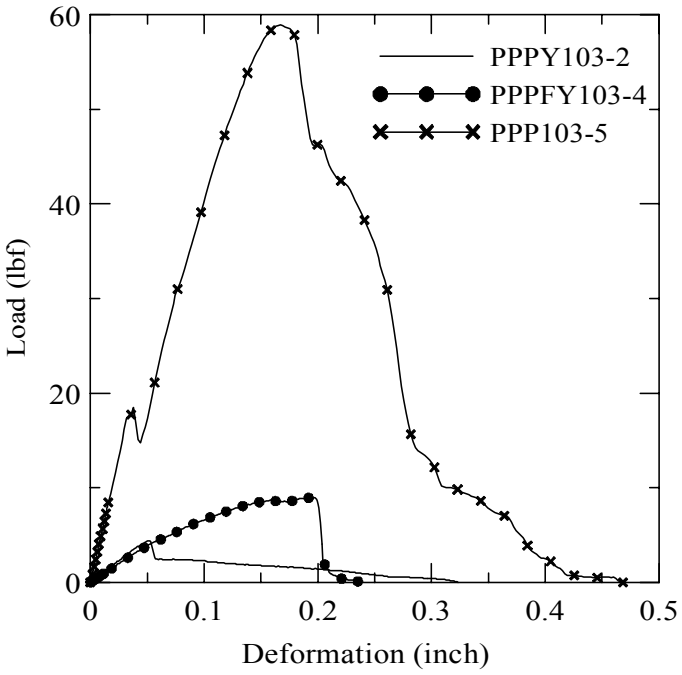

Fig. C-4. 1 and 8 yarns results for PP fiber with pultrusion procedure

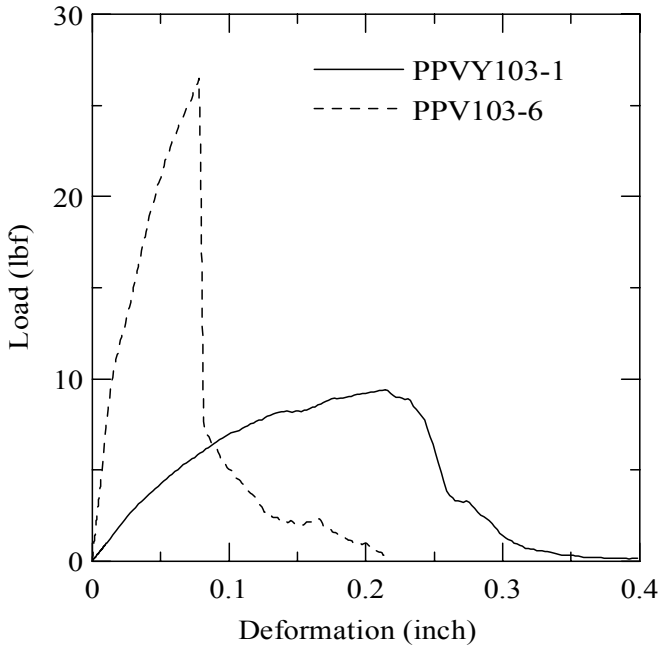

Fig. C-5. 1 and 8 yarns results for PP fiber with vacuum procedure

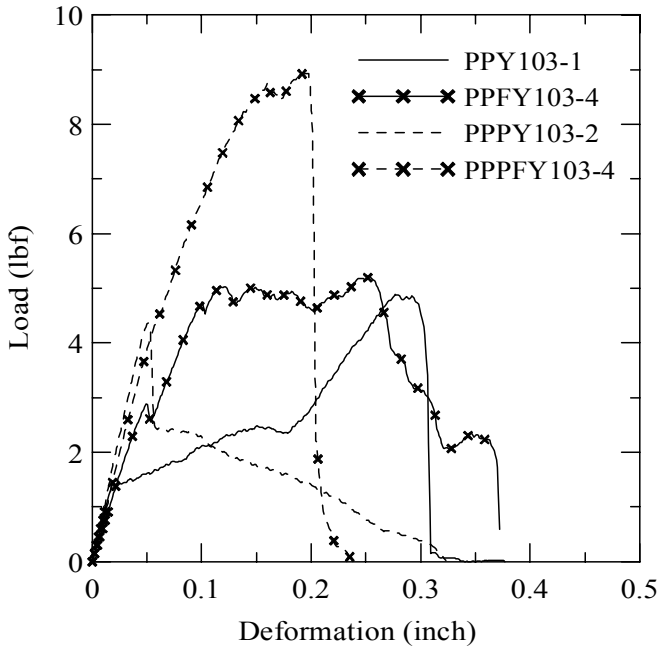

Fig. C-6. PP yarn pullout from the matrix embedded as single yarn or fiber for cast and pultrusion procedure

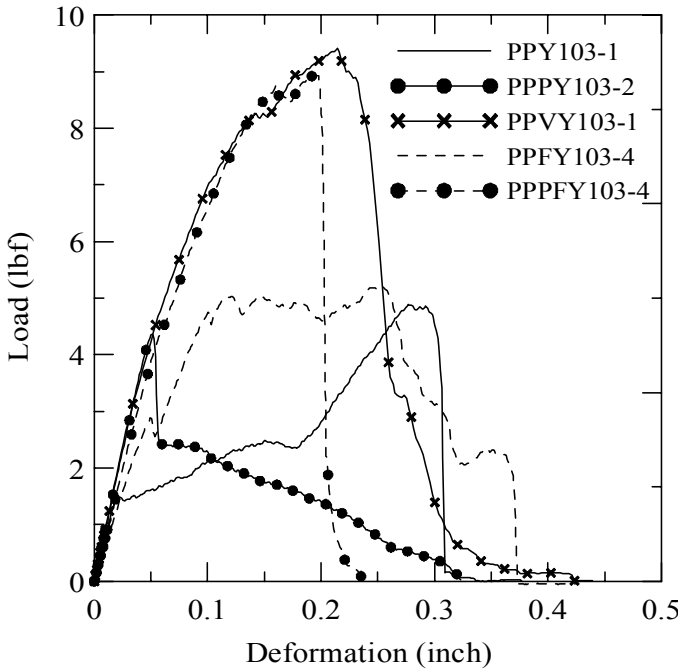

Fig. C-7. PP yarn samples for various conditions

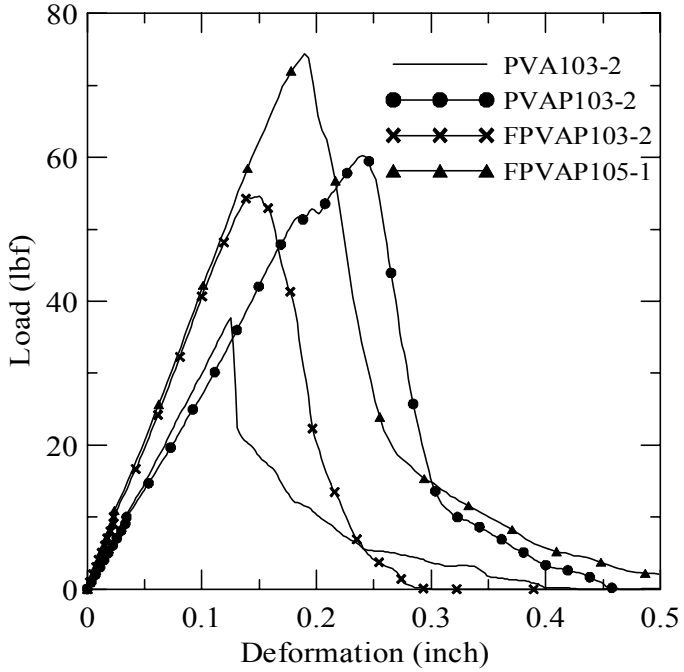

Fig. C-8. PVA fiber samples for various conditions